AD 685761

LATERAL WAVES ON DIFFUSE DIELECTRIC INTERFACES

by

ROGER LANG and JERRY SHMOYS

Polytechnic Institute of Brooklyn
Department of Electrophysics
Long Island Graduate Center
Farmingdale, New York 11735

D D C

R E C' D

APR 2 1 1969

C

Prepared for

LATERAL WAVES ON DIFFUSE DIELECTRIC INTERFACES

by

ROGER LANG and JERRY SHMOYS

Polytechnic Institute of Brooklyn
Department of Electrophysics
Long Island Graduate Center
Farmingdale, New York 11735

Prepared for

ABSTRACT

In the past the lateral wave has been investigated for the case of a sharply bounded transition layer and a layer with a linear velocity variation. The interpretation of the lateral wave given in these instances cannot be extended to an arbitrary smooth layer, and in many cases, the exact nature of the lateral wave contribution becomes unclear. It is our purpose to clarify these matters and to present the characteristics of lateral wave propagation on a layer of arbitrary variation. The models employed can simulate an inhomogeneous plasma having a number density profile, $n(z)$, which varies continuously between two homogeneous half spaces. An integral representation for the scattered field in the optically denser half space is found and evaluated asymptotically in the high frequency limit. This asymptotic evaluation is carried out in two parameter ranges: first, when the layer is thick compared with wavelength; and second, when the layer thickness is arbitrary but the observation point's distance along the interface is large compared with layer thickness.

When the layer thickness is large compared with wavelength, the asymptotic analysis of the scattered field shows that the interpretation of the lateral wave depends markedly upon the gradient of $n(z)$ at the junction with the optically rarer homogeneous half space. It is found that when a finite gradient of $n(z)$ exists, the conventional interpretation of the lateral wave contribution is correct; however, the lateral wave mechanism is different in the case of a zero gradient. For observation points situated at a large distance along a layer of arbitrary thickness, the asymptotic expression for the lateral wave contribution has an amplitude dependence on distance identical with that for the lateral wave on an abrupt interface. In addition, the lateral wave expression reduces to the thick layer result for large layer thickness and it reduces to the abrupt interface result for thin layer thickness.

ii

ACKNOWLEDGEMENT

TABLE OF CONTENTS

TABLE OF FIGURES

TABLE OF FIGURES (Cont'd)

TABLE OF FIGURES (Cont'd)

INTRODUCTION

This report is a study of the fields reflected from diffuse plasma interfaces with particular emphasis on lateral wave excitation and guiding. It was motivated to a large extent by the general lack of knowledge concerning lateral wave behavior on diffuse transitions. From an examination of the literature it became apparent that Nakamura[1] was the only investigator to treat lateral waves excited on a diffuse transition and, in his case, only a linear velocity profile was considered. The diffraction effect in question is relevant for such applications as the scattering of waves by inhomogeneous dielectric or plasma ducts and the radiation from antennae in the presence of ionospheric irregularities. In the latter case, the presence of a magnetic field may introduce additional complications ; however, the results obtained here for the isotropic problem should provide a basis for future study of lateral wave effects when a magnetic field is present.

The transition layers to be considered have a monotonically stratified number density profile, $n(z)$, which varies continuously between two homogeneous half spaces. The width or average width of these layers is proportional to the parameter L; as L becomes small compared with wavelength, the transition layers tend toward an abrupt transition. The equivalent dielectric constant for the medium is given by

$$\epsilon(z) = 1 - (\omega_p/\omega)^2 \quad , \qquad \omega_p^2 = n(z)\, e^2/m\epsilon_o \quad ,$$

and is representative of a cold electron plasma with a background of positively charged immobile particles. In the above formulae ω is the applied frequency, ω_p is the plasma frequency, e and m are the charge and mass of an electron, respectively, and ϵ_o is the free space permittivity. The field incident upon the layer is produced by an electric line current source placed parallel to the transition in the optically denser half space.

Before proceeding, a review of the past research concerning reflected fields from stratified transition layers will be useful. The major portion of this research can be divided into two sections. These are : first, the formulation and investigation of the reflection coefficients from transition layers ; second, the investigation of the reflected fields due to a point source located above these layers. The general problem of relating the dielectric profile of the layer to its reflection coefficient has been dealt with in a number of ways. Brekhovskikh[2] has derived two representations for the reflection coefficient. One of these converges rapidly when the layer is thin compared with wavelength, while the other makes use of the geometrical-optics approximation and converges rapidly when the layer is thick compared with wavelength. Since an explicit form of the reflection coefficient from an arbitrary layer is difficult to obtain , many investigators have studied particular profiles. Hartree[3] has studied the linear layer, and Epstein[4] has devised a layer which is completely continuous. He then studied the reflection properties from it. Heading[5] has recently generalized Epstein's results, and Wait[6] has summarized the results of many other studies.

Although the above reflection coefficient formulae are useful, they can only be employed to calculate the reflected field when a plane wave is incident upon the layer. When the excitation is in the form of a line source, a complete spectrum of plane waves is excited. The reflected field in this case can be represented as a continuous sum or integral over the plane wave spectrum weighted by the appropriate amplitude coefficients for each spectral component. These amplitude coefficients will depend on the reflection coefficient of the layer and, as a result, previous investigations of reflection coefficient properties become useful. It will be the main purpose of this report to approximate asymptotically the integral representation for the reflected field in the

high reequency limit. The asymptotic approximations will then be interpreted geometrically as rays, and the results will be co npared with the classical theory of geometrical-optics. This comparison will clearly distinguish the diffracted rays from those which are predicted solely by calssical geometrical optics.

As has been mentioned previously, all the layers considered here depend on the width parameter L. As L decreases, the layer approaches an abrupt transition. Since this is the case we should expect all of our results to approach the field reflected from an abrupt transition as $k_o L$ becomes small (k_o is the free space wavenumber). The requirement that $k_o L$ be small implies that the field does not vary appreciably over the layer's width. Lateral waves excited on abrupt transitions were first observed and studied by seismologists. Jeffery[7] and Muskart[8] investigated the observed waves theoretically by evaluating the transient field from a point source. Later Ott[9] and Brekhovskikh[10] investigated the time harmonic point source problems. Other investigators who contributed to the understanding of lateral waves on abrupt interfaces were Kruger[11], Gerjouy[12], and Tamir and Felsen[13]. Tamir and Felsen considered the lateral wave excited by a line source and they found that the lateral wave had essentially the same behavior as the lateral wave excited by a point source.

All of the above investigators found that the reflected field from an abrupt interface consisted of two contributions : a reflected and a lateral wave. In Fig. I the ray interpretation of both of these contributions is shown. We see that a ray, emitted from the source toward the layer, is reflected from the interface at the angle of incidence and then proceeds to the observation point. The ray contribution for a line source excitation has an amplitude dependence of $O(k_o^{-\frac{1}{2}})$. The lateral wave,

on the other hand, can be interpreted in terms of a ray that is emitted from the source at the critical angle $(\theta_c = \sin^{-1} \sqrt{\epsilon_1})$. This ray is refracted along the interface, and it then sheds energy into the reflected field. Its contribution to the reflected field for a line source excitation is given by

$$E_L \sim \frac{\alpha_a e^{ik_o[L_1 + L_p + L_2]}}{(k_o L_p)^{3/2}}$$

where the constant α_a is the excitation coefficient, and L_1, L_p, L_2 are defined in Fig. I. We r ould note that the wave has an algebraic decay with distance along the interface. This decay results from the continual shedding of energy into the reflected field as the lateral ray progresses along the interface.

Fig. I
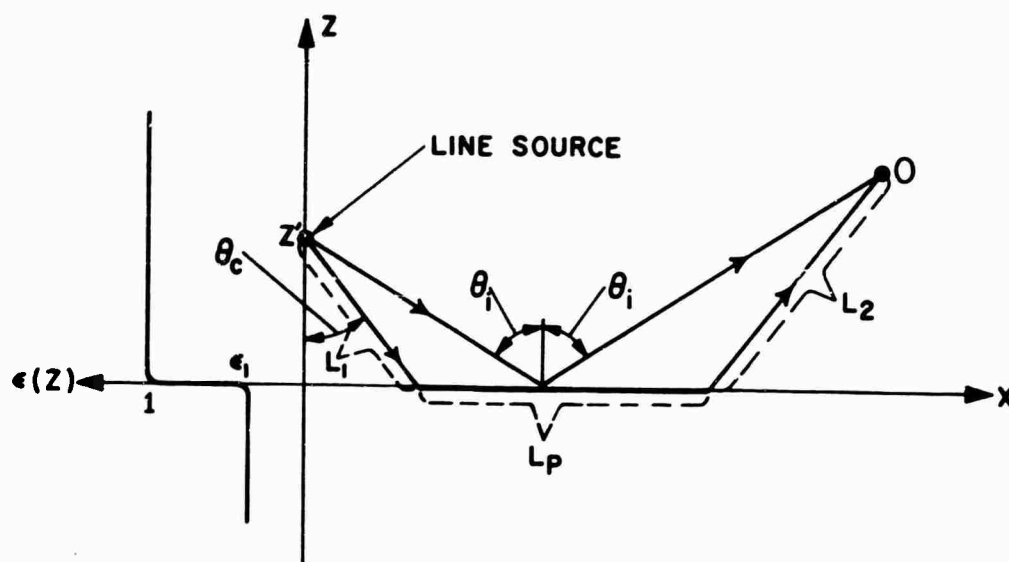
Reflected Field From an Abrupt Interface

An examination of the two contributions to the reflected field shows that the lateral wave contribution is smaller by a factor of k_o^{-1} than the reflected wave contribution ; nevertheless, in many physically meaningful situations, the lateral wave effect is of importance. For instance, when the transient field is observed at points located a large number of wavelengths along the interface, the lateral wave contribution is seen as a first arrival. For this reason it is sometimes known as a head wave. The lateral wave also becomes important in the time harmonic case when the medium containing the source has a slight amount of loss. The wave spends most of its time in the lower, lossless medium and, as a result, becomes the dominant effect for observation points located a large distance along the interface. In our study of lateral waves we shall restrict ourselves to time harmonic problems ; however, the results can be related to transient phenomena.

In an attempt to understand the nature of lateral waves excited on transition layers, the reflected field from four profiles is investigated here. These profiles are : linear, parabolic, Epstein and double exponential ; they are considered in Chapters 1 through 4, respectively. The profiles have not been chosen at random, but instead are selected because the wave functions for the transition can be related to well known functions, and because each successive transition demonstrates an aspect of lateral waves not shown by the previous profiles. Finally, in Chapter 5, the conclusions drawn from the first four chapters are extended to an arbitrary layer when possible . The general method of investigation is: first, to formulate the integral representation for the reflected field ; second, to evaluate the formal solution asymptotically for thick layers $(k_o L \gg 1)$; and third, to perform an asymptotic analysis for arbitrary layer thickness. It has been found that in order to obtain an asymptotic estimate of the reflected field for arbitrary layer thickness, it is necessary to assume that the observation point is far from the source.

CHAPTER 1.

THE LINEAR TRANSITION LAYER

1.1   Introduction

To begin our investigation of lateral waves we will study the
reflected field from a linear transition. This transition is composed of
a ramp dielectric variation between two homogeneous dielectric half spaces.
A source, placed in the denser half space, illuminates the transition and
causes a reflected field. This reflected field, which will be the main object
of our investigation, can be represented by a continuous sum or integral
over the reflection coefficient of the layer times the spectral components
excited by the source. The formulation and some of the properties of the
reflection coefficient have been investigated by Hartree . However, no
attempt has been made by him to investigate the source problem.

The integral representation for the reflected field is too complex to be
directly integrated and therefore it must be asymptotically approximated.
Two separate asymptotic evaluations of the integral representation are
carried out: first, when the layer thickness, L, is large compared to wave-
length, i.e., $k_0 L \gg 1$, and second, when the observation point is far from
the source. In the first case we will obtain an asymptotic approximation to
the reflected field for all observation points for large $k_0 L$. The asymptotic
approximation obtained by the second procedure, on the other hand, will be
valid for observation points which are far from the source compared to the
layer thickness. In both evaluations of the reflected field, special emphasis
will be placed on lateral wave contributions and their interpretation.

Before proceeding with our investigation, some of the pertinent work
that has been done on similar problems should be mentioned. Orlov [14]
has found the ray trajectories which are reflected from a ramp dielectric
variation as shown in Fig. 1.1 when $k_0 z_L \gg 1$. Here z_L is the width of
the   tion of the dielectric layer which supports propagating waves.
      ght modification, these results can be used to give the structure
of the reflected ray trajectories for the linear layer when $k_0 L$ is large.

In the text we have not used Orlov's results directly, but instead, have rederived them. An investigation of the lateral wave which is excited in a medium with a linear velocity transition, has been considered by Nakamura when the observation point is far from the source. Because of the analogous behavior of acoustic and electromagnetic waves in media of the type being considered here, Nakamura's profile is equivalent to an inverse square dielectric profile as shown in Fig. 1.2. A comparison between Nakamura's lateral wave and our results will be made in an attempt to determine some of the invariants of transition layers.

1.2   Formal Solution

An electric line current source of amplitude J is placed in a stratified dielectric medium, $\epsilon(z)$, at $x = 0$, $z = z'$ and parallel to the y axis, as is shown in Fig. 1.3. Under these conditions the only field components excited are E_y, H_x and H_z. The electric field obeys the inhomogeneous wave equation[15]

$$[\nabla^2 + k_o^2 \, \epsilon(z)] \, E_y = - \, i\omega\mu_o \, J \, \delta(x) \, \delta(z - z') \, . \tag{1.2.1}$$

We will assume that

$$J = 1/(i\omega\mu_o) \tag{1.2.2}$$

to simplify Eq. (1.2.1). The particular dielectric variation to be used is given by

$$\epsilon(z) = \begin{cases} 1 & , \quad z \geq 0 \\ \Delta z/L + 1 & , \quad -L < z < 0 \quad , \quad \Delta = 1 - \epsilon_1 \\ \epsilon_1 & , \quad z \leq -L \end{cases} \tag{1.2.3}$$

and is shown in Fig. 1.2. The dielectric constant of the homogeneous region, $z \geq 0$, has been chosen to be unity, but if the dielectric constant of this region is not unity, Eq. (1.2.1) can be scaled to produce an equivalent dielectric
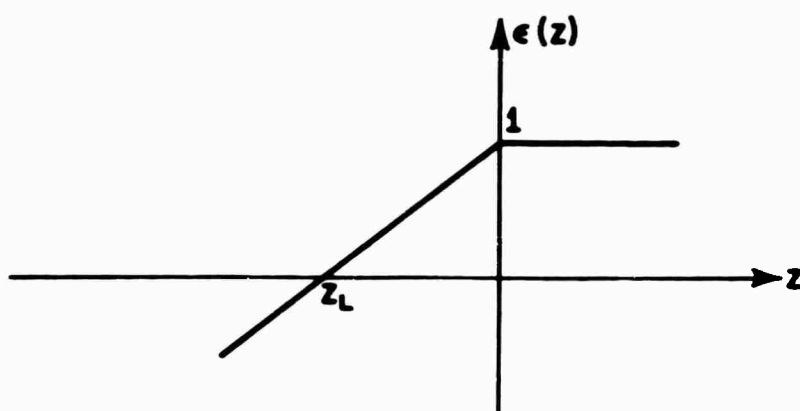
Fig. 1.1

Orlov's Dielectric Variation
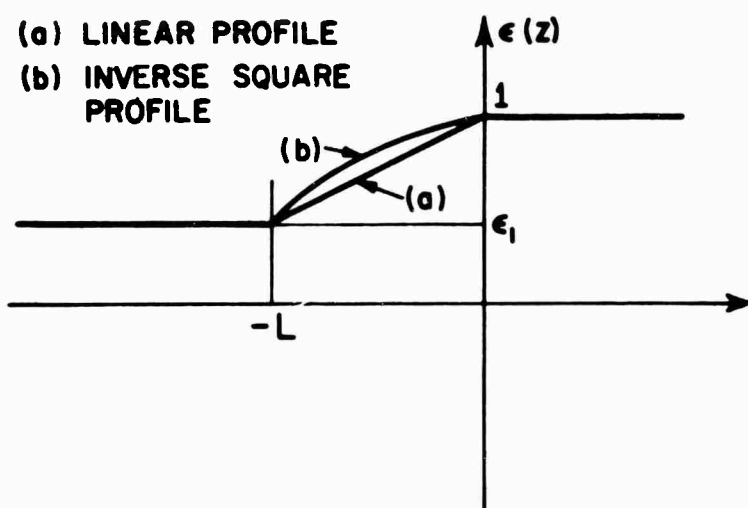
Fig. 1.2

Comparison of Nakamura's and Linear Dielectric Variation
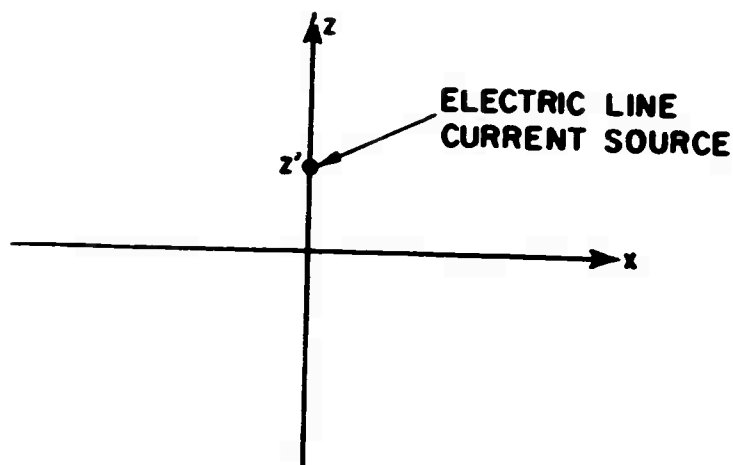
Fig. 1.3

Source Location
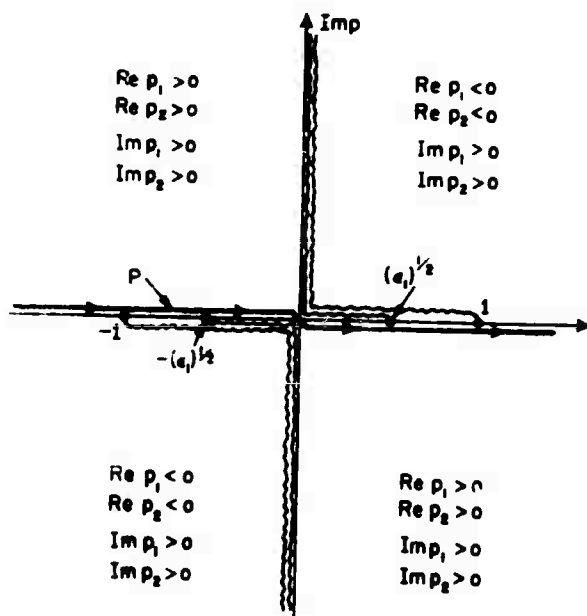
Fig. 1.4

Top Sheet of a Four Sheeted Riemann Surface,
p - plane

constant which is unity.

Since the medium is uniform in x, we will represent E_y by means of its Fourier transform $\Phi(z, p)$, i.e.,

$$E_y = \frac{k_o}{2\pi} \int_{-\infty}^{+\infty} \Phi(z, p) \, e^{ik_o px} \, dp. \tag{1.2.4}$$

By using the above representation for E_y, Eq. (1.2.1) reduces to the one-dimensional Green's function problem

$$\left\{ \frac{d^2}{dz^2} + k_o^2 \left[\epsilon(z) - p^2 \right] \right\} \Phi(z, p) = - \delta(z - z') \tag{1.2.5}$$

with the boundary conditions that $\Phi(z, p)$ must be an out-going wave as $z \to \pm \infty$.

In Appendix A the formal solution for the Green's function $\Phi(z, p)$ is obtained for an arbitrary layer variation in terms of a pair of independent homogeneous solutions to the wave equation in the layer region. For a layer with a linear variation such as the one under consideration here, two independent solutions to the wave equation in the layer region are $A_i(\xi^2 e^{\pm i\pi/3})$ where A_i is the Airy function[16] and $\xi^2 = (k_o L/\Delta)^{2/3} (\Delta z/L + 1 - p^2)$. By using these independent solutions in Eq. (A-13) and in Eq. (A-7) we obtain an explicit expression for $\Phi(z, p)$. We then substitute $\Phi(z, p)$ into Eq. (1.2.4) and obtain an integral representation for the field. It is

$$E_y = E_{yf} + E_{yr} \tag{1.2.6}$$

$$E_{yf} = \frac{i}{4\pi} \int_{-\infty}^{+\infty} \frac{e^{ik_o[p_2|z - z'| + px]}}{p_2} \, dp \tag{1.2.7}$$

$$E_{yr} = \frac{i}{4\pi} \int_{-\infty}^{+\infty} \frac{\bar{\Gamma} e^{ik_o[p_2(z + z') + px]}}{p_2} \, dp \tag{1.2.8}$$

where

$$\bar{\Gamma} = - \frac{\Delta_t}{\Delta_b} \qquad (1.2.9)$$

with

$$\Delta_t = \begin{vmatrix} \left\{ A_i'(\zeta_1^2 e^{-i\pi/3}) + \zeta_1 e^{i\,5\pi/6} A_i(\zeta_1^2 e^{-i\pi/3}) \right\} & \left\{ A_i'(\zeta_1^2 e^{+i\pi/3}) + \zeta_1 e^{i\pi/6} A_i(\zeta_1^2 e^{i\pi/3}) \right\} \\ \left\{ A_i'(\zeta_2^2 e^{-i\pi/3}) \pm \zeta_2 e^{i\,5\pi/6} A_i(\zeta_2^2 e^{-i\pi/3}) \right\} & \left\{ A_i'(\zeta_2^2 e^{+i\pi/3}) \pm \zeta_2 e^{i\pi/6} A_i(\zeta_2^2 e^{i\pi/3}) \right\} \end{vmatrix}$$

$$\zeta_{\substack{1\\2}} = (\tau/\Delta)^{1/3} p_{\substack{1\\2}} \quad , \qquad \tau = k_o L \quad ,$$

$$\qquad (1.2.10)$$

$$p_1 = [\epsilon_1 - p^2]^{\frac{1}{2}} \quad , \qquad p_2 = [1 - p^2]^{\frac{1}{2}} \quad .$$

In the above expression for the reflection coefficient, $\bar{\Gamma}$, the symbol $A_i'(z) = dA_i(z)/dz$. The branch cuts for the square root functions p_1 and p_2 must be specified if the integrals in Eqs. (1.2.7) and (1.2.8) are to be completely defined. This specification has been made in Fig. 1.4 where the top sheet of a four sheeted Riemann surface is shown. To clarify the designation of the top sheet, the sign of the real and imaginary parts of p_1 and p_2 have been given in each quadrant. On any particular sheet of this Riemann surface the integral is a single-valued function, however, the integration path was chosen on the top sheet so that the integral would converge properly as $p \to \pm \infty$.

The expression for the field has been divided into two parts : E_{yf} and E_{yr} as shown in Eq. (1.2.6) . The motivation for this is that E_{yf} is the direct field from the source, that is, it is the field which would exist if the entire medium were homogeneous while E_{yr} is the reflected field from

the layer. As expected, the direct field integral, Eq.(1.2.7) integrates to

$$E_{yf} = \frac{i}{4} H_0^{(1)} (k_o \sqrt{x^2 + (z - z')^2})$$ (1.2.11)

where $H_0^{(1)}$ is the Hankel function of the first kind and zero order. We see that E_{yr} can be interpreted as a cylindrical wave propagating away from the source. The integral for the reflected field is too complicated to be integrated directly, so approximate techniques must be used.

Before proceeding with the approximate evaluation of the reflected field, E_{yr}, we will transform the integral from the p to the p_1 plane. The result is

$$E_{yr} = - \frac{i}{4\pi} \int_C \frac{p_1 \bar{\Gamma}}{p p_2} e^{ i k_o [p_2(z + z') + px]} dp_1$$ (1.2.12)

where the square roots $p = \sqrt{\epsilon_1 - p_1^2}$ and $p_2 = \sqrt{\Delta + p_1^2}$ must again be defined on a four sheeted Riemann surface. The upper two sheets of this surface are shown in Figs. 1.5 and 1.6 along with the transformed integration path, C. This transformation was motivated by the fact that the interesting contributions to E_{yr} come from the region near the branch point $p = \sqrt{\epsilon_1}$. By transforming the integral to the p_1 plane, this branch point and the branch point at $p = \sqrt{\epsilon_1}$ are eliminated. The disappearance of these two branch points is accompanied by the appearance of two new branch points at $p_1 = \pm\sqrt{\epsilon_1}$. For a more detailed explanation of the transformation, consult Tamir and Felsen[13].

1.3   Evaluation of Reflected Field for $k_o L \gg 1$

1.3.1.   Geometrical Optics

Before attempting a rigorous asymptotic evaluation of the reflected field when $k_o L \gg 1$, we shall investigate the rays which are emitted from
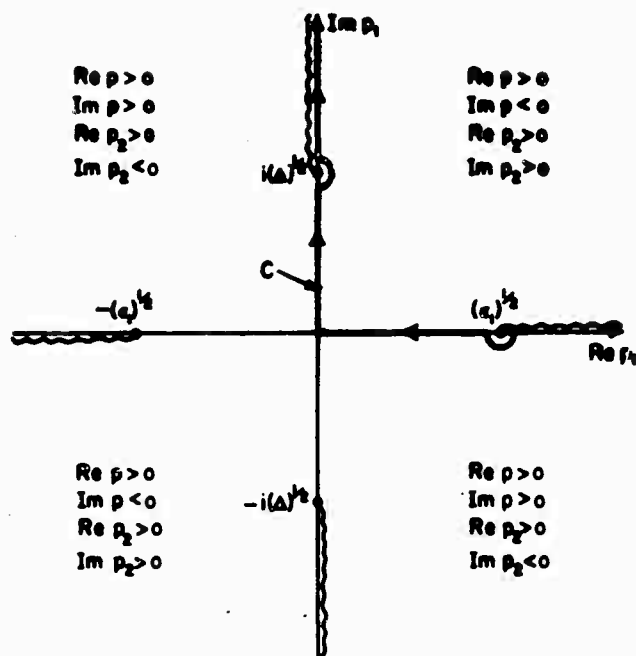
Fig. 1.5

Top Sheet of a Four Sheeted Riemann Surface, p_1 - plane
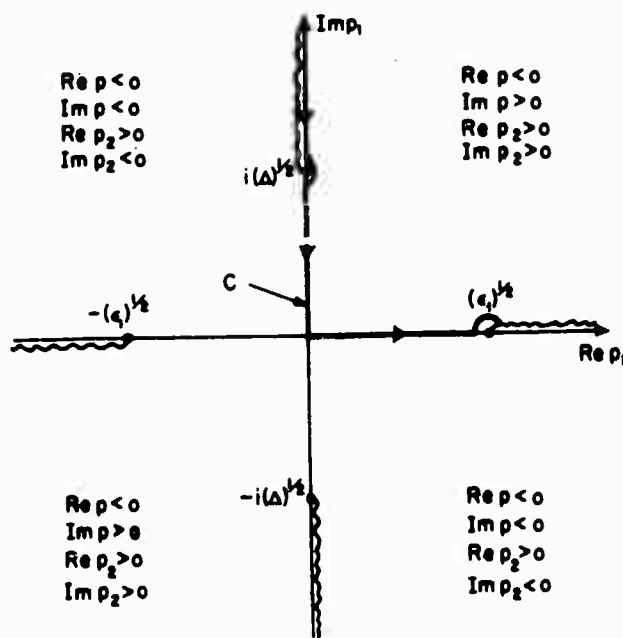
Fig. 1.6

Second Sheet of a Four Sheeted Riemann Surface, p_1 - plane

the source when the layer is thick compared to wavelength. These rays divide into three basic types : direct, transmitted and returning. The direct rays are emitted from the source in the angular range $-\pi/2 < \vartheta \leq 0$ where θ is the angle of emission of the ray from the source and is shown in Fig. 1.7. The returning and transmitted rays are emitted from the source in the angular ranges $0 < \theta < \theta_c$ and $\theta_c < \theta < \pi/2$ respectively, where the angle θ_c is the critical angle. This angle is defined as the angle whose corresponding ray (critical ray) has its turning point on the lower interface. The three basic types of rays and the critical ray are shown in Fig. 1.7.

An examination of this figure shows that the direct and transmitted rays are of a much simpler character than the reflected rays. The simplifying feature of these ray types is that neighboring ray trajectories do not cross one another, thus making the formation of caustics impossible. No such statement can be made about the returning rays which shall now be examined in further detail.

The returning ray trajectories for $x > x_t$ can be found by integrating the ray equation

$$x = x_t + \int_{z_t}^{z} \frac{p\,d\tau}{\sqrt{\epsilon(\tau) - p^2}} \tag{1.3.1}$$

where

$$x_t = - \int_{z'}^{z_t} \frac{p\,d\tau}{\sqrt{\epsilon(\tau) - p^2}} \quad , \quad p = \sin\theta$$

and

$$\epsilon(z_t) = p^2 \quad .$$

The ray parameter p is the same as the integration variable in Eq. (1.2.8). We will not investigate the returning rays in the region before they turn $(x < x_t)$ since the rays do not cross one another in this region. Upon integrating Eq. (1.3.1) , for $x > x_t$ we obtain
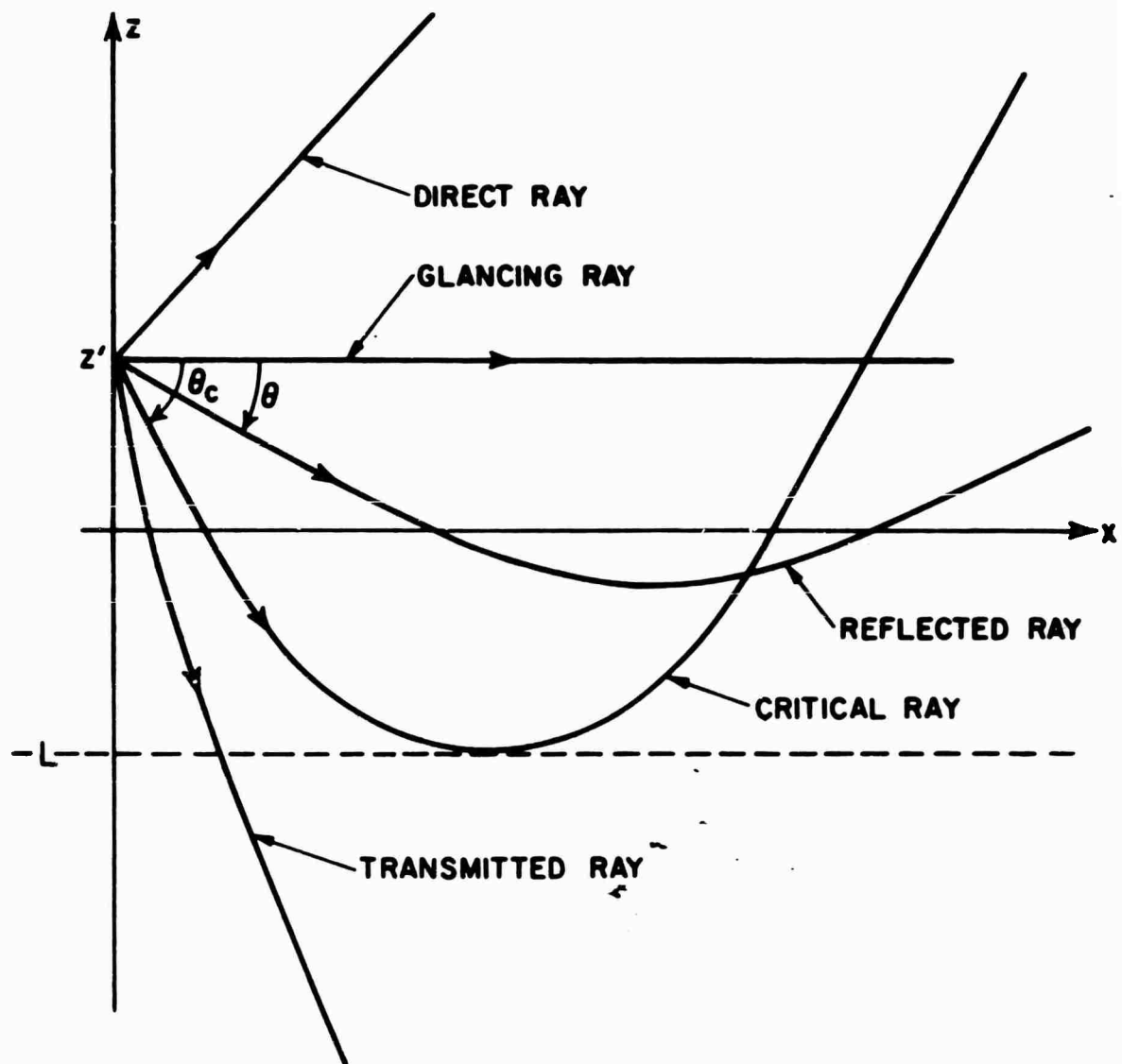
Fig. 1.7

Typical Ray Types for Linear Layer

$$\bar{z} = \bar{z}' + \frac{p_2 \bar{x}}{p} - 4 p_2^2 \quad , \quad z \geq 0$$

$$\bar{z} = (\frac{\bar{x}}{2p} - \frac{\bar{z}'}{2p_2} - p_2)^2 - p_2^2 \quad , \quad z \leq 0 \qquad (1.3.2)$$

where

$$\bar{z} = \Delta z / L \quad , \quad \bar{x} = \Delta x / L \quad , \quad \bar{z}' = \Delta z' / L$$

and $\epsilon_1 \leq p^2 < 1$. It is interesting to note that $p^2 = \epsilon_1$ is the critically reflected ray. When the ray parameter $p^2 < \epsilon_1$, the rays correspond to transmitted rays and are no longer given by Eq. (1.3.2) .

An inspection of Eq. (1.3.2) shows that it appears in a normalized form in terms of barred coordinates, i.e., $\bar{x}$, $\bar{z}$ and $\bar{z}'$. As a function of these new coordinates, the ray trajectories depend only on the source coordinates $\bar{z}'$, however, the equations are still only valid for $\epsilon_1 \leq p^2 < 1$. Since we would like to investigate the nature of the rays for arbitrary ϵ_1 , i.e., $0 \leq \epsilon_1 < 1$ we will assume $0 \leq p^2 < 1$. This corresponds to a layer with $\epsilon_1 = 0$. If we are considering a layer where ϵ_1 is finite, then we just use the results of the $\epsilon_1 = 0$ case and eliminate those rays with $0 \leq p^2 < \epsilon_1$.

The returning rays for $x > x_t$ cross over one another in such a way that they form a caustic. This caustic can be found by solving the constraint equation,

$$0 = \bar{x} - 2 p_2 p^3 \qquad\qquad , \quad \bar{z} \geq 0$$

$$(1.3.3)$$

$$0 = \bar{x}^2 + \frac{\bar{z}' \bar{x}(2p^3 - p)}{p_2^3} - \frac{2p\bar{x}}{p_2} - \frac{p^2 \bar{z}'}{p_2^4} \quad , \quad \bar{z} \leq 0$$

simultaneously with the ray equation (1.3.2). The constraint equation can be found by taking the partial derivative of the ray equation with respect to p.

The elimination of the ray parameter p between Eqs. (1.3.2) and (1.3.3) can be accomplished only when $\bar{z} > 0$. The result is quite complicated and will not be presented here.

As an alternative method of finding the equation of the caustic directly we shall investigate its behavior near $\theta = 0$ and $\theta = \pi/2$. With this information and with the location of the focal points, we shall have a fair understanding of the caustic's configuration.

From the ray and constraint equation we find that the point on the caustic, corresponding to $\theta = 0$, is located at $x = 0$, $\bar{z} = -\bar{z}'(1 - \bar{z}'/4)$. The slope of the caustic at this point is zero, i.e., $dz/dx = 0$. As the angle $\theta \to \pi/2$, the parameter p_2 becomes small and the equations simplify which allows us to obtain an asymptote to the caustic in this region. It is

$$\bar{z} = -\frac{\bar{z}'}{\bar{x}^2} \quad , \quad p_2 \approx 0 . \tag{1.3.4}$$

To complete the description of the caustic, the second constraint equation must be found. This equation, together with the ray and first constraint equation, will give the location of the foci. The second constraint equation, obtained by taking the partial derivative of Eq. (1.3.3) with respect to p, is

$$0 = 4 p_2^2 - 1 \qquad , \qquad \bar{z} \geq 0$$

$$0 = \bar{x} - \frac{4 \bar{z}'^2 p^3}{p_2 [\bar{z}'(4 p^2 - 1) - 2 p_2^2]} \qquad , \qquad \bar{z} \leq 0 . \tag{1.3.5}$$

For $\bar{z} \geq 0$, the location of the focus can be found explicitly in a simple form. It is

$$\bar{x} = 3\sqrt{3}/2 \quad , \quad \bar{z} = \frac{1}{2} - \bar{z}' \quad , \quad p_2 = \frac{1}{2} . \tag{1.3.6}$$

From these equations we see that there is one focus when $\bar{z}' \leq 1/2$ while no foci exist for $\bar{z} \geq 0$ when $\bar{z}' > 1/2$. For $\bar{z} < 0$ we find that the foci occur at ray parameters

$$p_2^2 = \frac{\bar{z}'}{2}\left[\frac{5 \pm 2\sqrt{4-6\bar{z}'}}{8\bar{z}'+3}\right].\tag{1.3.7}$$

When $\bar{z}' > 2/3$, the ray parameters p_2 are complex and no foci occur. In the interval $1/2 < \bar{z}' < 2/3$, two real p_2 exist and two foci occur for $\bar{z} < 0$. When $0 < \bar{z}' < 1/2$, two real p_2 still exist but one of the ray parameters leads to a $\bar{z} > 0$.

To summarize our investigation of the foci, we have found : first, for large $\bar{z}'$, no foci exist; second, as $\bar{z}'$ becomes less than $2/3$, two foci appear in the layer; and third, as $\bar{z}'$ becomes less than $1/2$, one of the two foci in the layer region moves into the homogeneous region. It is also interesting to note that at $\bar{z}' = 2/3$, two foci are located at the same spot. A check shows that the third constraint equation is zero at this point.

A graph of the caustic has been plotted for each of the three cases given above. These graphs appear in Figs. 1.8, 1.9. and 1.10 along with the locus of turning points and the critical ray. The portion of the caustic near $p = 0$ is not shown in these figures since $z_1 > 0$. To alleviate this, we have presented a sketch of the caustic for $c_1 = 0$ and $\bar{z}' > 2/3$ in Fig. 1.11. The behavior of the portion of the caustic, corresponding to rays with small θ, remains essentially the same when $\bar{z}' < 2/3$.

1.3.2   Asymptotic Evaluation

As mentioned in the previous section, the integral representation for the reflected field, appearing in Eq. (1.2.8), is too complicated to be integrated directly. To effect its evaluation we will expand the reflection coefficient in

$\epsilon_1 = .5$
$\bar{Z}' = .15$

———— CAUSTIC
– – – – LOCUS OF TURNING POINTS
—·—·— CRITICAL RAY
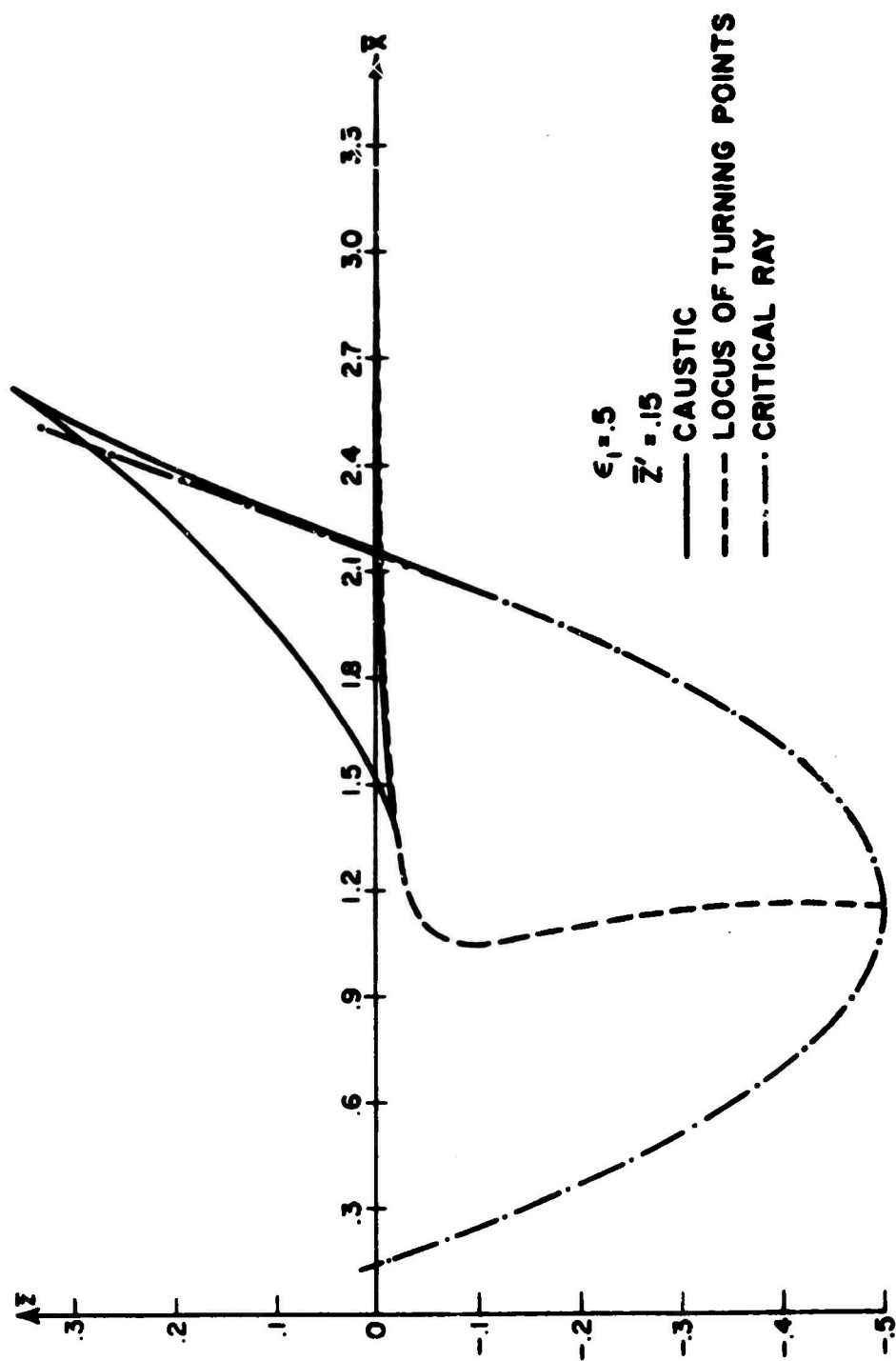
Fig. 1.8

Caustic Formed by a Linear Layer ($\bar{E}' = .15$)
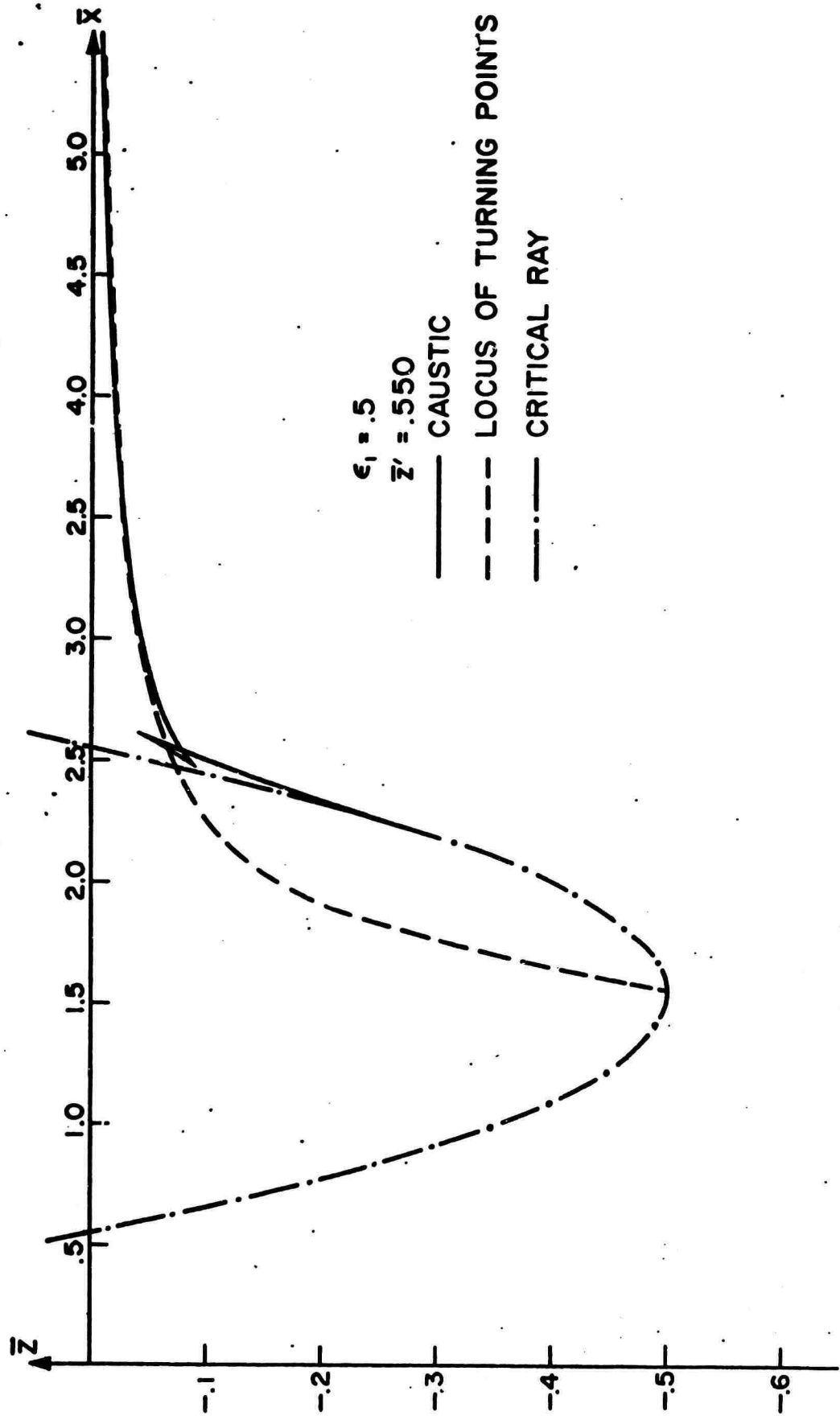
Fig. 1.9

Caustic Formed by a Linear Layer ($\bar{z}' = .55$)
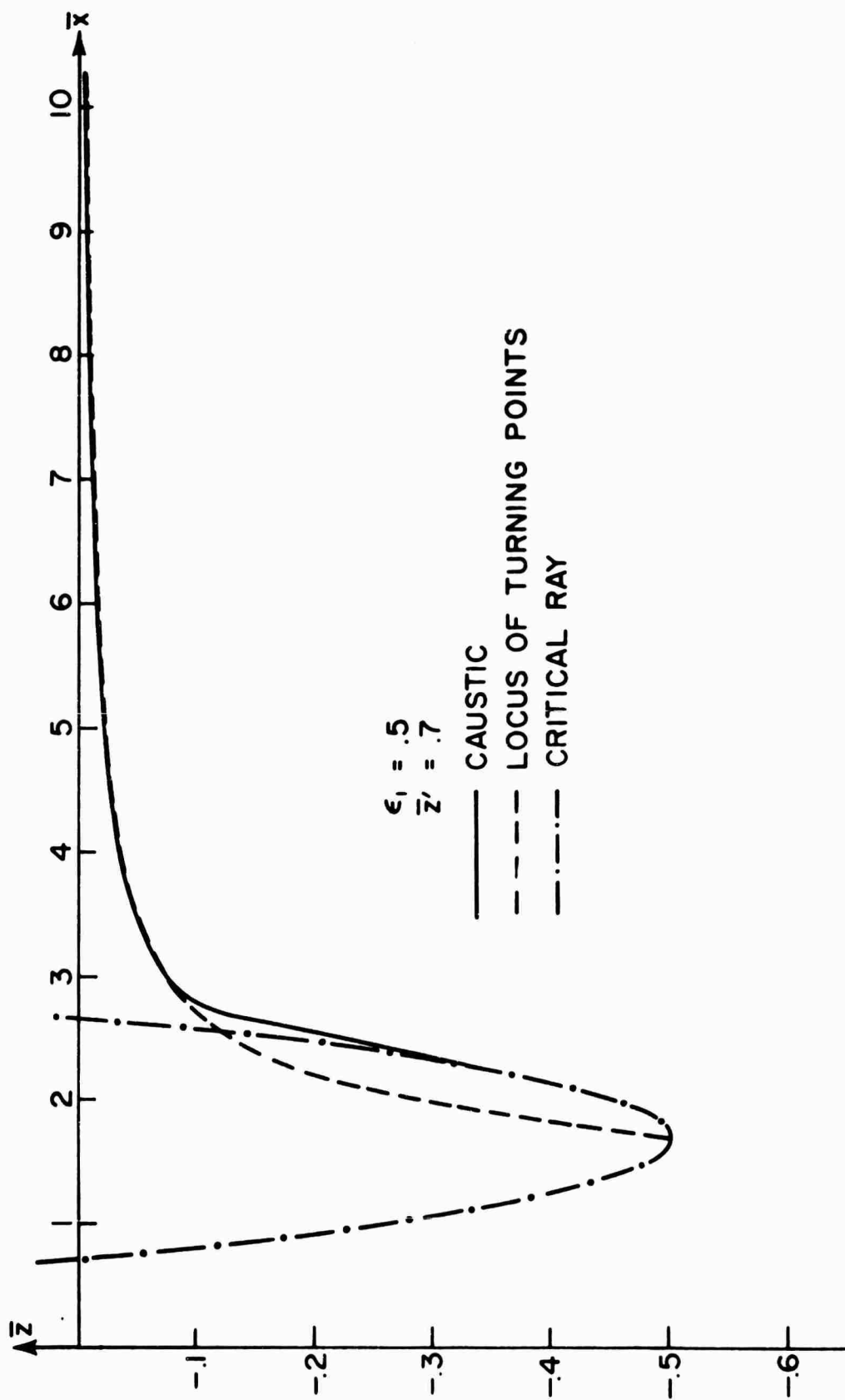
Fig. 1.10

Caustic Formed by a Linear Layer($\bar{z}' = .7$)
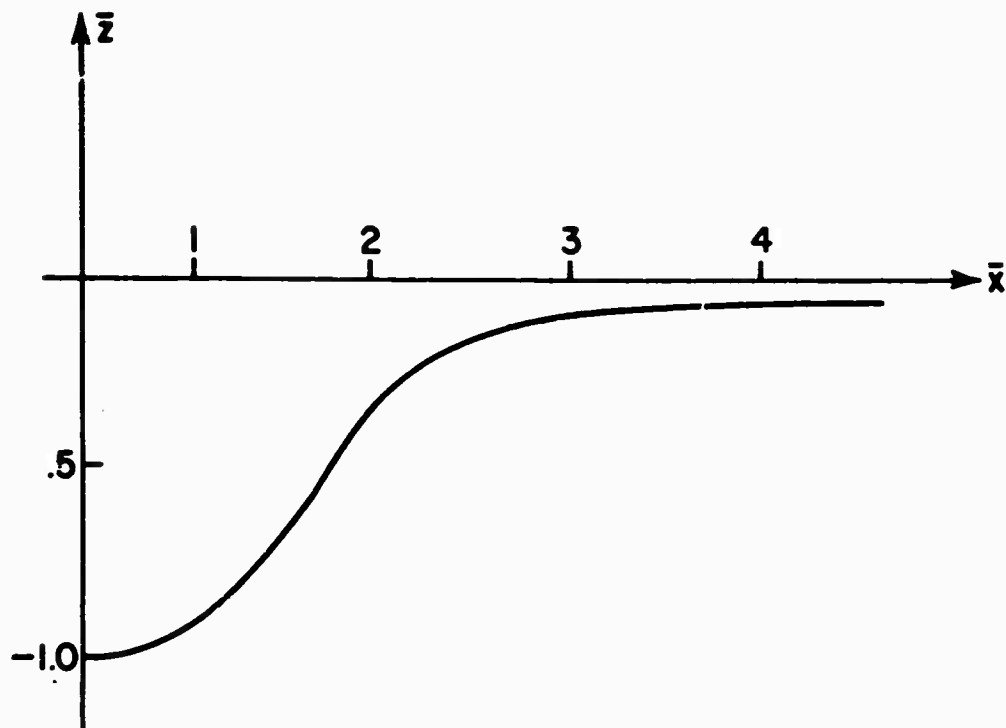
Fig. 1.11

Sketch of Caustic for $\epsilon_1 = 0$ and $\bar{z}' > 2/3$

a geometric series and then make use of asymptotic techniques to integrate each term of the series individually. This will result in a representation for the reflected field, E_{yr}, which can be interpreted in terms of geometrical-optic ray contributions.

The reflection coefficient given by Eq. (1.2.9) can be written as

$$\bar{\Gamma} = \Gamma_{oa} + \frac{\Gamma_{oa} \Gamma_L (\Gamma_{ob} - \Gamma_{oc})}{1 - \Gamma_L \Gamma_{o_b}} \qquad (1.3.8)$$

where

$$\Gamma_{oa} = \frac{A_i'(\varsigma_2^2 e^{i\pi/3}) + \varsigma_2 e^{i\pi/6} A_i(\varsigma_2^2 e^{i\pi/3})}{A_i'(\varsigma_2^2 e^{i\pi/3}) - \varsigma_2 e^{i\pi/6} A_i(\varsigma_2^2 e^{i\pi/6})} \qquad (1.3.9)$$

$$\Gamma_{ob} = -\frac{A_i'(\varsigma_2^2 e^{-i\pi/3}) - \varsigma_2 e^{i5\pi/6} A_i(\varsigma_2^2 e^{-i\pi/3})}{A_i'(\varsigma_2^2 e^{+i\pi/3}) - \varsigma_2 e^{i\pi/6} A_i(\varsigma_2^2 e^{+i\pi/3})} \qquad (1.3.10)$$

$$\Gamma_{oc} = \frac{A_i'(\varsigma_2^2 e^{-i\pi/3}) + \varsigma_2 e^{i5\pi/6} A_i(\varsigma_2^2 e^{-i\pi/3})}{A_i'(\varsigma_2^2 e^{+i\pi/3}) + \varsigma_2 e^{i5\pi/6} A_i(\varsigma_2^2 e^{+i\pi/3})} \qquad (1.3.11)$$

$$\Gamma_L = \frac{A_i'(\varsigma_1^2 e^{i\pi/3}) + \varsigma_1 e^{i\pi/6} A_i(\varsigma_1^2 e^{i\pi/3})}{A_i'(\varsigma_1^2 e^{-i\pi/3}) + \varsigma_1 e^{i5\pi/6} A_i(\varsigma_1^2 e^{-i\pi/3})} \qquad (1.3.12)$$

The denominator of the second term in Eq. (1.3.8) can be expanded in a geometric series if $|\Gamma_L \Gamma_{ob}| < 1$. This condition must be met at all points along the integration path C. An evaluation of $\Gamma_L \Gamma_{ob}$ shows that its magnitude is less than one, except for the portion of the path $\operatorname{Re} p_1 = 0$, $\sqrt{\Delta} < \operatorname{Im} p_1 < \infty$. Along this portion of the path $|\Gamma_L \Gamma_{ob}| = 1$, however, we can show that a slight deformation of the integration path C to the right of the $\operatorname{Im} p_1$ axis in this region makes $|\Gamma_L \Gamma_{ob}| < 1$. The use of this series expansion in the reflection coefficient gives us

$$\bar{\Gamma} = \Gamma_{oa} + \sum_{n=0}^{\infty} \Gamma_n \qquad (1.3.13)$$

where

$$\Gamma_n = \Gamma_{oa} (\Gamma_{oa} - \Gamma_{oc}) \Gamma_{ob}^n \Gamma_L^{n+1} \qquad (1.3.14)$$

We now use the series expansion for $\bar{\Gamma}$ in Eq. (1.2.8) and interchange the intergration and summation signs. We obtain

$$E_{yr} = E_{ro} + \sum_{n=0}^{\infty} E_n \tag{1.3.15}$$

where

$$E_{ro} = -\frac{i}{4\pi} \int_C \frac{P_1 \Gamma_{oa}}{P P_2} e^{i k_o [p_2(z+z') + px]} dp_1 \tag{1.3.16}$$

and

$$E_n = -\frac{i}{4\pi} \int_C \frac{P_1 \Gamma_n}{P P_2} e^{i k_o [p_2(z+z') + px]} dp_1 . \tag{1.3.17}$$

The integrals E_{ro} and E_n will now be evaluated by the method of steepest descents when k_o is large. Before doing this however, we will assume $k_o L \gg 1$ and replace Γ_{oa} and Γ_n by their asymptotic approximations. These approximations are obtained by using the asymptotic expansions for the Airy function and its derivative. The expansion for $A_i(z)$ is given by

$$A_i(z) \sim -\frac{1}{2\sqrt{\pi}} z^{-1/4} e^{-\zeta} \sum_{n=0}^{\infty} (-1)^k C_k \zeta^{-k} , \quad |\arg z| < \pi \tag{1.3.18}$$

where

$$\zeta = 2z^{3/2}/3 , \quad C_o = 1 , C_1 = 5/72$$

while $A_i'(z)$ can be obtained by formally differentiating Eq. (1.3.18). The additional coefficients C_k can be found in Abramawitz[17]. When the $\arg z$ is close to $\pm \pi$ Eq. (1.3.18) is no longer valid and another asymptotic expansion including this sector of $\arg z$ must be used [18]. The expressions for Γ_{oa} and Γ_n contain the Airy functions with four different arguments.

The locus of possible p_1 values, when the argument is constrained to have an angle of $\pm\pi$, have been drawn in Fig. 1.12 for the four 'iry functions. This figure serves to make the region of validity of Eq. (1.3.18) in the p_1 plane clear. The curves shown in Fig. 1.12 are the same on both the top and on the second sheet of the Riemann surface since the Airy functions are even functions of p.

The asymptotic approximations for Γ_{oa} and Γ_n on the integration path between $p_1 = \sqrt{\epsilon_1}$ and $p_1 = i\sqrt{\Delta}$ are

$$\Gamma_{oa} \sim - \frac{A_1}{k_o L p_2^3} e^{-i\pi/3} \tag{1.3.19}$$

and

$$\Gamma_n \sim \frac{A_n \Gamma_L^{n+1}}{(k_o L)^n p_2^{3n}} e^{i 4(n+1)\xi_2^3/3 + in\pi/2} \tag{1.3.20}$$

where $A_n = (-1)^{n+1} (15\Delta C_1/2)^n$. If we restrict p_1 to lie between the origin and $p_1 = i\sqrt{\Delta}$, making sure that p_1 does not come too close to the origin, then Eq. (1.3.20) reduces to

$$\Gamma_n \sim \frac{A_n}{(k_o L) p_2^{3n}} e^{i 4(n+1)\xi_2^3/3 + i(n-2)\pi/6} \tag{1.3.21}$$

while if we restrict p_1 to the real axis $(0 < \text{Re}\, p_1 < \sqrt{\epsilon_1})$ and again keeping p_1 away from the origin, Eq. (1.3.20) reduces to

$$\Gamma_n \sim \frac{A_n}{(k_o L)^{2n+1} p_2^{3n} p_1^{3(n+1)}} e^{i 4(n+1)(\xi_2^3 - \xi_1^3)/3 + i(n-2)\pi/6} \qquad . \tag{1.3.22}$$
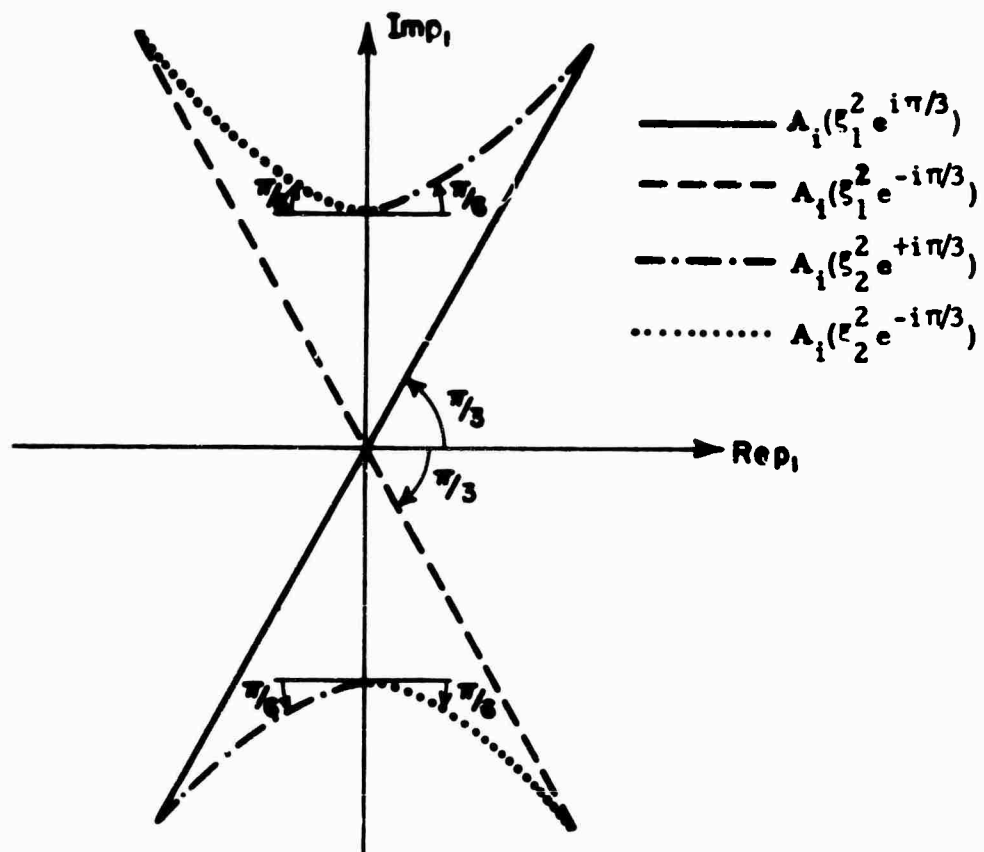
Fig. 1.12

Regions of Validity for Asymptotic Expansions of Airy Functions
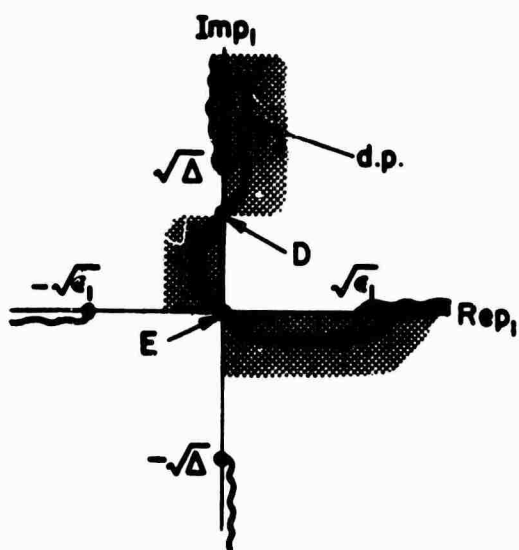
Fig. 1.13

Deformed Path for I_r (Top Sheet)
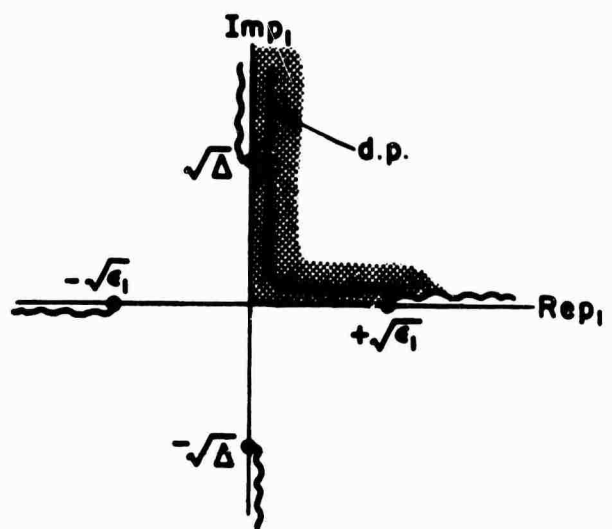
Fig. 1.14

Deformed Path for I_r (Second Sheet)

By using the asymptotic approximation for Γ_{oa} in the integral E_{ro}, the saddle point equation can be determined by taking the derivative with respect to p_1 of the argument of the exponential term in the integrand. The result is

$$p_1 \left(\frac{s+z'}{p_2} \mp \frac{x}{p} \right) = 0 \qquad \begin{cases} - \text{ top sheet} \\ + \text{ second sheet .} \end{cases} \qquad (1.3.23)$$

There are two relevant solutions to this equation on the top sheet which are denoted by D and E in Fig. 1.13; there are no relevant solutions on the second sheet. The saddle point D can occur anywhere on the integration path between $p_1 = \sqrt{\epsilon_1}$ and $p_1 = i\sqrt{\Delta}$ while the saddle point E is always located at $p_1 = 0$. If we restrict the saddle point D to lie on the imaginary axis and deform the integration path C into the decay regions, (Figs. 1.13 and 1.14), the field E_{ro} is asymptotically approximated by the two saddle point contributions D and E. The contribution of E is exponentially small however, since the integrand is an odd function of p_1 integrated over a symmetric interval. The contribution from D can be interpreted as a ray reflected from the $z = 0$ interface as shown in Fig. 1.19. The asymptotic order of contributions of D and E are shown in Table 1.1. If now we restrict the saddle point D to the real axis, the saddle point E is not intercepted when the integration path C is deformed and the total contribution to the integral comes from D. The interpretation of D is as before. We should mention at this point that the assumption has been made that no isolated pole singularities exist between the original and deformed paths which contribute to the asymptotic evaluation of E_{ro}. This same assumption will apply to the other path deformations which shall occur in this chapter.

Type	Asymptotic Order
A_n	$O(k_o^{-(n+1/2)})$
B_n	$O(k_o^{-(2n+3/2)})$
C_n	$O(k_o^{-(n-7/6)})$
D	$O(k_o^{-3/2})$
E	$O(e^{-\alpha k_o}), \alpha > 0$

Table 1.1

Asymptotic Order of Geometrical

Optic Contributions

The asymptotic evaluation of the integral E_n can be treated in a similar way to E_{ro}. The asymptotic approximations for Γ_n given in Eqs. (1.3.20), (1.3.21) and (1.3.22) are substituted in the integrand of E_n and the saddle point equations are then obtained. They are:

$$P_1\left(\frac{z+z'}{P_2} \mp \frac{x}{p} + \frac{4(n+1)P_2 L}{\Delta}\right) = 0, \quad \text{Re}\, p_1 = 0, \quad 0 < \text{Im}\, p_1 < \sqrt{\Delta} \qquad (1.3.24)$$

$$P_1\left(\frac{z+z'}{P_2} \mp \frac{x}{p} + \frac{4(n+1)(P_2-P_1) L}{\Delta}\right) = 0, \quad 0 < \text{Re}\, p_1 < \sqrt{\epsilon_1}, \quad \text{Im}\, p_1 = 0 \qquad (1.3.25)$$

and

$$P_1 = C, \quad k_o L |p_1|^3 < 1 \qquad (1.3.26)$$

where the upper sign in Eqs. (1.3.24) and (1.3.25) refers to the top
sheet and the lower sign to the bottom. Equation (1.3.26) is valid on
both sheets.

Upon obtaining the saddle point locations from the above equations,
we deform the contour C through these saddle points and into the decay
regions. Since the contribution due to the portion of the integral lying in
the decay region is exponentially small, the integral E_n will be asymptotic-
ally equal to the sum of the saddle point contributions. The contributions
arising from saddle points obeying Eq. (1.3.24), (1.3.25) and (1.3.26) will
be known as type A_n, B_n and C_n contributions respectively. The subscript
n indicates the integral in which the saddle points occur. It can be shown
that no relevant saddle points occur on the second sheet for any n and there-
fore the deformed path will be the same as that shown in Fig. 1.14 .

At this point we shall focus our attention on the relevant saddle points
on the top sheet, their contributions to the reflected field and the geometrical
interpretation of these contributions. We shall first consider the integral
E_o since E_o contributes the dominant terms to the reflected field for $k_o L$
large and then, at a later time, we shall consider the integrals E_n, n = 1, 2, 3, ..

Saddle point contributions of type A_o will be considered first. A
comparison of Eq. (1.3.24) with the ray equation for returning rays (z ≥ 0) ,
Eq. (1.3.2) , shows that the two are identical. This means that saddle
point contributions in the interval $\operatorname{Re} p_1 = 0$, $0 < \operatorname{Im} p_1 < \sqrt{\Delta}$ correspond to
returning ray contributions. At this point we can use our knowledge of the
returning ray trajectories to find the location and number of saddle points
in the interval $\operatorname{Re} p_1 = 0$, $0 < \operatorname{Im} p_1 < \sqrt{\Delta}$. Before proceeding however, we
shall divide the portion of the x-z plane with z ≥ 0 in two parts separated by
the critical ray as shown in Fig. 1.19. To the right of the critical ray
(region 2) there is either one or there are three returning rays passing

through an observation point. If the observation point is located inside
the cusp region there are three rays while outside, there is only one.
To the left of the critical ray (region 1) there are either two saddle points
in the interval $\operatorname{Re} p_1 = 0$, $0 < \operatorname{Im} p_1 < \sqrt{\Delta}$ or there are none. The two saddle
points occur when the cusp region lies to the left of the critical ray, and the
observation point is located inside the cusp region. The saddle points are
shown for the four cases, considered above in Figs. 1.15 - 1.18, where
they are denoted by $A_n (n=0)$. The contributions to the reflected field at
these saddle points are of $O(k_o^{-1/2})$ as would be expected since they repre-
sent returning ray contributions.

Saddle point contributions of type B_o will be considered next. An
examination of Eq. (1.3.25) shows that one saddle point exists in the interval
$0 < \operatorname{Re} p_1 < \sqrt{\epsilon_1}$, $\operatorname{Im} p_1 = 0$ when the observation point is in region 1 while no
saddle points exist in the interval when the observation point is in region 2.
The saddle point contributing to region 1 can be interpreted as a ray reflected
from the interface at $z = -L$. A ray of this type is shown in Fig. 1.19. Its
asymptotic contribution to the reflected field is of $O(k_o^{-3/2})$ which is $1/k_o$
lower than the returning ray contribution. This is expected, however since
the ray under consideration is reflected at an interface when the dielectric
profile has a discontinuous first derivative.

Finally, the saddle point contribution of type C_o will be considered.
An examination of Eq. (1.3.26) shows that only one saddle point exists and
its location ($p_1 = 0$) is independent of the location of the observation point.
An analysis of the decay regions, the results of which are presented in
Fig. 1.15 - 1.18, has shown that the saddle point is only intercepted when
the observation point is located in region 2.

We will now attempt to asymptotically evaluate E_o. The integral E_o
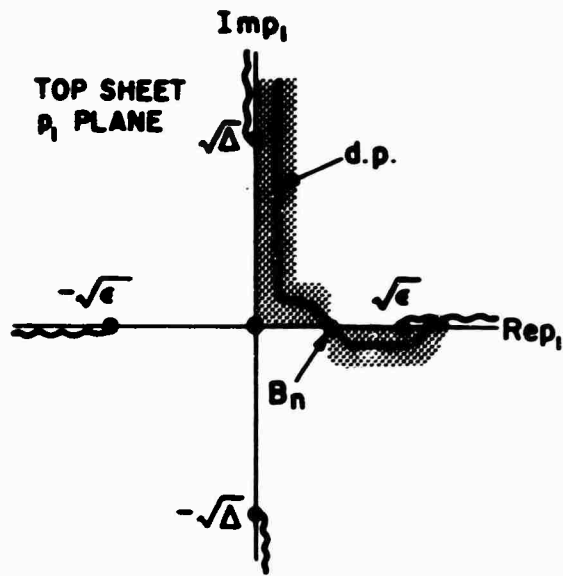
Fig. 1.15

Deformed Path for I_n (Region 1)
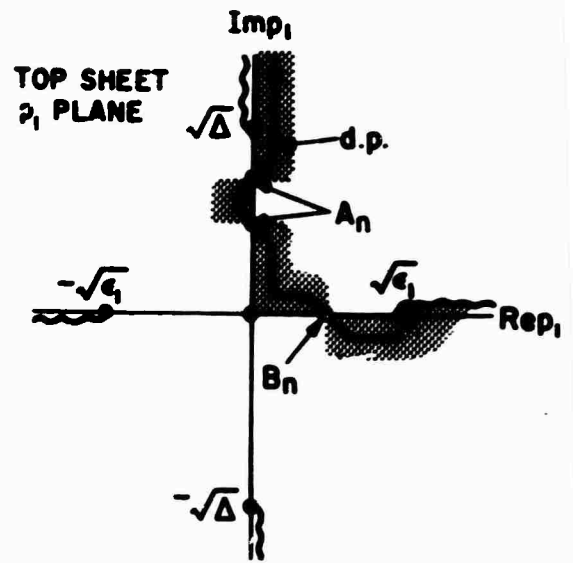
Fig. 1.16

Deformed Path for I_n (Region 1)
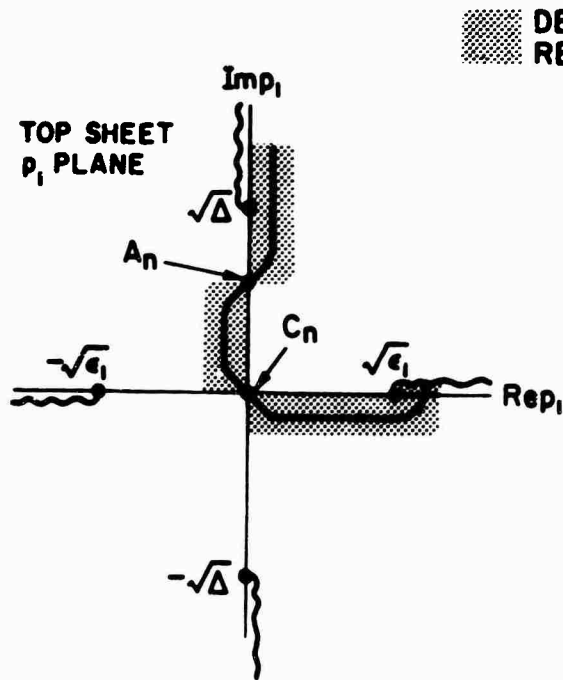
Fig. 1.17

Deformed Path for I_n (Region 2)
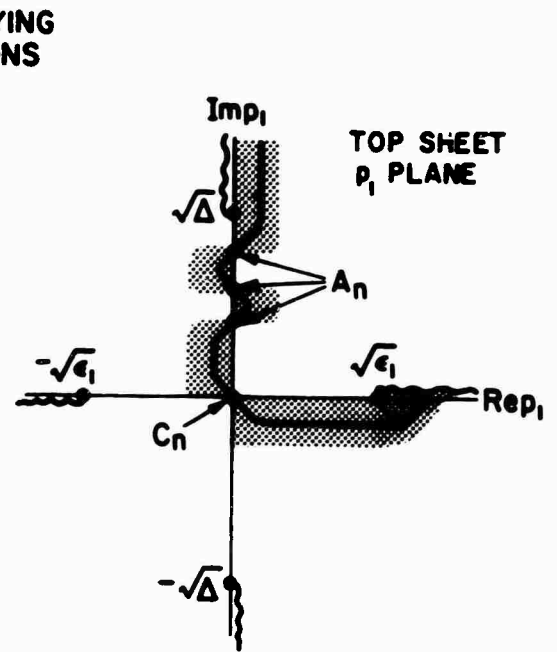
Fig. 1.18

Deformed Path for I_n (Region 2)
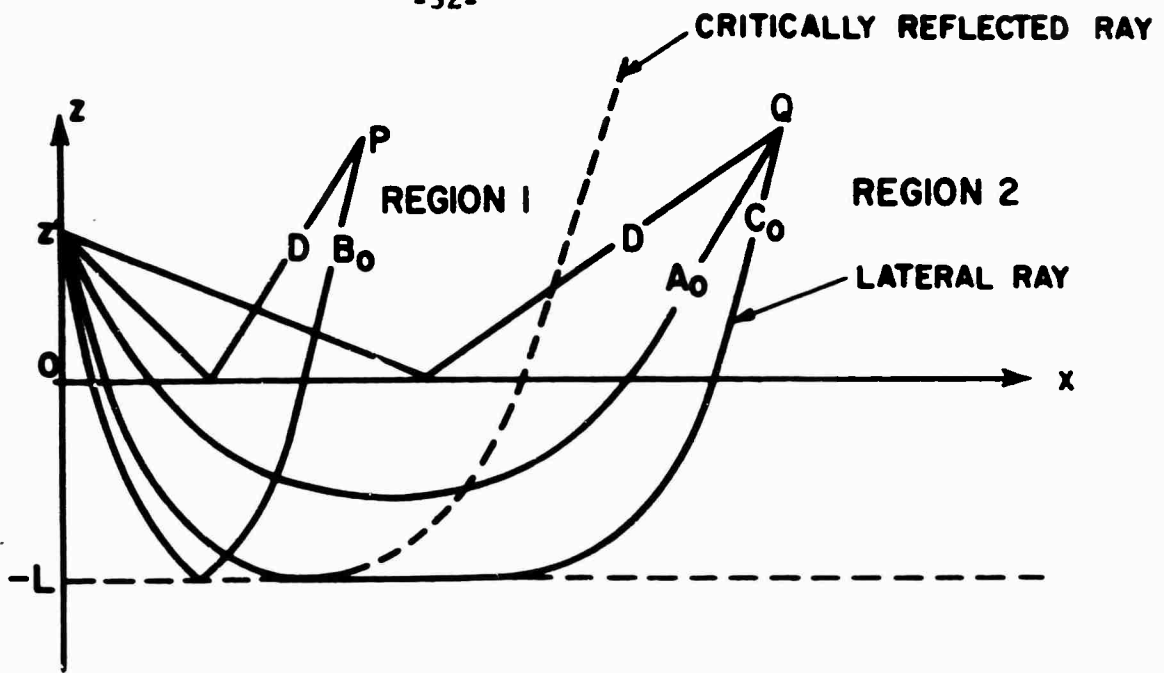
Fig. 1.19

Ray Contributions from I_r and I_o
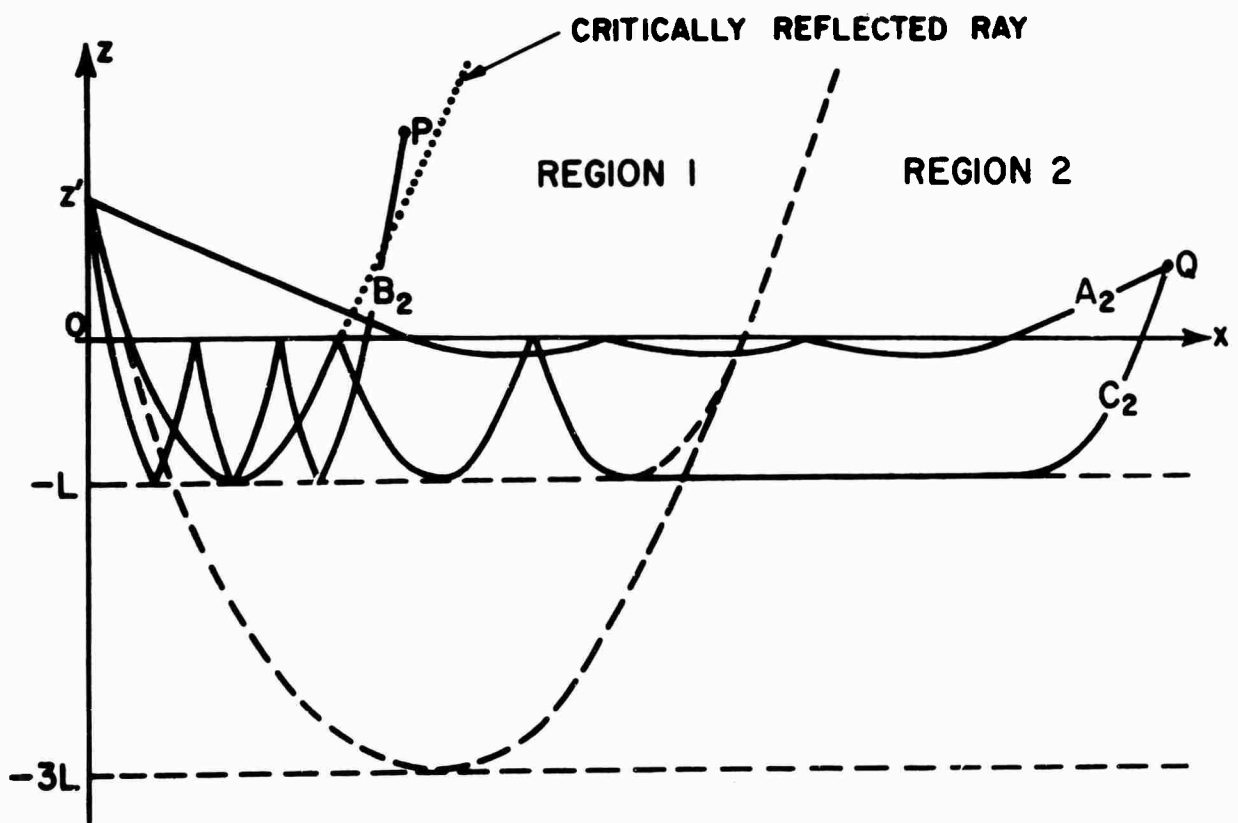
Fig. 1.20

Ray Contributions from I_2

in the vicinity of the origin does not appear to be a simple steepest descent integral since Γ_L is a complicated function of k_o . The situation can be clarified by making the change of variables $\xi_1 = (\tau/\Delta)^{1/3} p_1$ in the integral. The portion of the integral in the vicinity of the origin, E_L , becomes

$$E_L = - \frac{i\Delta^{2/3}}{4\pi \tau^{2/3}} \int_{C'} \frac{\xi_1 \Gamma_L}{p p_2} e^{ik_o [p_2(z+z') + px + \frac{4L}{3\Delta} p_2^2]} d\xi_1 \qquad (1.3.27)$$

where

$$p_2 = \sqrt{\Delta + (\Delta/\tau)^{2/3} \xi_1^2} \quad , \qquad p = \sqrt{\epsilon_1 - (\Delta/\tau)^{2/3} \xi_1^2}$$

and C' is the transformed path C in the vicinity of the origin. Now Γ_L is no longer a function of k_o but p and p_2 are. Because of the simpler dependence of p and p_2 upon k_o , it becomes possible to show that the standard steepest descent techniques [19] can be applied to Eq. (1.3.27) . Upon the application of these techniques we find

$$E_L \sim \frac{A_L e^{ik_o [\sqrt{\Delta}(z+z') + \sqrt{\epsilon_1}x + 4\sqrt{\Delta}L/3] + i7\pi/12}}{(L_p + 4\sqrt{\epsilon_1}L/\sqrt{\Delta})^{3/2}} \qquad (1.3.28)$$

where

$$A_L = \frac{3^{2/3} \Gamma^2(1/3) \epsilon_1^{1/4} L^{1/3}}{2(2\pi)^{3/2} \Delta^{5/6} k_o^{7/6}} \quad , \qquad L_p = x - \sqrt{\epsilon_1/\Delta} (z+z') \qquad (1.3.29)$$

and $\Gamma(z)$ is the gamma function of argument z . This result can be interpreted as the contribution from a ray which is excited by the critical ray at the $z = -L$ interface. This newly formed ray travels along the lower interface for a distance $L_p + 4\sqrt{\epsilon_1} L/\sqrt{\Delta}$ and sheds energy into the upper region.

A typical ray trajectory is shown in Fig. 1.19. The lateral wave exicted on an abrupt transition has a similar ray interpretation and amplitude dependence with distance along the interface. The two lateral waves, however, have different excitation coefficients. The excitation coefficient, A_L, for a lateral wave on a thick linear transition, depends on $k_o^{-7/6}$ while the excitation coefficient for a lateral wave on an abrupt transition has a dependence of $k_o^{-3/2}$.

Now we will not require n to be zero and we will investigate the asymptotic contributions to the integral E_n. To do this we must locate the relevant saddle points and then find their contributions to the reflected field. As mentioned earlier, the general saddle point equations are given by Eqs. (1.3.24), (1.3.25) and (1.3.26). By replacing (n+1) L by $\overline{L}$ in the first two of these saddle point equations we see that the equations are the same as the n = 0 case with L replaced by $\overline{L}$. Since the n = 0 case was done for arbitrary L, the location of saddle points of type A_n and B_n has already been investigated. However, there is one basic change. The demarcation between region # 1 and region # 2 is no longer the critical ray reflected from a layer of thickness L but is rather the critical ray reflected from a layer of thickness of $\overline{L}$. This cirtical ray is shown for n = 2 in Fig. 1.20. The third saddle point equation given in Eq. (1.3.26) has one saddle point at $p_1 = 0$ for any n. From the above argument we conclude that the basic structure of the deformed paths are again given by Figs. 1.15 - 1.18.

The method of steepest descents can then be used to evaluate the asymptotic contributions at each saddle point. Those contributions of type A_n correspond to returning rays reflected n times from the z = 0 interface while those of type B_n correspond to rays reflected n + 1 times from the interface at z = - L. The C_n are lateral wave contributions. These are excited by the critical ray which is reflected n times from the z = 0 interface.

The ray trajectories for these contributions are shown in Fig. 1.20 for $n = 2$. The order of each type of contribution is given in Table 1. We see from this table that as n increases, the order of the asymptotic contribution decreases. This results from the fact that the order of a ray contribution is reduced by $O(1/k_0)$ each time the ray is reflected from the $z = 0$ or $z = - L$ interface.

To summarize briefly we have found that the reflected field from a gradual linear layer ($k_0 L \gg 1$) can be decomposed into a geometric - optic series. The dominant terms of this series in region #2 are the returning rays which are of $O(k_0^{-1/2})$, and a lateral wave contribution which is of $O(k_0^{-7/6})$. This lateral wave has a great similarity to the lateral wave occurring on an abrupt transition except for a difference in its excitation coefficient.

1.4 Evaluation of Reflected Field for Large $k_0 L_p$

In this section we shall explore the connection between the lateral wave contribution observed on a thick linear transition (section 1.3) and the lateral wave excited on an abrupt interface. The linear layer provides an excellent opportunity to do this, since for small $k_0 L$, the layer appears to be an abrupt transition, while for large $k_0 L$ the layer thickness is large compared with wavelength. It can be shown, in fact, that the reflected coefficient, Eq. (1.2.9), reduces to the reflection coefficient for an abrupt transition as $k_0 L \rightarrow 0$.

Our investigation of the lateral wave's character shall be carried out by performing an asymptotic evaluation of the reflected field for observation points which are far from the source compared with layer thickness. To be more specific we shall assume that $k_0 L_p \gg 1$ and $L_p \gg L$. This says that we

shall consider those observation points which are a large number of wavelengths and a large number of layer thicknesses to the right of the reflected ray, $x = \sqrt{\epsilon_1/\Delta}\,(z + z')$.

The integral representation for the reflected field is given by

$$E_{yr} = -\frac{i}{4\pi} \int_C \frac{p_1 \overline{\Gamma}}{pp_2}\, e^{ik_o[p_2(z+z')+px]}\, dp_1 \qquad (1.4.1)$$

where

$$\overline{\Gamma} = -\frac{\Delta_{tn}}{\Delta_{tb}} \qquad (1.4.2)$$

with

$$\Delta_{tn}_{tb} = \begin{vmatrix} \left\{ A_i'(-\xi_1^2) - i\xi_1 A_i(-\xi_1^2) \right\} & \left\{ B_i'(-\xi_1^2) - i\xi_1 B_i(-\xi_1^2) \right\} \\[2mm] \left\{ A_i'(-\xi_2^2) \mp i\xi_2 A_i(-\xi_2^2) \right\} & \left\{ B_i'(-\xi_2^2) \mp i\xi_2 B_i(-\xi_2^2) \right\} \end{vmatrix} .$$

The representation given in Eq. (1.4.1) is the same as that presented in Eq. (1.2.12) except that a different form of the reflection coefficient has been used. The alternate form of this reflection coefficient was obtained by choosing $\phi_1(z)$ and $\phi_2(z)$ in Appendix A as $B_i(-\xi^2)$ and $A_i(-\xi^2)$ respectively. These two functions are independent of one another and thus satisfy the requirement for choosing $\phi_1(z)$ and $\phi_2(z)$. The $B_i(-\xi^2)$ not encountered previously, is the Airy function of the second kind. The reason for using an alternative form of reflection coefficient is that it will allow us to put our results in a form which is more suitable for computation.[*]

---

[*] The advantage of the original form of the reflection coefficient was that it contained Airy functions whose asymptotic expansions were of a simpler form in the vicinity of the integration path .

If we now use the assumption that $k_o L \ll k_o L_p$ then the reflection coefficient in Eq. (1.4.1) is slowly varying compared to the exponential in the integrand, and the standard steepest descent techniques can be used to asymptotically evaluate the integral representation. The saddle points are found by taking the derivative with respect to p_1 of the argument of the integrand's exponential and setting it equal to zero. The result is

$$p_1 \left(\frac{z+z'}{p_2} \mp \frac{x}{p} \right) = 0 \qquad \begin{cases} - \text{ top sheet} \\ + \text{ second sheet} \end{cases} \qquad (1.4.3)$$

This is the same saddle point equation encountered in the asymptotic evaluation of E_{ro} . The relevant saddle points which occur on the top sheet of the Riemann surface are located at

$$p_1 = 0 \quad , \quad p_1 = i \sqrt{x^2 \Delta - (z+z')^2 \epsilon_1} \qquad (1.4.4)$$

where we have assumed that $x > \sqrt{\epsilon_1 / \Delta} \, (z+z')$ or $L_p > 0$. The original integration path is deformed through the two saddle points given above and into the decay regions. We will assume that there are no singularities of importance lying between the two paths. The decay regions and the deformed path are shown in Figs. 1.13 and 1.14 .

We see now that when $k_o L_p$ is large, the reflected field is composed of two contributions. The first of these occurring at $p_1 = i \sqrt{x^2 \Delta - (z+z')^2 \epsilon_1}$ is a reflected ray from the interface at $z = 0$. When $1 \ll k_o L \ll k_o L_p$ this reflected ray corresponds to a returning ray that has its turning point close to the $z = 0$ interface. When $k_o L$ is small the contribution is the same as a reflected ray from an abrupt interface. The contribution from the saddle point is of $O(k_o^{-1/2})$ as would be expected.

The second contribution to the reflected field comes from the saddle point at $p_1 = 0$ and is the lateral wave contribution. This contribution was

obtained by the application of steepest descent methods and is given by

$$E_L \sim \frac{\epsilon_1^{1/4} A(\sigma) e^{ik_o[\sqrt{\Delta}(z+z')+\sqrt{\epsilon_1}x]+i\psi(\sigma)+i3\pi/4}}{\sqrt{2\pi}\,\Delta\,(k_o L_p)^{3/2}}, \quad \sigma = (\sqrt{\Delta}\,\tau)^{1/3}$$

(1.4.5)

where

$$A(\sigma) = -\left.\frac{\sqrt{\Delta}}{2}\left|\frac{d\Gamma}{dp_1}\right|\right|_{p_1=0} = \frac{\sigma^2}{\pi^2(D_1^2+D_2^2)}$$

(1.4.6)

and

$$\psi(\sigma) = 2\tan^{-1}\frac{D_1}{D_2}$$

(1.4.7)

with

$$D_1 = B_i'(0)A_i'(-\sigma^2) - A_i'(0)B_i'(-\sigma^2)$$

(1.4.8)

and

$$D_2 = \sigma\left[B_i'(0)A_i(-\sigma^2) - A_i'(0)B_i(-\sigma^2)\right].$$

(1.4.9)

In the above we have denoted the lateral wave contriubtion by E_L as was done in the previous section, Eq. (1.3.27) . The amplitude, $A(\sigma)$ and phase $\psi(\sigma)$ functions have been plotted by computer and are shown in Figs. 1.21 and 1.22 . Those figures also show the approximate lateral wave amplitude and phase when the layer is thick compared with wavelength.

The physical interpretation of the lateral wave contribution can best be gotten from examination of small and large limits. When τ is small or when the layer appears to be abrupt, we find $A(\sigma) \to 1$ and $\psi(\sigma) \to 0$. By using these limits in Eq. (1.4.5), we find that E_L reduces to the lateral wave contribution on an abrupt interface. On the other hand, when $1 << k_o L << k_o L_p$ then E_L reduces to
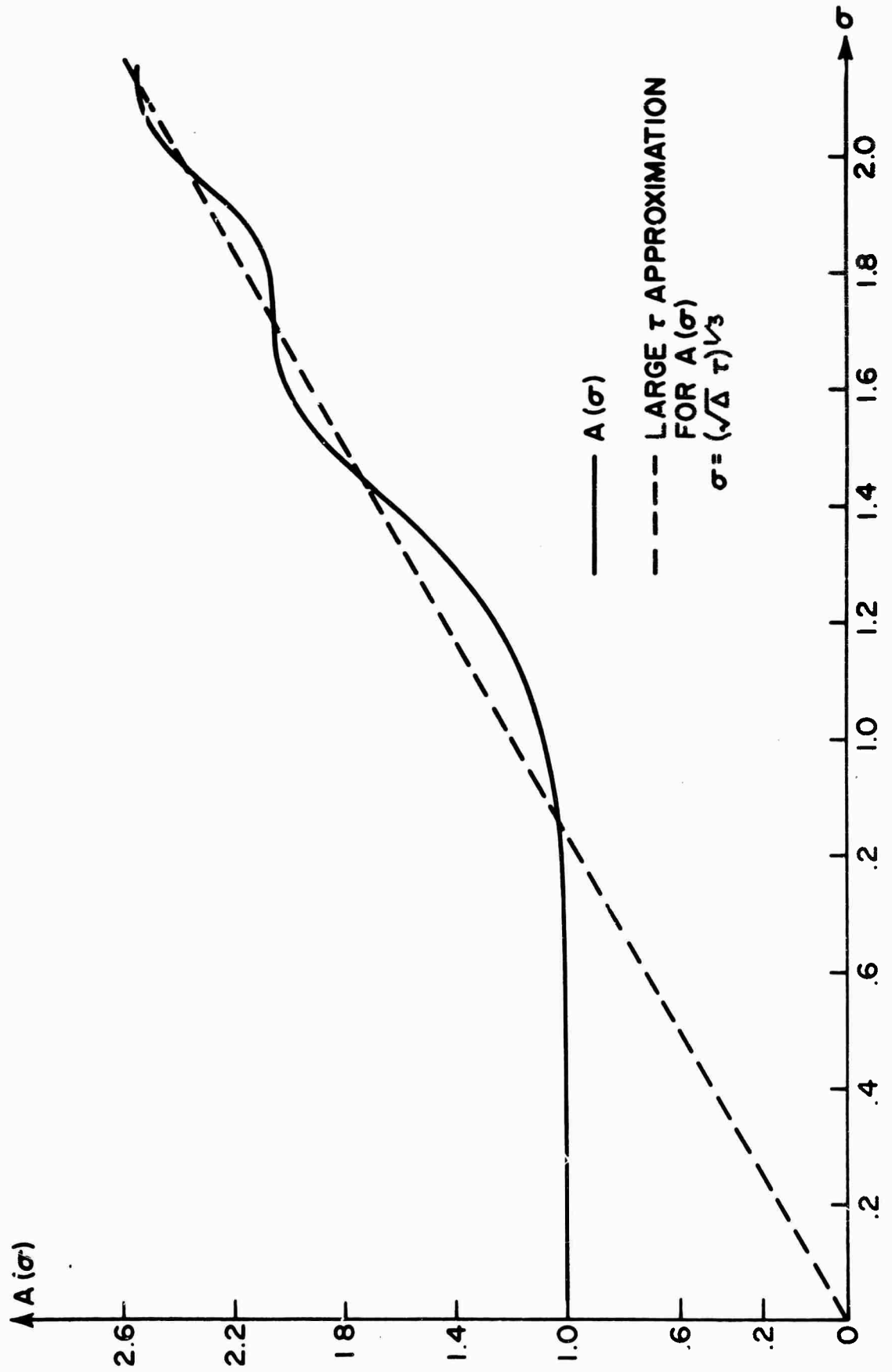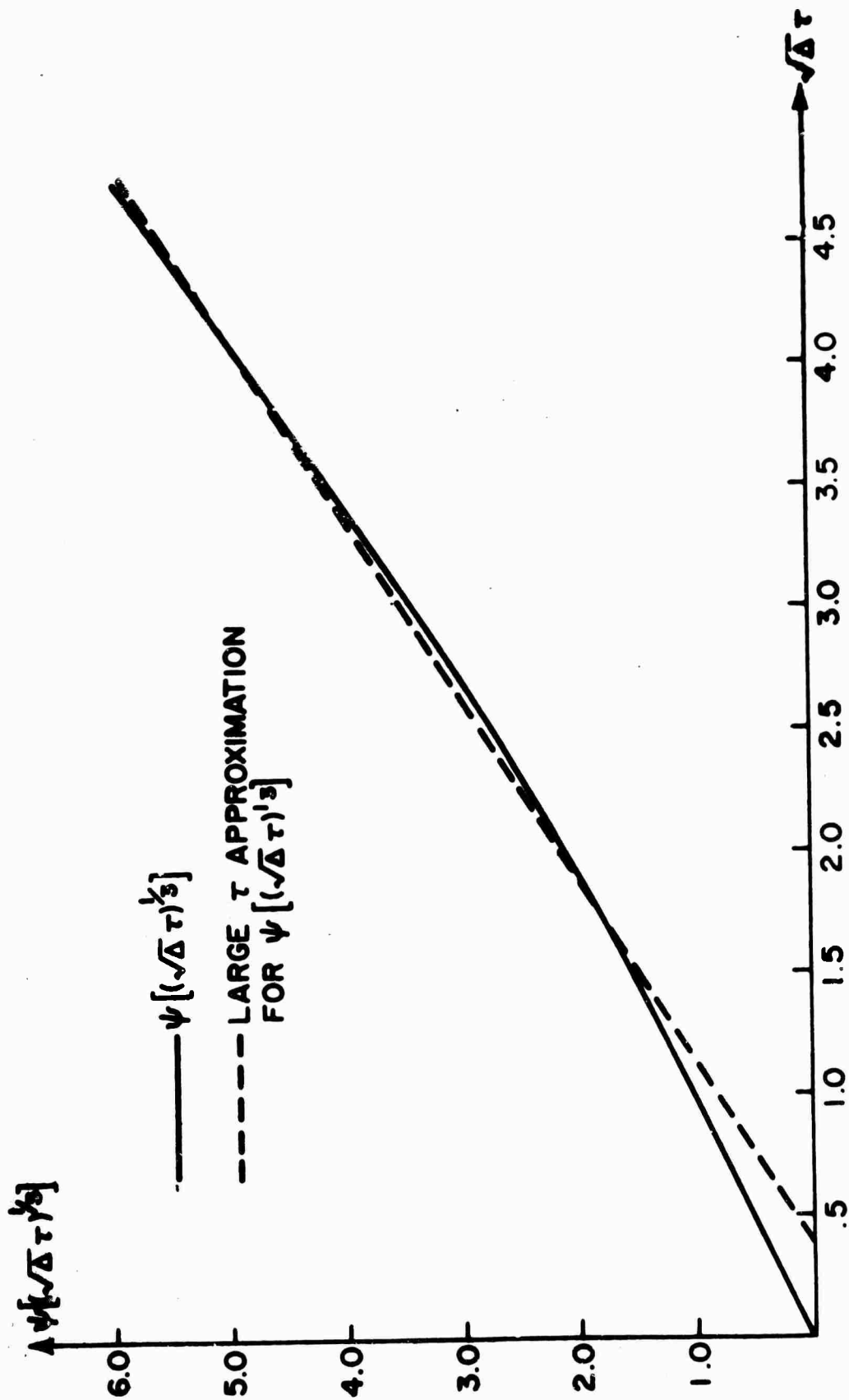
Fig. 1.22 Lateral Wave Phase vs. Normalized Transition Thickness

$$E_L \sim \frac{A_L \, e^{i k_o \left[\sqrt{\Delta}(z+z') + \sqrt{\epsilon_1} \, x + 4\sqrt{\Delta} \, L/3 \right] + i \, 7\pi/12}}{L_p^{3/2}} \tag{1.4.10}$$

where A_L is given by Eq. (1.3.29). When this result is compared with Eq. (1.3.28) and use is made of the fact that $k_o L \ll k_o L_p$, we find that the two expressions are identical.

As was stated in the introduction, Nakamura has obtained a uniform expression for the lateral wave excited on an inverse square dielectric profile which is valid under the same conditions assumed in this section. A comparison between our result, Eq. (1.4.5), and Nakamura's shows that a lateral wave is excited for all layer thicknesses in both cases and both have amplitude dependences of $L_p^{-3/2}$. However, the excitation coefficient as a function of layer thickness appears to depend on the detailed behavior of the wave functions in each particular medium, and nothing in general can be said. When the layer thickness becomes large compared with wavelength, the excitation coefficient simplifies and both results have a wavenumber dependence which is $O(k_o^{-7/6})$.

CHAPTER 2.

THE PARABOLIC TRANSITION LAYER

2.1   Introduction

In Chapter 1 a detailed study of the reflected field from a linear transition layer was made. There, it was found that a lateral wave was excited on the layer for all layer thicknesses. In this chapter, we will continue our study of lateral waves by considering the reflected field from a parabolic transition. Other parameters influencing the reflected field, such as source location and orientation, will remain the same as in Chapter 1. The dielectric profile to be considered is given by

$$\epsilon(z) = \begin{cases} 1 & z > 0 \\ \Delta (z+L)^2/L^2 + \epsilon_1 & -L \leq z \leq 0 \quad , \quad \Delta = 1 - \epsilon_1 \\ \epsilon_1 & z < -L \end{cases} \qquad (2.1.1)$$

and is shown in Fig. 2.1 . The basic similarities between the parabolic and linear transitions are their thickness L , height Δ and finite slope at $z = 0$. Their fundamental difference, on the other hand, is the slope of the profiles at $z = -L$. The linear layer's slope at that point is finite while the parabolic profile has zero slope there.

Our investigation of the parabolic transition has been motivated by the behavior of the critical ray trajectory when the layer is thick compared to wavelength. This critical ray, unlike the critical ray in a linear transition, never becomes tangent to the lower interface but only approaches it asymptotically as $x \to \infty$. In the previous chapter the lateral wave contribution has been interpreted as a wave excited at the point that the critical ray becomes tangent to the lower interface. If this supposition is true for the parabolic transition, no lateral wave will be excited when the parabolic transition thickness is large compared to wavelength. In an attempt to clarify the above
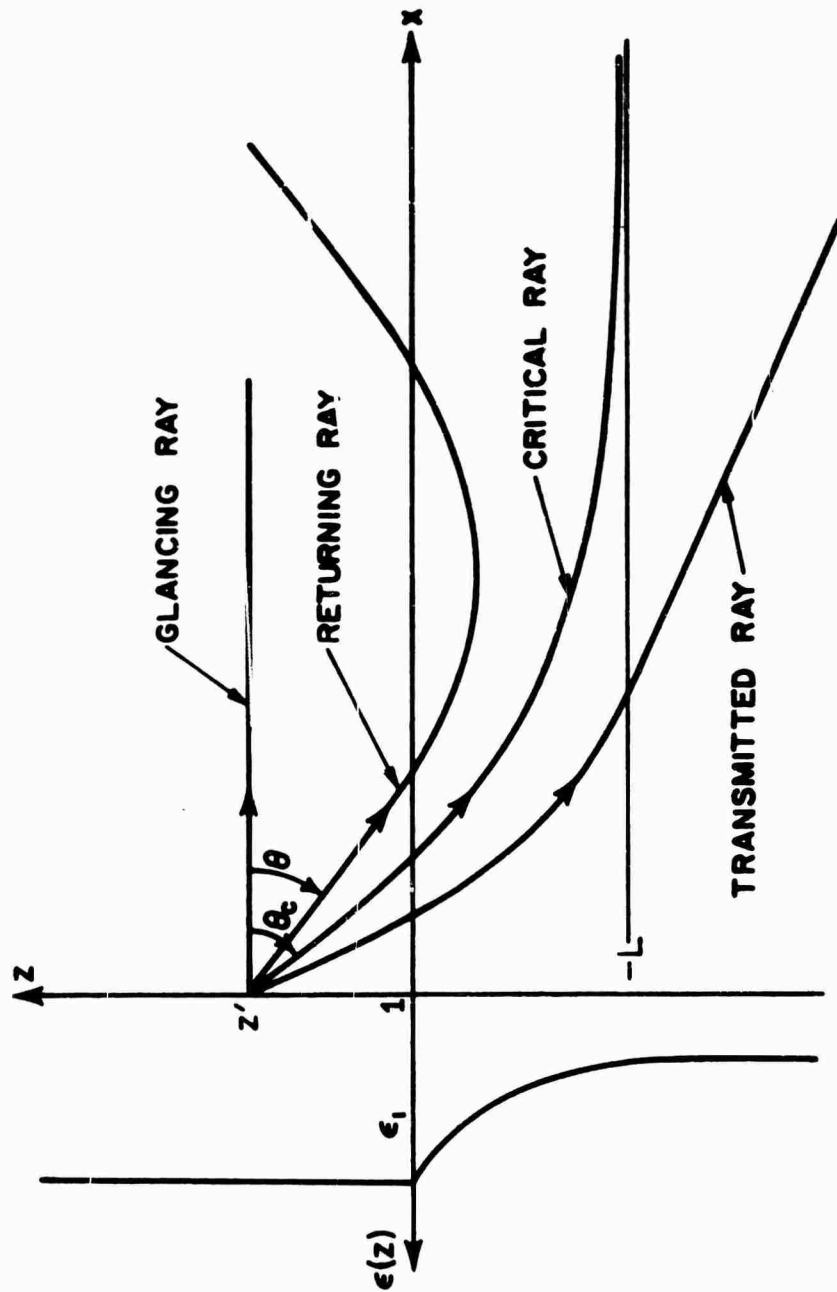
Fig. 2.1

Parabolic Dielectric Profile and Typical Ray Types

question we shall asymptotically approximate the formal solution first for large $k_o L$ and then for large $k_o L_p$ with $L_p \gg L$. Here L_p is the same as that defined in Chapter 1. When $k_o L \gg 1$ or the layer thickness is large compared to wavelength, a knowledge of reflected ray trajectories will be necessary to carry out an asymptotic evaluation of the integral representation. These ray trajectories have been considered in some detail by Orlov[20] for $z > 0$; his results will be used in the text.

2.2. Formal Solution

The integral representation for the field, due to a line source located above a parabolic transition, is obtained in an analogous way to the integral representation found in Chapter 1. The only component of the electric field which is excited is E_y which obeys the inhomogeneous wave equation

$$[\nabla^2 + k_o^2 \epsilon(z)] \, E_y = - i \omega \mu_o \, J \, \delta(x) \, \delta(z - z')$$
(2.2.1)

where $\epsilon(z)$ is given by Eq. (2.1.1).

The application of Fourier integral techniques to the above equation reduces it to a one-dimensional Green's function problem. The formal solution to this Green's problem has been presented in Appendix A in terms of two independent solutions to the wave equation in the layer region. For the parabolic transition which is being considered in this chapter, two independent solutions to the wave equation in the layer region are $E(-a_1^2, \xi)$ and its conjugate, $E^*(-a_1^2, \xi)$. These two functions which are defined by Abramowitz[21] have an order $-a_1^2$ and an argument ξ given by

$$a_1 = (\tau/2\sqrt{\Delta})^{\frac{1}{2}} \, p_1 \quad , \quad \xi = [2 k_o \sqrt{\Delta}/L]^{\frac{1}{2}} (z+L) \quad , \quad \tau = k_o L$$
(2.2.2)

In the above p_1 is related to the Fourier transform variable p as it was in Chapter 1, i.e., $p_1 = (\epsilon_1 - p^2)^{\frac{1}{2}}$. By using these independent solutions in Eq. (A-13) and in Eq. (A-7) we can obtain an explicit expression for the one-dimensional Green's function and, from this, an integral representation for the field. The representation for E_y is given by

$$E_y = E_{yf} + E_{yr} \tag{2.2.3}$$

where E_{yf} is given in Eq. (1.2.7) and represents the direct field from the source in the region $z \geq 0$. The second term in Eq. (2.2.3), E_{yr}, is given by

$$E_{yr} = \frac{i}{4\pi} \int_{-\infty}^{+\infty} \frac{\overline{\Gamma}}{p_2} e^{i k_o [p_2(z + z') + \rho x]} dp \tag{2.2.4}$$

where

$$\overline{\Gamma} = - \Delta_t / \Delta_b \tag{2.2.5}$$

with

$$\Delta_t \atop b = \begin{vmatrix} \left\{ E'(-a_1^2, 0) + i a_1 E(-a_1^2, 0) \right\} & \left\{ E^{*'}(-a_1^2, 0) + i a_1 E^*(-a_1^2, 0) \right\} \\ \left\{ E'(-a_1^2, c) \pm i a_2 E(-a_1^2, c) \right\} & \left\{ E^{*'}(-a_1^2, c) \pm i a_2 E^*(-a_1^2, c) \right\} \end{vmatrix}$$

$$a_2 = (\tau/2\sqrt{\Delta})^{\frac{1}{2}} p_2 \ , \quad p_2 = (1-p^2)^{\frac{1}{2}} \ , \quad c = (2\tau\sqrt{\Delta})^{\frac{1}{2}} \ . \tag{2.2.6}$$

In the above expressions for $\Delta_t \atop b$ the symbol $E'(-a_1^2, \xi) = dE(-a_1^2, \xi)/d\xi$. The square roots P_1 are defined as in Chapter 1 by Fig. 1.4. The integral for the reflected field, Eq. (2.2.4) is transformed to the p_1 plane. The result is given in Eq. (1.2.12) where the integration path C and the square roots are defined as in Chapter 1, Fig. 1.5 and 1.6.

2.3 Evaluation of Reflected Field for Large Layer Thichness ($k_o L \gg 1$

2.3.1 Geometrical-Optics

Before performing the asymptotic evaluation of the reflected field for $k_o L \gg 1$ we shall make use of the method of geometrical-optics to predict the ray contributions to the reflected field. Then, in the next section, we shall asymptotically evaluate the integral representation for the reflected field and compare the two results. In this way we will see the limitation on the theory of geometrical-optics when applied to a parabolic layer.

The rays emitted from the source can be divided into three types: direct, transmitted and returning. They are defined in the same manner as in Chapter 1. There the reflected and transmitted ray types have been separated by a critical ray. This is also the case here, however the critical ray has a different behavior as is shown in Fig. 2.1.

The trajectory for this ray is obtained by integrating the ray equation

$$x = \int_{z'}^{z} \frac{p \, d\tau}{\sqrt{\epsilon(\tau) - p^2}} \tag{2.3.1}$$

with the appropriate value of p for the critical ray ($p = \sqrt{\epsilon_1}$). The result is

$$x = \sqrt{\epsilon_1/\Delta} \; [z' + L \ln(\frac{L}{z+L})] \tag{2.3.2}$$

where we see that as $z \to -L$, $x \to \infty$.

The difference between the behavior of the critical ray in a linear transition and its behavior in a parabolic transition can be understood better by applying the reciprocity prinicple. Consider a ray that is progressing

along the $z = -L$ interface of a linear transition.[*] This ray will be forced to turn away from the interface since it has a finite radius of curvature, $(d\epsilon(z)/dz\big|_{z=-L} \neq 0)$. The situation is not the same for a ray travelling along a parabolic interface. There $d\epsilon(z)/dz\big|_{z=-L} = 0$ and the radius of curvature is infinite. In this case the ray continues to propagate along the interface. Now, applying the principle of reciprocity to the parabolic layer, we see that if a ray starting in the interface, cannot escape then a ray outside the interface cannot become tangent to the interface unless it has an infinite radius of curvature. The critical ray in the parabolic layer only obtains an infinite radius of curvature as $x \to \infty$.

As in Chapter 1 we shall now focus our attention on the returning rays. By substituting the parabolic dielectric variation into the ray equation for returning rays, Eq. (1.3.1), and integrating it we obtain

$$x = p(z'+z)/p_2 + \frac{2pL}{\sqrt{\Delta}} \cosh^{-1} \frac{\sqrt{\Delta}}{|P_1|} \qquad , \qquad z \geq 0$$

$$\text{(2.3.3)}$$

$$x = pz'/p_2 + \frac{pL}{\sqrt{\Delta}} \cosh^{-1} \frac{\sqrt{\Delta}}{|P_1|} + \frac{pL}{\sqrt{\Delta}} \cosh^{-1} \frac{\sqrt{\Delta}(z+L)}{|P_1| L} , \quad z < 0$$

where $p_1 = i|p_1|$ and $\epsilon_i < p^2 < 1$. A typical ray is shown in Fig. 2.1 . Since these rays cross over one another, we shall require the constraint equation for the caustic. This is obtained by taking the derivative with respect to p of Eq. (2.3.3). The result is

---

[*] To be more accurate, we must say that the ray is not exactly on the interface but just a small amount above it. This removes the ambiguity in $d\epsilon(z)/dz\big|_{z=-L}$.

$$0 = (z+z')/p_2^3 + \frac{2L}{\sqrt{\Delta}} \cosh^{-1} \frac{\sqrt{\Delta}}{|p_1|} - 2Lp^2/|p_1|^2 p \ , \quad z \geq 0$$

$$0 = z'/p_2^3 + \frac{L}{\sqrt{\Delta}} \left[\cosh^{-1} \frac{\sqrt{\Delta}}{|p_1|} + \cosh^{-1} \frac{\sqrt{\Delta}(z+L)}{|p_1|\,L}\right]$$

$$- \frac{Lp^2}{|p_1|^2} \left[\frac{1}{p_2} + \frac{z+L}{[\Delta(z+L)^2 - |p_1|^2 L^2]^{\frac{1}{2}}}\right] \ , \quad z < 0 .$$

(2.3.4)

The caustic is obtained by choosing a value of p and solving for z; then by using the ray equation to find x. We see that the first equation, $z \geq 0$, can be solved explicitly for z while the equation for $z < 0$ cannot.

It will also be of interest to know the number and the location of the foci formed by the returning rays. The constraint equation for the foci is obtained by taking the derivative of Eq. (2.3.4) with respect to p. Upon doing this, we obtain

$$0 = \frac{3(z+z')}{p_2^5} - \frac{2L(|p_1|^2 - 2c_1)}{|p_1|^4 p_2} - \frac{2Lp^2}{|p_1|^2 p_2^3} \qquad z \geq 0$$

$$0 = \frac{3z'}{p_2^5} - \frac{L(|p_1|^2 - 2c_1)}{|p_1|^4} \left[\frac{1}{p_2} + \frac{z+L}{\sqrt{\Delta(z+L)^2 - |p_1|^2 L^2}}\right]$$

(2.3.5)

$$- \frac{Lp^2}{|p_1|^2} \left\{\frac{1}{p_2^3} + \frac{(z+L)L^2}{[\Delta(z+L)^2 - |p_1|^2 L^2]^{3/2}}\right\} \ , \quad z < 0 .$$

To obtain the location of the foci we must solve Eq. (2.3.4) in conjunction with Eq. (2.3.5). This will give us the z coordinates of the foci; then the ray equation can be used to obtain the x coordinate.

As has been mentioned in the introduction, Orlov h studied these
returning rays. To be more specific, he has made a det   l analytic
study of the caustic and foci for $z \geq 0$. He has then plotted the caustic for
some typical values of parameters when both $z \geq 0$ and $z < 0$. We have
redrawn two of his graphs which are representative of the caustic's general
behavior. These are shown in Fig. 2.2. In the upper graph (a) we see that
five cusps appear on the caustic while, in the lower graph, two of the cusps
disappear when $2\Delta > (1.076) L$. We note that the bow tie configuration which
was observed in Chapter 1 occurs twice in   ` and once in (b). As L
becomes smaller the remaining bow tie configuration disappears and only
one focus is left. This is shown in Fig. 2.3 where the caustic has been
plotted rather than just sketched for $L = .1$.

The caustic appearing in the three previous graphs share two character-
istics in common. We see that at large distances from the source, the lower
branch of the caustic approaches the interface while the upper branch appears
to have corrdinates that become unbounded. The asymptote to the lower
branch of the caustic can be obtained from Eq. (2.3.4) with $z < 0$ if we assume
that $p_2 \rightarrow 0$ as $z \rightarrow 0$. By usin , this procedure we find the asymptote to be

$$x = z' \sqrt{L}/(2\Delta(-z))^{\frac{1}{2}} \quad . \tag{2.3.6}$$

In addition we can also find an asymptote to the upper branch of the caustic
by assuming that as $p_1 \rightarrow 0$, $z \rightarrow \infty$. By using this assumption in Eq. (2.3.4)
with $z \geq 0$, we find that

$$x \approx \sqrt{\epsilon_1/\Delta}(z + z') + \sqrt{\epsilon_1/\Delta} \; L \ln\left(\frac{z + z'}{2 \epsilon_1 L}\right) \tag{2.3.7}$$

with

$$z + z' = 2 L \epsilon_1 \Delta / |p_1|^2 \quad . \tag{2.3.8}$$
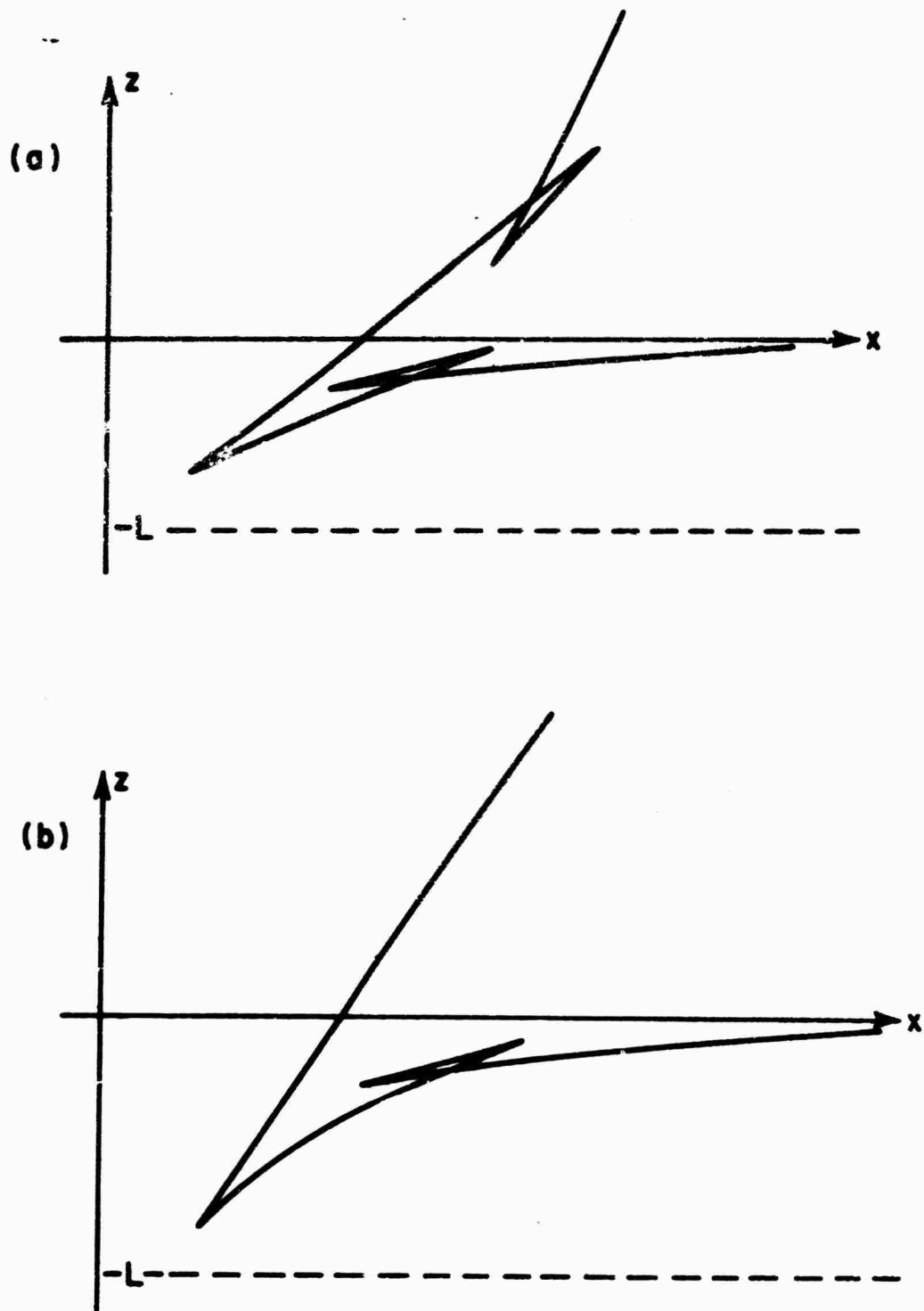
Fig. 2.2

Two Sketches of Caustics in a Parabolic Medium
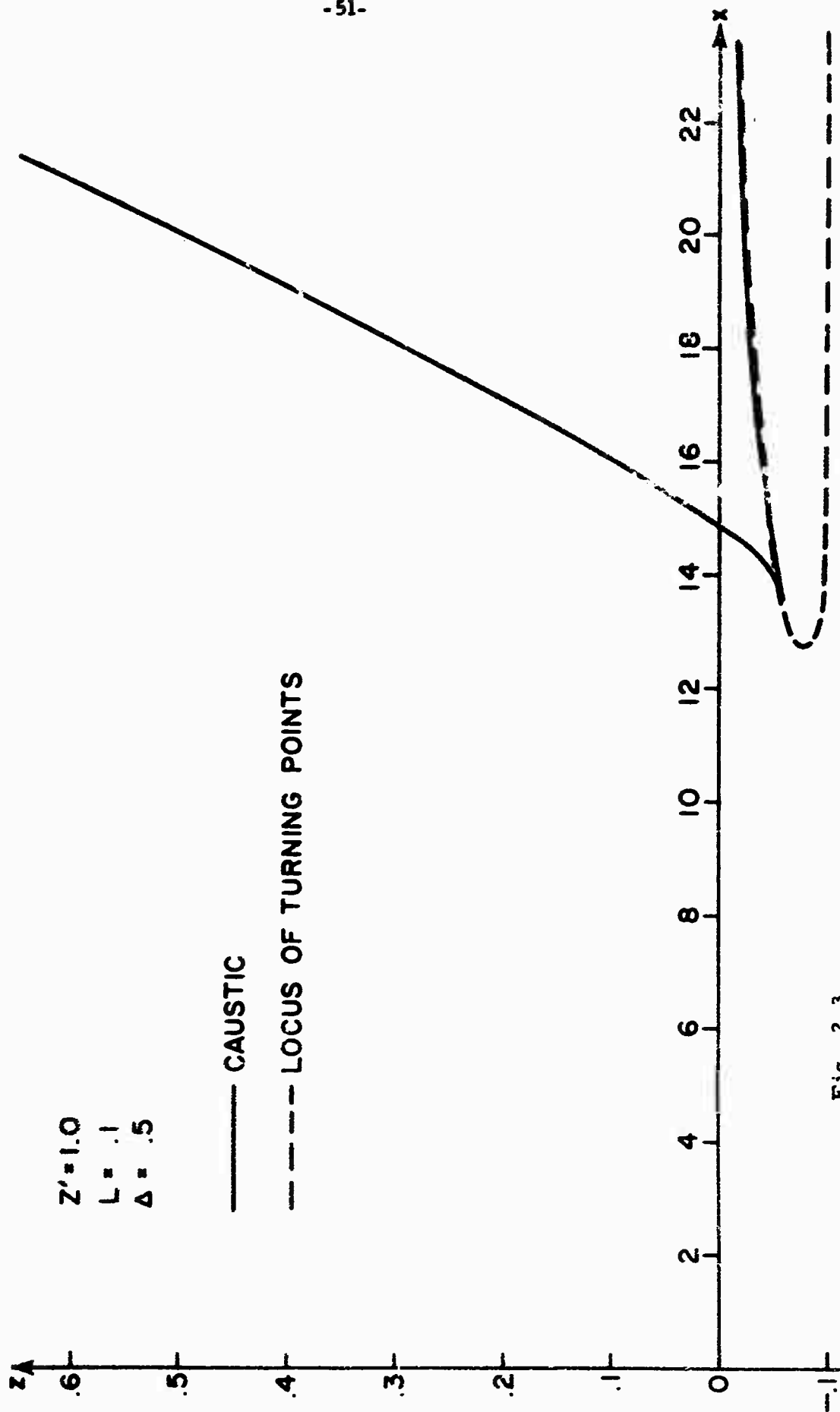
Fig. 2.3

Caustic Formed by a Parabolic Layer

We see that as the rays are emitted closer to the critical angle $(p_1 \to 0)$, the caustic formed by these rays tends closer to $x = \sqrt{\epsilon_1/\Delta}\,(z + z')$. We note that this equation represents the reflected critical ray from an abrupt transition.

When L is small the asymptote given in Eqs. (2.3.6) and (2.3.7) describes the caustic except for the region near the focus. The approximate location of the focus can be obtained by assuming

$$z \approx -L + AL^{3/2} \quad , \quad |p_1| \approx BL^{1/2} \quad , \quad \frac{L}{z} \ll 1 \qquad (2.3.9)$$

where A and B are constants to e determined. When these assumptions are used in Eqs. (2.3.4) and (2.3.5) they lead to an asymptotic approximation for the focus. The approximate location of the focus which is obtained is given by

$$x = \sqrt{\epsilon_1/\Delta} \left[z' + \frac{L}{2} \ln\left(z'/3\epsilon_1 L\right) \right] \qquad (2.3.10)$$

and

$$z = -L + 2\sqrt{\epsilon_1/z'}\,L^{3/2} \qquad . \qquad (2.3.11)$$

As $L \to 0$ the rays that make up the lower and upper branches of the caustic appear to have the same ray trajectories respectively as the reflected and lateral rays associated with an abrupt transition. We also note that the focus tends toward the point at which the critical ray is reflected from an abrupt transition. The comparison made above, says nothing about the ray contributions but only states that the two layers being compared have similar ray trajectories.

2.3.2   Asymptotic Evaluation

We will now asymptotically evaluate the formal solution for the reflected field, Eq. (2.2.4) when $k_o L \gg 1$ and compare our results to the prediction of geometrical-optics given in the last section. To effect the evaluation of the integral in Eq. (2.2.4) in physical terms we will expand the reflection coefficient in a geometric series and then asymptotically evaluate each term individually. The manner of development of this section will parallel section 1.3.2. quite closely.

The reflection coefficient given in Eq. (2.2.5) can be written as

$$\overline{\Gamma} = \Gamma_{oa} + \frac{\Gamma_{oa} \Gamma_L (\Gamma_{ob} - \Gamma_{oc})}{1 - \Gamma_L \Gamma_{ob}} \qquad (2.3.12)$$

where

$$\Gamma_L = \frac{E^{*'}(-a_1^2, o) + i a_1 E^*(-a_1^2, o)}{E'(-a_1^2, o) + i a_1 E(-a_1^2, o)} \qquad (2.3.13)$$

$$\Gamma_{oa} = -\frac{E^{*'}(-a_1^2, c) + i a_2 E^* -a_1^2, c)}{E^{*'}(-a_1^2, c) - i a_2 E^*(-a_1^2, c)} \qquad (2.3.14)$$

$$\Gamma_{ob} = \frac{E'(-a_1^2, c) - i a_2 E(-a_1^2, c)}{E^{*'}(-a_1^2, c) - i a_2 E^*(-a_1^2, c)} \qquad (2.3.15)$$

$$\Gamma_{oc} = \frac{E'(-a_1^2, c) + i a_2 E(-a_1^2, c)}{E^{*'}(-a_1^2, c) + i a_2 E^*(-a_1^2, c)} \qquad (2.3.16)$$

If $\left|\Gamma_L \Gamma_{ob}\right| < 1$ along the integration path C, the denominator of the second term in the reflection coefficient, Eq. (2.3.12), can be expanded in a geometric series. A calculation of $\left|\Gamma_L \Gamma_{ob}\right|$ shows that in the intervals $0 < \operatorname{Re} p_1 < \infty$, $\operatorname{Im} p_1 = 0$ and $\operatorname{Re} p_1 = 0$, $0 < \operatorname{Im} < \sqrt{\Delta}$, the term is less than one, however, for the interval $\operatorname{Re} p_1 = 0$, $\sqrt{\Delta}\operatorname{Im} p_1 < \infty$, we find $\left|\Gamma_L \Gamma_{ob}\right| = 1$. In Chapter 1 a similar problem had arisen and it was circumvented by deforming the integration path C a slight amount to the right of the $\operatorname{Im} p_1$ axis. We will perform a similar deformation of the path C at this point, however it must be assumed that $k_o L \gg 1$ in order to show that $\left|\Gamma_L \Gamma_{ob}\right| < 1$ along the deformed path.

We will make use of the series expansion in Eq. (2.3.12). The result is

$$\overline{\Gamma} = \Gamma_{oa} + \sum_{n=0}^{\infty} \Gamma_n \tag{2.3.17}$$

where Γ_n is defined in Eq. (1.3.14) and where it is assumed that the Γ_L, Γ_{oa}, Γ_{ob} and Γ_{oc} of Chapter 1 are replaced by those of Chapter 2. By substituting the series form of the reflection coefficient given above in the integral representation for the reflected field, Eq. (2.2.4) and interchanging orders of summation and integration, we find that

$$E_{yr} = E_{ro} + \sum_{n=0}^{\infty} E_n \tag{2.3.18}$$

where E_{ro} and E_n are defined by Eqs. (1.3.16) and (1.3.17) respectively.

Before evaluating E_{ro} and E_n by the method of steepest descents we will asymptotically approximate Γ_{oa} and Γ_n to reduce the complexity of the integrands. These expressions, Γ_{oa} and Γ_n, are composed of parabolic cylinder functions whose asymptotic approximations along the integration path C appear in Table 2.1. The functions E^* and $E^{*'}$ do not appear in the table, however, their asymptotic approximations can be obtained by

taking the complex conjugate of the asymptotic expansions for E and E^*.,

The asymptotic approximations for E and E^* will be needed close to the integration path C when subsequent path deformations are made. These asymptotic approximations can be obtained by analytically continuing the formulae in Table 2.1 if we exclude the regions near $p_1 = 0$, $\sqrt{\Delta}$. In these regions we can use

$$E(-a_1^2 , x) = \sqrt{2} e^{-\pi a_1^2/4 + i\pi/8 + i\$_2/2} \quad U(-ia_1^2, x e^{-i\pi/4}) \qquad (2.3.19)$$

$$E^*(-a_1^2, x) = \sqrt{2} e^{-\pi a_1^2/4 - i\pi/8 + i\$_2/2} \quad U(+ia_1^2, x e^{+i\pi/4}) \qquad (2.3.20)$$

where U is another form of parabolic cylinder function, $x = 0$ or $x = c$ and $\$_2 = \arg \Gamma(1/2 - ia_1^2)$, $\$_2 = 0$. Olver[21b] has obtained the asymptotic expansions of U and $U' (dU(a, x)/dx = U'(a, x))$ for large a_1 , and any x and $\arg a_1$. His expansions for U and U' can be used near $p_1 = 0$ and $p_1 = \sqrt{\Delta}$, however, we cannot come too close to $p_1 = 0$ since $a_1 = (\tau/2\sqrt{\Delta})^{\frac{1}{2}} p_1$ and the asymptotic parameter a_1 will tend to zero. The functions U and U' could have been used over the whole integration path, however, their asymptotic expansions are more complex and unwieldy.

By using the asymptotic expansions found in Table 2.1 to calculate Γ_{oa} and Γ_n in the region $\text{Re} \, p_1 \approx 0$, $\sqrt{\Delta} < \text{Im} \, p_1 < \infty$, and then by substituting these approximations in the appropriate integrals, we find the E_{ro} and E_n have no asymptotic contribution ($k_o L \gg 1$) from this section of their integration path on the top or second sheet. In a similar manner by the use of Eqs. (2.3.19) and (2.3.20) along with Olver's asymptotic expansions, we can show that the integration path in the region of the branch point, $p_1 = \sqrt{\Delta}$, gives no asymptotic contribution.

	$0 < \mathrm{Re}\, P_1 < \infty$, $\mathrm{Im}\, P_1 = \infty$	$\mathrm{Re}\, P_1 = 0$, $0 < \mathrm{Im}\, P_1 < \sqrt{\Delta}$	$\mathrm{Re}\, P_1 = 0$, $\sqrt{\Delta} < \mathrm{Im}\, P_1 < \infty$
$E(-a_1^2, 0)$	$\dfrac{1}{\sqrt{a_1}}\left(1+\dfrac{1}{32a_1^4}\right)e^{i\pi/4}$	$\dfrac{e^{-\pi a_1^2}}{\sqrt{a_1}}\left(1-\dfrac{1}{32a_1^2}\right)$	⟵ Same as
$E'(-a_1^2, 0)$	$-\sqrt{a_1}\left(1-\dfrac{1}{32a_1^4}\right)e^{-i\pi/4}$	$-\dfrac{e^{-\pi a_1^2}}{\sqrt{a_1}}\left(1+\dfrac{1}{32a_1^2}\right)$	⟵ Same as
$E(-a_1^2, c)$	$\dfrac{e^{i\theta_1}}{\sqrt{a_2}}(i - d_3/8a_2^3)$	$\dfrac{e^{i\theta_2}}{\sqrt{a_2}}(1 - d_3/8a_2^3)$	$\dfrac{i\,e^{\pi a_1^2 + \theta_3}}{\sqrt{a_2}}$
$E'(-a_1^2, c)$	$i\sqrt{a_2}\,e^{i\theta_1}\left[1 + \dfrac{(ic - d_3)}{8a_2^3}\right]$	$i\sqrt{a_2}\,e^{i\theta_2}\left[1 + \dfrac{(ic - d_3)}{8a_2^3}\right]$	$\sqrt{a_2}\,e^{\pi a_1^2 + \theta_3}$

$$\theta_1 = \tfrac{1}{2}\tau\left[P_2 + \frac{P_1^2}{\sqrt{\Delta}}\sinh^{-1}\frac{\sqrt{\Delta}}{P_1}\right] + \frac{\pi}{4}, \qquad \theta_3 = \tfrac{1}{2}\tau\left[|F_2| + \frac{|P_1|^2}{\sqrt{\Delta}}\sin^{-1}\frac{\sqrt{\Delta}}{|P_1|}\right]$$

$$\theta_2 = \tfrac{1}{2}\tau\left[P_2 - \frac{|P_1|^2}{\sqrt{\Delta}}\cosh^{-1}\frac{\sqrt{\Delta}}{|P_1|}\right] + \frac{\pi}{4}, \qquad d_3 = c\left(\frac{c^2}{48} + \frac{a_1^2}{2}\right)\Big/a_1^2, \qquad |P_1| = -iP_1$$

Table 2.1 Asymptotic forms of parabolic cylinder functions on the integration path

If we again use the asymptotic approximations from Table 2.1, we find that

$$\Gamma_{oa} \sim i\Delta/4\tau p_2^3 \tag{2.3.21}$$

when p_1 is on the integration path between $p_1 = \sqrt{\epsilon_1}$ and $p_1 = i\sqrt{\Delta}$. We now use this approximation in the integral for E_{ro} and apply the method of steepest descents. We will not go into the details since they exactly parallel the asymptotic evaluation of E_{ro} in Chapter 1. It will suffice to say that there are two relevant saddle points denoted by D and E, as before. The contribution from E is exponentially small while the contribution from D can be interpreted as a ray reflected from the $z = 0$ interface as shown in Fig. 1.19. The asymptotic order of these contributions are shown in Table 2.2.

We now asymptotically approximate E_n. First, the formulae in Table 2.1 will be used to simplify Γ_n along the portion of the integration path between $p_1 = \sqrt{\epsilon_1}$ and $p_1 = i\sqrt{\Delta}$. When $0 < \operatorname{Re} p_1 < \sqrt{\epsilon_1}, \operatorname{Im} p_1 = 0$ we find that

$$\Gamma_n \sim \frac{\Delta^{2n+1}}{4^{2n+1} p_2^{3n} p_1^{4n+4} \tau^{3n+2}} e^{i[2(n+1)\theta_1 - n\pi/2]} \tag{2.3.22}$$

and when $\operatorname{Re} p_1 = 0$, $0 < \operatorname{Im} p_1 < \sqrt{\Delta}$ we find that

$$\Gamma_n \sim \frac{\Delta^{n/2}}{8^n p_2^{3n} \tau^n} e^{i2(n+1)\theta_2} \tag{2.3.23}$$

where θ_1 and θ_2 are defined in Table 2.1.

Type	Asymptotic Order
A_n	$O(k_o^{-(n+1/2)})$
B_n	$O(k_o^{-(3n+5/2)})$
D	$O(k_o^{-3/2})$
E	$O(e^{-\alpha k_o}), \alpha > 0$

Table 2.2

Asymptotic Order of Geometrical-Optic Contributions

The above approximations are good in the vicinity of the integration path except near the origin, i.e., $(\tau/2\sqrt{\Delta}) p_1^2 \ll 1$.

If we now replace the Γ_n appearing in the integrand of Eq. (1.3.17), by its asymptotic approximation and find the saddle point equations as in the previous chapter, we obtain

$$p_1 \left(\frac{z+z'}{p_2} \mp \frac{x}{p} + 2(n+1) L \sinh^{-1} \frac{\sqrt{\Delta}}{p_1} \right) = 0 \qquad (2.3.24)$$

$$0 < \mathrm{Re}\, p_1 < \sqrt{\epsilon_1} \quad , \quad \mathrm{Im}\, p_1 = 0$$

and

$$|p_1| \left(\frac{z+z'}{p_2} \mp \frac{x}{p} + \frac{2(n+1) L}{\sqrt{\Delta}} \cosh^{-1} \frac{\sqrt{\Delta}}{|p_1|} \right) = 0 \qquad (2.3.25)$$

$$\mathrm{Re}\, p_1 = 0 \quad . \quad 0 < \mathrm{Im}\, p_1 < \sqrt{\Delta}$$

where the upper sign in the above equations refers to the top sheet while the lower sign refers to the second sheet.

Upon obtaining the saddle point locations from the above equations, we deform the contour C through the saddle points and into the decay regions. Since the contribution due to the portion of the integral lying in the decay region is exponentially small, the integral E_n will be asymptotically equal to the sum of the saddle point contributions. The contributions arising from saddle points obeying Eqs. (2.3.25) and (2.3.24) will be known as type A_n and B_n contributions, respectively. It can be shown that no relevant saddle points occur on the second sheet for any n and therefore the deformed path will be the same as that shown in Figs. 1.13 and 1.14.

We shall now focus our attention on the relevant saddle points on the top sheet and their contributions to the reflected field. The integral E_0 will be considered first, since it contributes the dominant terms to the reflected field for large $k_0 L$.

We will now investigate the saddle points of type A_0. A comparison of Eqs. (2.3.3) and (2.3.25) shows us that the two are identical. This means, as in Chapter 1, that each saddle point corresponds to a returning ray. If we now recall our discussion of returning rays, we will remember that there are two basic regions divided by a caustic. To the right of the caustic there are two returning rays; to the left there are none. For certain parameters, the caustic can assume a bow tie configuration for $z > 0$ as shown in Fig. 2.2(a). Inside the bow tie there are four returning rays while outside the bow tie there is the same number of returning rays as before. With the above information we see that there are 0, 2 or 4 solutions, depending upon the location of the observation point, to Eq. (2.3.25).

We shall next examine saddle points of the type B_o . An investigation of Eq. (2. 3. 24) shows that there is one saddle point for any given observation point. The saddle point contribution can be interpreted as a ray reflected from the lower interface. The amplitude factor of this ray has $O(k_o^{-5/2})$.

As stated previously, the reflected field, E_o , is composed of a sum of A_o and B_o type contributions. The deformed path on the top sheet is shown in Figs. 1. 15 and 1. 16 when there are no saddle points or there are two saddle points of the A_o type, respectively. When there are four saddle points of type A_o the path is similar to the ones shown, but it is not shown here. An approximation of the deformed path shows that it can be deformed around the origin for any given observation point and, therefore no contribution, similar to type C_o , arises as we observed in Chapter 1 . This means that there is no lateral wave contribution. However, there are two (assume that the bow tie is not present) rays through each point to the right of the caustic while in a similar region, in Chapter 1, there is only one ray through each point. When the observation point is located far from the source compared to layer thickness we observe: first, that the returning ray in Chapter 1 has a similar trajectory to one of the returning rays of Chapter 2; and second, that the trajectory of the lateral ray in Chapter 1 is similar to the trajectory of the other returning ray observed in Chapter 2 .

We will now evaluate explicitly the contribution due to the ray whose trajectory is similar to a lateral ray. The evaluation will be limited to observation points which are located far from the source compared to layer thickness and also those observation points where $L_p \gg L$. Here L_p is defined as in Chapter 1. The last condition has the following physical explanation. When the observation point is located far from the source, the upper branch of the caustic is approximately described by $L_p = 0$. The condition, $L_p \gg L$, says that the observation point should be many layer thicknesses from this portion of the caustic.

By using the above approximations on the saddle point equation, Eq. (2.3.25) , we obtain the approximate location for the two saddle points in question. They are :

$$P_{1r} = \sqrt{x^2 \Delta - (z+z')^2 \epsilon_1} \qquad , \qquad |P_{1L}| = 2\sqrt{\Delta} \; e^{-\sqrt{\Delta} L_p / 2\sqrt{\epsilon_1} L} \qquad (2.3.26)$$

The notation used is motivated by the fact that the contributions from saddle points P_{1r} and P_{1L} are similar to reflected and lateral rays from an abrupt transition. The first saddle point P_{1r} is obtained by assuming that the last term in Eq. (2.3.25) is small while the saddle point P_{1L} is obtained by assuming $p_1 \approx 0$. From Eq. (2.3.25) we see that there appears to be a saddle point at $p_1 = 0$, however the asymptotic approximations used to simplify the integrand are not valid there.

Now by evaluating the integral E_o at the saddle point P_{1L} we obtain

$$E_L \sim \frac{\Delta^{1/4} \; e^{-\sqrt{\Delta} L_p / 2\sqrt{\epsilon_1} L}}{2\sqrt{\pi \epsilon_1 k_o L}} \; e^{i k_o [\sqrt{\Delta}(z+z') + \sqrt{\epsilon_1} x + \sqrt{\Delta} L] + i 3\pi/4} \qquad (2.3.27)$$

where E_L is the contribution from E_o which is due to the saddle point P_{1L} . The phase of the above contribution corresponds to a lateral ray, however the amplitude is of $O(k_o^{-1/2})$ which makes this contribution a classical geo-metrical-optic result.

An examination of Eq. (2.3.26) reveals one basic difficulty. As L_p / L becomes increasingly large $|P_{1L}| \to 0$. In order for the asymptotic forms of Table 2.1 to be valid $a_1^2 \gg 1$ or using Eq. (2.3.26) we find

$$\tau \; e^{-\sqrt{\Delta} L_p / 2\sqrt{\epsilon_1} L} \gg 1 . \qquad (2.3.28)$$

This inequality essentially says that as L_p/L gets very large compared to τ, the geometrical-optic result, appearing in Eq. (2.3.27), is no longer valid. We see rays emitted from the source close to the critical angle resemble geometrical-optic rays with lateral ray type trajectories, but, as the emission angle becomes closer to the critical ray, the geometrical-optic interpretation can no longer be given.

An evaluation of E_n for arbitrary n will show E_o to be the dominant term in the series. We will not go into detail since the evaluation exactly parallels a similar development in Chapter 1 . It will suffice to say that the contributions of types A_n and B_n will be encountered. Those of type A_n are returning rays reflected from the $z = 0$ interface n times. On the other hand, the B_n contributions are those rays reflected $n+1$ times from the $z = -L$ interface. The asymptotic order of those contributions is shown in Table 2.2 .

2.4   Evaluation of Reflected Field for Large $k_o L_p$

In this section we will investigate the reflected field from the parabolic transition when $k_o L_p \gg 1$ and $L_p \gg L$. From this investigation we hope to learn what the pertinent field contributions are, when the layer is thick compared to wavelength, i.e.: $k_o L_p \gg k_o L \gg 1$. In addition, we want to relate these contributions to the field constituents that occur when $k_o L \gg k_o L_p \gg 1$ and when $k_o L_p \gg 1$, $k_o L \ll 1$.

The integral representation for the reflected field is given by Eq. (1.4.1) where the reflection coefficient used there is replaced by

$$\overline{\Gamma} = - \Delta_{tn} / \Delta_{tb} \tag{2.4.1}$$

where

$$
\Delta_{\substack{tn \\ bn}} = \begin{Vmatrix} \left\{ W'(-a_1^2, 0) - ia_1 W(-a_1^2, 0) \right\} & \left\{ -W'(-a_1^2, 0) - ia_1 W(-a_1^2, 0) \right\} \\ \left\{ W'(-a_1^2, -c) \mp ia_2 W(-a_1^2, -c) \right\} & \left\{ -W'(-a_1^2, c) \mp ia_2 W(-a_1^2, c) \right\} \end{Vmatrix} ,
$$

$W(-a_1^2, \pm \zeta)$ are another form of parabolic cylinder functions which are defined by Abramowitz[22] and $W'(-a_1^2, \zeta) = dW(-a_1^2, \zeta)/d\zeta$. We see that the integral representation employed here is the same as that used in the last section, except with a different reflection coefficient. This reflection coefficient is derived via Appendix A. by choosing $\phi_1(z) = W(-a_1^2, \zeta)$ and $\phi_2(z) = W(-a_1^2, \zeta)$ where ζ has been defined in the beginning of Chapter 2. This alternative form of reflection coefficient makes the computations, that will follow, easier since the $W(-a_1^2, \pm \zeta)$ are real functions .

If we now use the assumption that $k_0 L \ll k_0 L_p$ then the reflection coefficient in Eq. (2.4.1) is slowly varying compared to the exponential in the integrand, and the standard steepest descent techniques can be used to asymptotically evaulate the integral representation. We will not go into detail since the development parallels Chapter 1, Section 1.4.

The results of this asymptotic analysis are that there are two saddle point contributions which make up the reflected field. The first of these is simply the reflected ray contribution. The contribution has an $O(k_0^{-1/2})$ for all layer thicknesses considered here.

The second contribution to the reflected field comes from the saddle point occuring at $p_1 = 0$ and it reduces to the lateral wave contribution on an abrupt interface when $k_0 L \to 0$. The contribution will be denoted by E_L and it is given by

$$E_L \sim \frac{c_1^{1/4} A(\sqrt{\Delta}\,\tau)\, e^{i k_o [\sqrt{\Delta}(z+z') + \sqrt{c_1}\,x] + i \psi(\sqrt{\Delta}\,\tau) + i 3\pi/4}}{\sqrt{2\pi}\,\Delta\,(k_o L)^{3/2}} \tag{2.4.2}$$

where

$$A(\sqrt{\Delta}\,\tau) = \frac{\sqrt{\Delta}}{2} \left| \frac{d\bar{\Gamma}}{dp_1} \right|\Bigg|_{p_1=0} = -\frac{\tau\sqrt{\Delta}\,\Gamma(1/4)}{\sqrt{2}\,\Gamma(3/4)}\,\frac{[W'(0,c)W(0,-c) + W(0,c)\,W'(0,-c)]}{\left[(W'(0,-c) - W'(0,c))^2 + \dfrac{c^2}{4}\,(W(0,c) + W(0,-c))^2 \right]} \tag{2.4.3}$$

and

$$\psi(\sqrt{\Delta}\,\tau) = 2 \tan^{-1}\left[\frac{2}{c}\,\frac{W'(0,-c) - W'(0,c)}{W(0,c) + W(0,-c)} \right] . \tag{2.4.4}$$

The amplitude $A(\sqrt{\Delta}\,\tau)$ and the phase $\psi(\sqrt{\Delta}\,\tau)$ have been plotted by computer and are shown in Figs. 2.4 and 2.5. In these figures the thick layer approximations to $A(\sqrt{\Delta}\,\tau)$ and $\psi(\sqrt{\Delta}\,\tau)$ are also shown.

The physical interpretation of E_L can best be found from an investigation of the small and large τ limits. When τ is small, as we have already stated, E_L reduces to the lateral wave on an abrupt interface. We see this from the fact that as $\tau \to 0$, $A(\sqrt{\Delta}\,\tau) \to 1$ and $\psi(\sqrt{\Delta}\,\tau) \to 0$. When $k_o L \gg 1$, or the layer is large compared wavelength, E_L reduces to

$$E_L \sim -\frac{\Gamma^2(1/4)\,c_1^{1/4}\,L^{1/2}}{2(2\pi)^{3/2}\Delta^{3/4} L_p^{1/2}\,(k_o L_p)}\, e^{i k_o\left[\sqrt{\Delta}(z+z') + \sqrt{c_1}\,x + L\sqrt{\Delta}\right] + i\pi/2} . \tag{2.4.5}$$

If we compare the lateral wave contributions excited on a linear and parabolic layer for $k_o L$ large, as given in Eqs. (1.4.10) and (2.4.2)
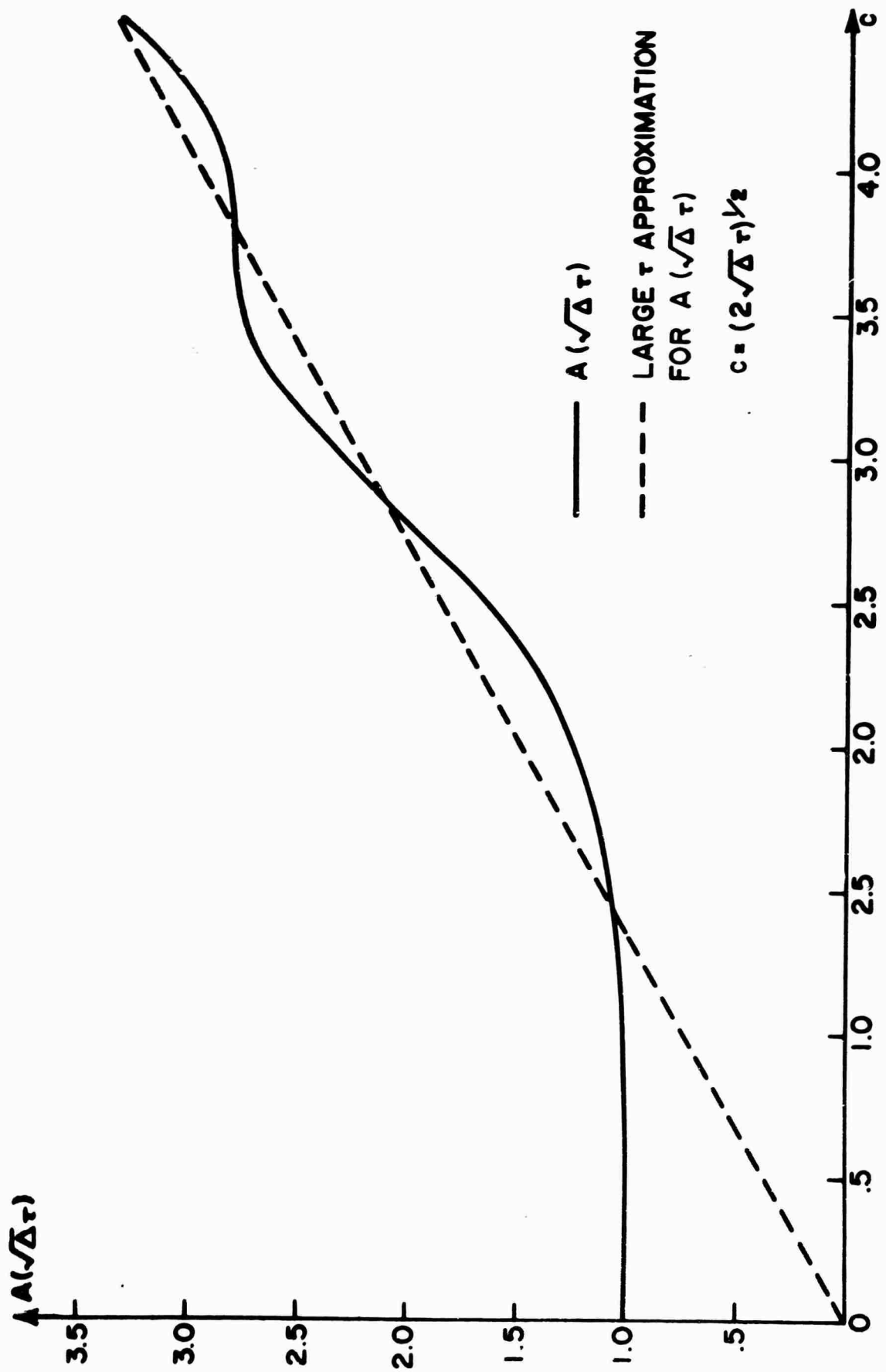
Fig. 2.4

Lateral Wave Amplitude vs. Normalized Transition Thickness to the One Half Power
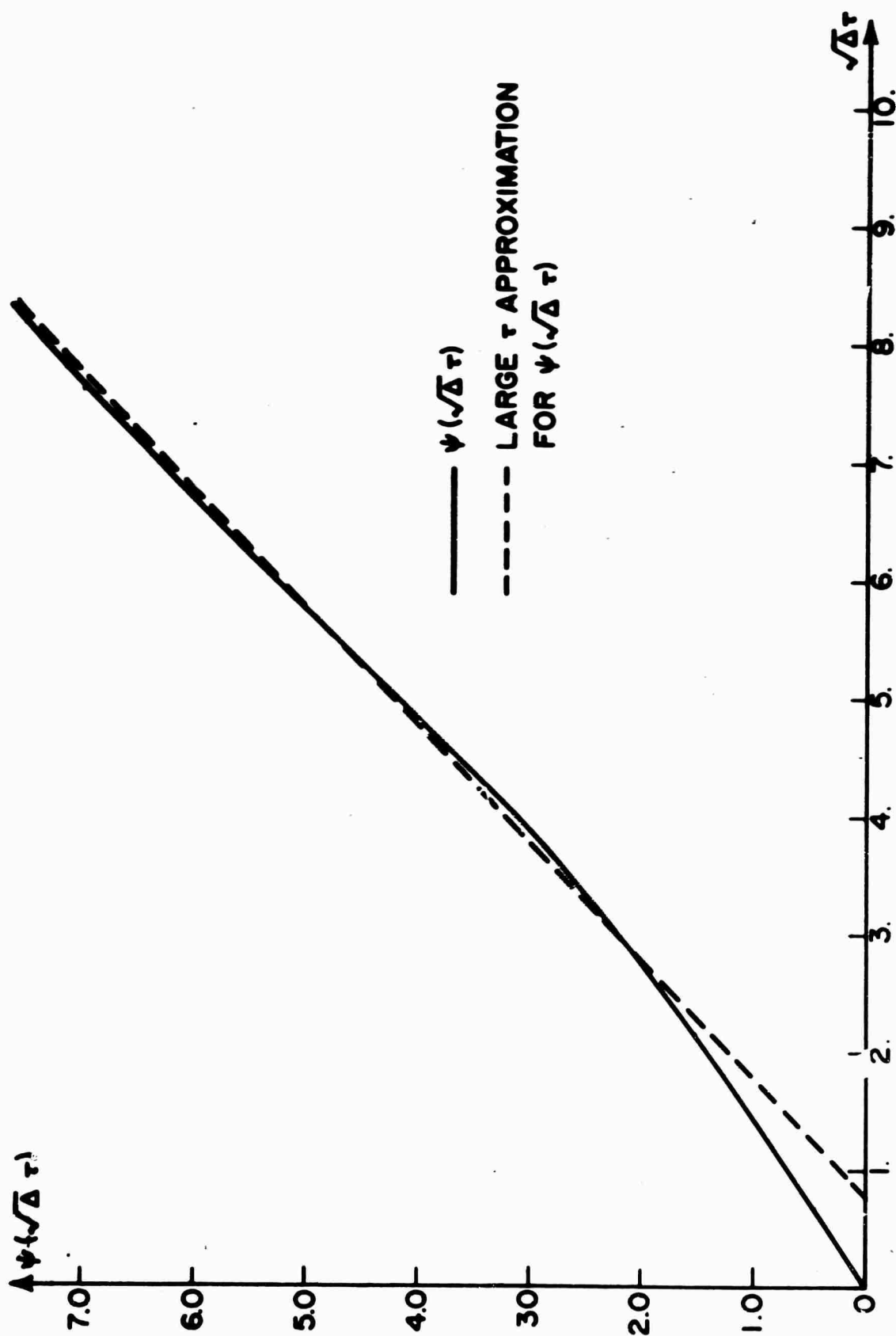
Fig. 2.5

Lateral Wave Phase vs. Normalized Transition Thickness

respectively, we observe that both have a similar phase dependence and an amplitude dependence on distance of $O(L_p^{-3/2})$. The outstanding difference between the two contributions is that the lateral wave, excited on a linear layer, has an excitation coefficient of $O(k_o^{-7/6})$ while the lateral wave, found on a parabolic layer, has a coefficient of $O(k_o^{-1})$. We see for high frequency that the parabolic layer wave is excited more strongly.

The lateral wave contribution given in Eq. (2.4.5) also sheds some light on another area. In the previous section, a geometrical-optic ray contribution was found. It has a ray trajectory similar to a lateral ray, however, as the observation points move away from the source, $L_p \gg L$, the geometrical-optic contribution becomes invalid. We see now that this contribution transforms into a true lateral wave contribution when $k_o L_p \gg k_o L \gg 1$. The transition between the two regions of validity for the E_L contribution is quite complex and, as yet, transition functions have not been found.

CHAPTER 3.

THE SYMMETRICAL EPSTEIN TRANSITION LAYER

3.1 Introduction

In Chapters 1 and 2 the reflected field from a linear and parabolic transition has been studied. There it was found that a lateral wave was excited for all layer thicknesses, and that its character was changed as the normalised layer thickness, $k_o L$, was varied. For both of the above mentioned cases the thick layer limit was particularly interesting. In this limit the lateral wave discussed in Chapter 1 appeared to be excited at the point that the critical ray was tangent to the lower interface. In Chapter 2, no such interpretation was possible, but instead, the lateral rays resulted from returning rays emitted close to the critical angle.

In an examination of the above problems, we had noted that the continuity of the layer at the lower interface was the critical factor in determining the type of lateral wave that could be excited. A logical extension of the studies undertaken in the first two chapters could consist of an investigation of the reflected field from a layer that was completely continuous at the lower interface. Wave functions for the layer mentioned above could not be found, therefore we resorted to the study of a layer of infinite extent. The symmetrical Epstein layer, to be considered in this chapter, is such a layer. Its dielectric profile is given by

$$
\epsilon(z) = \begin{cases} 1 & , \quad z \geq 0 \\ \\ \epsilon_1 + \Delta \, \text{sech}^2 z/L & , \quad z < 0 \end{cases} \quad , \quad \Delta = 1 - \epsilon_1 \quad . \quad (3.1.1)
$$

This layer has the property that as $z \to -\infty$, $\epsilon(z) \to \epsilon_1$ and all derivatives of $\epsilon(z)$ approach zero. Thus, we see that the layer is completely continuous

at the lower homogeneous medium which occurs at minus infinity. The
dielectric layer also has the required property that as $L \to 0$ the layer
approaches an abrupt interface.

In this chapter we will first investigate the structure of the returning
ray trajectories when $k_o L \gg 1$. Following this, a uniform asymptotic
approximation for the reflected field will be derived which will be valid for
abritrary values of $k_o L$. By means of this approximation we can relate the
lateral wave on a sharp interface to the geometric-optic rays observed when
the layer is thick compared with wavelength.

3.2   Formal Solution

The integral representation for the reflected field in the region $z \geq 0$ is
obtained in a manner similar to that used in Chapters 1 and 2. The source
configuration is the same as before and again only the E_y component of the
electric field is excited. This component satisfies the wave equation,
Eq. (1.2.1), where the source amplitude has been assumed to be normalized
as in Eq. (1.2.2). The representation for E_y is obtained by the application
of Fourier integral techniques to Eq. (1.2.1). The result is given by a sum
of direct and reflected fields

$$E_y = E_{yf} + E_{yr}$$

where

$$E_{yf} = -\frac{1}{4\pi i} \int_{-\infty}^{+\infty} e^{ik_o[p_2|z-z'| + px]} dp \quad , \quad z \geq 0 \qquad (3.2.2)$$

and

$$E_{yr} = -\frac{1}{4\pi i} \int_{-\infty}^{+\infty} \frac{\bar{T}}{p_2} e^{ik_o[p_2(z+z') + px]} dp \quad , \quad z \geq 0 \quad . \qquad (3.2.3)$$

with

$$\bar{\Gamma} = \frac{ik_o P_2 + \theta'(0)/\theta(0)}{ik_o P_2 - \theta'(0)/\theta(0)} \qquad , \qquad (3.2.4)$$

$$P_2 = \left(1-p^2\right)^{\frac{1}{2}} \quad , \qquad P_1 = \left(\epsilon_1 - p^2\right)^{\frac{1}{2}} \quad . \qquad (3.2.5)$$

The function $\theta(z)$ used in the reflection coefficient $\bar{\Gamma}$ is defined as the solution of the differential equation

$$\left[\frac{d^2}{dz^2} + k_o^2 \left(\Delta \ \text{sech}^2(z/L) + p_1^2\right)\right] \theta(z) = 0 \qquad (3.2.6)$$

which satisfies the radiation condition as $z \to -\infty$. The derivative of $\theta(z)$ with respect to z will be denoted by $\theta'(z)$. In order to define the integrals appearing in (3.2.2) and (3.2.3) completely, the square roots p_1 and p_2 must be specified. This specification is shown in Fig. 1.4 where the four branch cuts have been chosen. The integration path P is also shown in the same figure.

We will now solve (3.2.6) exactly Transforming (3.2.6) by

$$\zeta = \tanh(z/L) \qquad (3.2.7)$$

reduces it to

$$\left\{(1-\zeta^2)\frac{d^2}{d\zeta^2} - 2\zeta\frac{d}{d\zeta} + \left[\nu(\nu+1) - \mu^2/(1-\zeta^2)\right]\right\} \theta = 0$$

$$(3.2.8)$$

with

$$\mu = +i\tau p_1 \quad , \quad \nu = -1/2 + (1/4 + \tau^2\Delta)^{\frac{1}{2}} \ , \quad \tau = k_o L \ . \qquad (3.2.9)$$

This is the Associated Legendre equation whose two independent solutions are $P_\nu^\mu(\zeta)$, $Q_\nu^\mu(\zeta)$. If we represent $P_\nu^\mu(\zeta)$ as an hypergeometric function[23] and let $z \to -\infty$ we see that it obeys the radiation condition. The solution to (3.2.6) is then

$$\theta(z) = P_\nu^\mu\left[-\tanh(z/L)\right] \ . \qquad (3.2.10)$$

The initial value (z=0) of this Associated Legendre function and its derivative are given in terms of Gamma function[24]. Using these relations, one obtains

$$\frac{\theta'(0)}{\theta(0)} = -\frac{2\Gamma(\nu/2 + \mu/2 + 1)\ \Gamma(\nu/2 - \mu/2 + 1)}{L\Gamma(\nu/2 + \mu/2 + 1/2)\Gamma(\nu/2 - \mu/2 + 1/2)}\tan\left[\pi(\nu + \mu)/2\right]$$

or
$$\tag{3.2.11}$$

$$\frac{\theta'(0)}{\theta(0)} = \frac{2\Gamma(1/2 - \nu/2 - \mu/2)\ \Gamma(\nu/2 - \mu/2 + 1)}{L\Gamma(-\nu/2 - \mu/2)\ \Gamma(\nu/2 - \mu/2 + 1/2)} \ .$$

$$\tag{3.2.12}$$

In order to determine the asymptotic properties of the reflection co-efficient the location of the poles of the gamma function will be necessary. Consider the poles of $\Gamma(\nu/2 + \mu/2 + 1)$, for example. They occur when

$$-1/4 + \frac{1}{2}\ (1/4 + \tau^2\Delta)^{\frac{1}{2}} + i\tau p_1/2 + 1 = -n\ , \quad n = 0, 1, 2, \ldots \tag{3.2.13}$$

is satisfied. Since

$$\tau(\Delta)^{\frac{1}{2}} < 3/2 + (1/4 + \tau^2\Delta)^{\frac{1}{2}} \tag{3.2.14}$$

for all $\tau(\Delta)^{\frac{1}{2}}$, the first pole lies in the range $\mathrm{Re}\,p_1 = 0$, $(\Delta)^{\frac{1}{2}} < \mathrm{Im}\,p_1$. Poles corresponding to $n = 1$ and higher have larger values of $|p_1|$ and therefore occur in the same range as the first pole. The pole locations of the various gamma functions appearing in (3.2.11) and (3.2.12) are shown in Table 3.1. Since these poles occur on the $\mathrm{Re}\,p$ axis for $|\mathrm{Re}\,p| > (\epsilon_1)^{\frac{1}{2}}$ they lie directly on the integration path. If a small amount of loss is added to the dielectric medium, the poles with $\mathrm{Re}\,p > 0$ shift into the first quadrant of the p plane while the remaining poles shift into the third quadrant. With this information, the integration path can be deformed around the poles in the correct manner in the limit of zero loss.

Gamma Functions	Pole Locations	
$\Gamma(\nu/2 + \mu/2 + 1)$	$\mathrm{Re}\ p_1 = 0$	$\mathrm{Im}\ p_1 > (\Delta)^{\frac{1}{2}}$
$\Gamma(\nu/2 + \mu/2 + 1/2)$	$\mathrm{Re}\ p_1 = 0$	$\mathrm{Im}\ p_1 > (\Delta)^{\frac{1}{2}}$
$\Gamma(\nu/2 - \mu/2 + 1)$	$\mathrm{Re}\ p_1 = 0$	$\mathrm{Im}\ p_1 < -(\Delta)^{\frac{1}{2}}$
$\Gamma(\nu/2 - \mu/2 + 1/2)$	$\mathrm{Re}\ p_1 = 0$	$\mathrm{Im}\ p_1 < -(\Delta)^{\frac{1}{2}}$
$\Gamma(1/2 - \nu/2 - \mu/2)$	$\mathrm{Re}\ p_1 = 0$	$\mathrm{Im}\ p_1 < (\Delta)^{\frac{1}{2}}$
$\Gamma(-\nu/2 - \mu/2)$	$\mathrm{Re}\ p_1 = 0$	$\mathrm{Im}\ p_1 < (\Delta)^{\frac{1}{2}}$

Table 3.1   Pole Locations

Before proceeding we shall check the convergence of the integral.

To do this we asymptotically evaluate (3.2.10) as $|p| \to \infty$. We find

$$\theta'(0)/\theta(0) \sim k_o |p_1|$$ (3.2.15)

which gives a reflection coefficient

$$\bar{\Gamma} = \frac{|p_2| - |p_1|}{|p_2| + |p_1|}$$ (3.2.16)

when p is large. Since the exponential in the integral decays for large p, the integral converges.

To simplify future calculations, the branch points at $p = \pm(\epsilon_1)^{\frac{1}{2}}$ are now removed by means of the transformation

$$p = (\epsilon_1 - p_1^2)^{\frac{1}{2}} \quad , \quad p_2 = (\Delta + p_1^2)^{\frac{1}{2}} \quad .$$ (3.2.17)

This transforms the integral in (3.2.3) to

$$E_R = +\frac{1}{4\pi i} \int_C \frac{p_1 \Gamma}{p p_2} e^{i k_o [p_2(z+z')+px]} dp_1 \, , \quad z \geq 0$$ (3.2.18)

where the multivalued functions p, p_2 are defined on a four sheeted Riemann surface. The first two sheets of this surface are shown in Figs. 1.5 and 1.6. The multivalued character of the mapping (3.2.17) leads to a transformed integration path, C, in the p_1 plane. Parts of this path appear on different sheets since any two points symmetrically located on path p lead to the same value of p_1^2.

3.3   Ray Trajectories

When the parameter L of the Epstein layer is large in comparison with a wavelength, the medium can be considered slowly varying, and the methods of geometrical optics can be used to find the ray trajectories. In this section, the ray family will be found by using the ray equation for a stratified medium given in Kelso [25]. The caustics of this family of rays will also be found and the

detailed behavior of these caustics as $L \to 0$ will be investigated and related to the half space problem.

First, the reflected rays in the homogeneous medium, $z \geq 0$, will be considered. These rays are straight lines given by

$$x/p - (z + z')/p_2 - L\pi/|p_1| = 0 \qquad (3.3.1)$$

where p_1 is imaginary for reflected rays, i.e., $p_1 = i|p_1|$. The same ray equation is recovered from the exact solution, (3.2.18), if $\bar{\Gamma}$ is replaced by its asymptotic approximation ($k_0 L \gg 1$) and then the saddle point condition is applied to the resulting integrand. The caustic is found by eliminating $|p_1|$ between (3.3.1) and the derivative of (3.3.1) with respect to $|p_1|$. We obtain

$$x^{2/3} = \left(\epsilon_1/\Delta\right)^{1/3} (z + z')^{2/3} + \left[(\pi L)^2/\Delta\right]^{1/3}. \qquad (3.3.2)$$

This caustic coincides with the critically reflected ray found in the half space problem in the limit as $L \to 0$.

The rays in the medium $z < 0$ are divided into three types: transmitted rays; critical ray; and, totally reflected rays. The transmitted rays are not of great interest to us. The critical ray is given by

$$x = \left(\epsilon_1/\Delta\right)^{\frac{1}{2}} \left[z' - L \sinh(z/L)\right], \quad |p_1| = 0. \qquad (3.3.3)$$

This ray never turns since z is a monotonically decreasing function of x. The totally reflected rays satisfy the equation

$$\cos w = 1 - 2|p_1|^2 p_2^{-2} \sinh^2(z/L) \qquad (3.3.4)$$

where

$$w = 2|p_1|(pL)^{-1}(x-x_0), \quad x_0 = p\, z'/p_2, \quad 0 \leq w \leq 2\pi.$$

These rays enter the inhomogeneous medium at $x = x_o$, turn at $x = x_o + x_t$, $\left(x_t = \pi p L (2 |p_1|)^{-1} \right)$ and return to the linear medium at $x = x_o + 2x_t$. A typical ray is shown in Fig. 3.1. The rays have been plotted for some typical parameters in Fig. 3.2.

The caustic formed by these returning rays is found by eliminating $|p_1|$ between the derivative of (3.3.4) with respect to $|p_1|$, i.e.,

$$\frac{\epsilon_1 x}{p^3 L} - \frac{\Delta z'}{p_2^3 L} = \frac{\epsilon_1 \Delta}{|p_1| p_2^2} \tan (\omega/2) \qquad (3.3.5)$$

and the ray equation, (3.3.4). The caustic is shown in Fig. 3.2. It consists of two branches: one that crosses the $z = 0$ line and connects to the caustic in the homogeneous space, and another that tends asymptotically toward the $z = 0$ line as $x \to \infty$. The ray and constraint equations can be solved exactly for the exit point of the first branch into the homogeneous medium. A calculation shows the exit point lies on the beginning of the free space caustic. The asymptotic character of the second branch can be found by assuming $p_2 \ll 1$. Using this approximation in the ray and constraint equations gives the asymptote

$$z/L = - z \left[(\Delta)^{\frac{1}{2}} x \right]^{-1} . \qquad (3.3.6)$$

This asymptote tends toward the interface as $L \to 0$.

As the two branches progress deeper into the inhomogeneous medium they meet in a cusp. The location of this cusp can be obtained with the additional constraint equation found by taking the derivative of (3.3.5) with respect to $|p_1|$. The result is
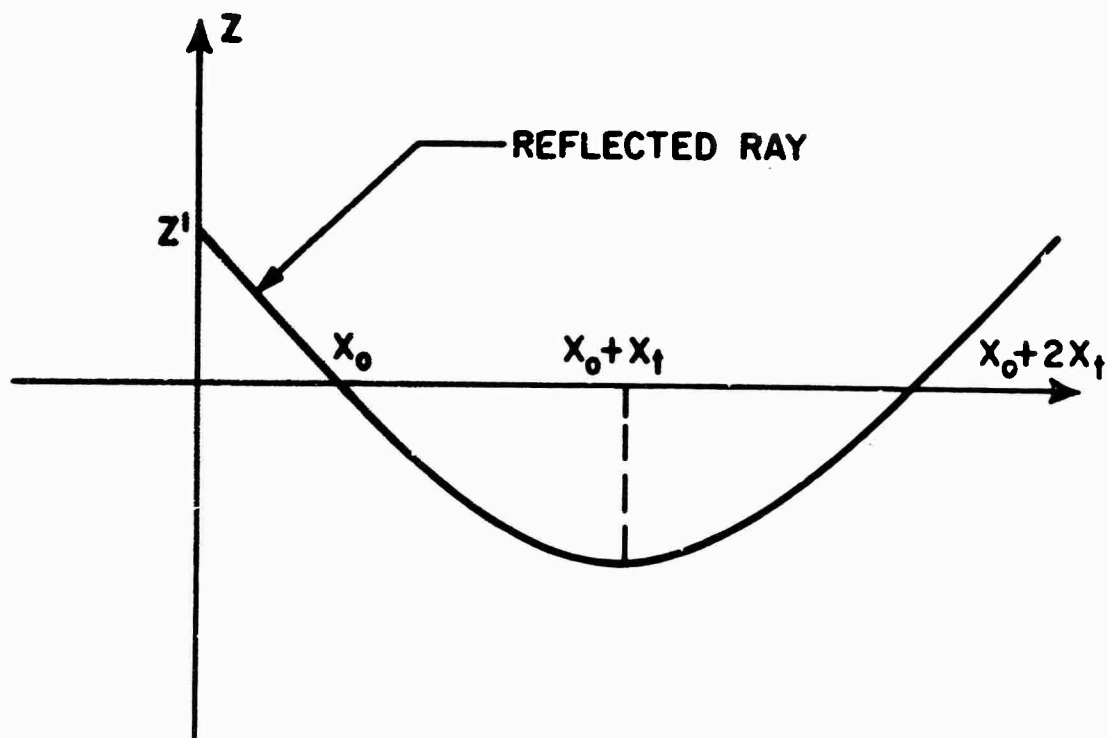
Fig. 3.1

Typical Reflected Ray
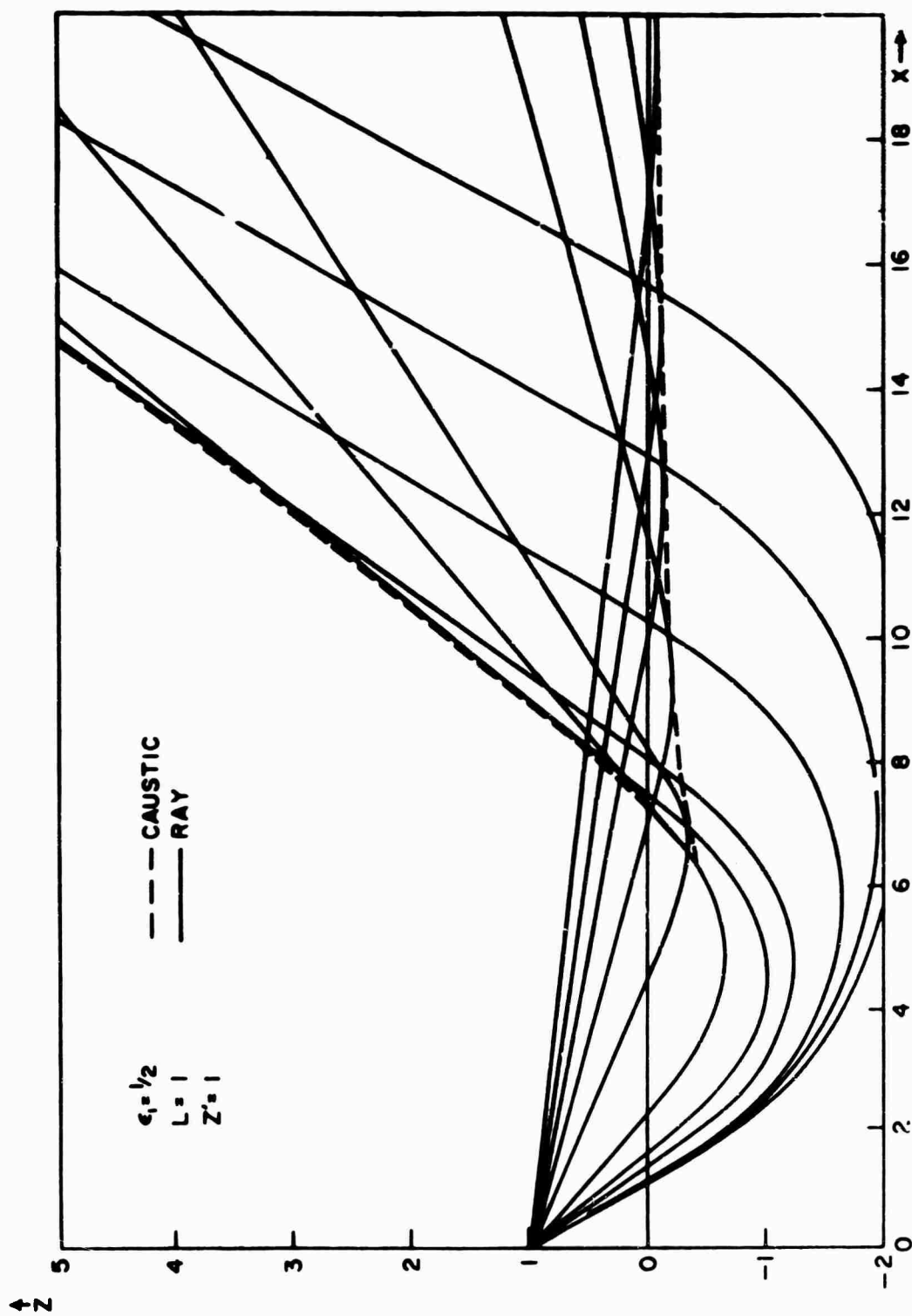
Fig. 3.2

Reflected Rays and Caustics From an Epstein Layer

$$\frac{3\epsilon_1 |p_1|^3 p_2^2 x}{\Delta^2 p^5 L} = -\tan^3(\psi/2) . \tag{3.3.7}$$

The simultaneous solution of (3.3.4), (3.3.5) and (3.3.7), will give us the coordinates of the cusp. Unfortunately, they could not be solved explicitly ; however, an asymptotic solution was obtained as $L \to 0$. The only nontrivial solution to this system of equations with small L is obtained when the $\tan(\psi/2)$ remains finite and non zero and $|p_1|$ is small. From (3.3.7), we then have

$$|p_1| \simeq \beta L^{1/3} , \tag{3.3.8}$$

where β is a constant to be determined. Putting this into (3.3.4) , (3.3.5) and (3.3.7) we find β obeys the transcendental equation.

$$\pi - \tan^{-1}\left[\beta\left(\frac{3z'}{\epsilon_1 \Delta^3/2} \right)^{1/3} \right] - \frac{\beta^3 z'}{\epsilon_1 \Delta^{3/2}} = -(3z' \epsilon_1^2)^{1/3} \Delta^{-\frac{1}{2}} \tag{3.3.9}$$

and the approximate location of the cusp for small L is

$$x = (\epsilon_1/\Delta)^{\frac{1}{2}} z' + O(L^{2/3}) ; \tag{3.3.10}$$

as $L \to 0$ the caustics and cusp approach the interface and transition region of the half space problem.

3.4 Uniform Asymptotic Solution

Writing the reflection coefficient in exponential form

$$\bar{\Gamma} = e^{i\psi} \tag{3.4.1}$$

and putting this into (3.2.18) gives us

$$E_{yr} = \frac{1}{4\pi i} \int_C \frac{p_1}{pp_2} e^{ik_0\left[p_2(z+z') + px + \frac{1}{k_0} \psi(p_1, (\Delta)^{\frac{1}{2}} \tau) \right]} dp_1 \tag{3.4.2}$$

where

$$\psi(p_1, (\Delta)^{\frac{1}{2}}\tau) = 2 \tan^{-1}\left\{\frac{2\Gamma(\nu/2 + \mu/2 + 1)\,\Gamma(\nu/2 - \mu/2 + 1)}{\tau p_2 \Gamma(\nu/2 - \mu/2 + 1/2)\Gamma(\nu/2 + \mu/2 + 1/2)}\tan\left[\frac{\pi}{2}(\nu + \mu)\right]\right\} \tag{3.4.3}$$

The multivaluedness of the function $\tan^{-1}$ does not appear in the overall integrand since $e^{2i\tan^{-1}}$ is single valued.

The uniform asymptotic evaluation of the above integral is performed by first finding the saddle points for all values of $0 < \tau < \infty$. In general, these saddle point locations will depend on the large parameter k_o and the normalized length τ. The location of these saddle points can be found: first, by the method of successive approximations and second, by using an asymptotic approximation to the function ψ for large τ. The first method is a generalized sharp interface technique and is valid when the length L is small compared to z' and k_o is large, while the second method gives the geometric-optic result and holds when τ is large. Since the two methods overlap for a restricted range of τ, the saddle point locations can be found for any τ.

The saddle point equation is given by

$$p_1\left[(z + z')/p_2 - x/p\right] + k_o^{-1}(d\psi/dp_1) = 0 \tag{3.4.4}$$

on the top sheet and

$$p_1\left[(z + z')/p_2 + x/p\right] + k_o^{-1}(d\psi/dp_1) = 0 \tag{3.4.5}$$

on the second sheet First, we will apply the method of successive approximations to (3.4.4) and (3.4.5). The solutions to (3.4.5) neglecting the perturbing term $k_o^{-1}(d\psi/dp_1)$ are

$$p_{1L}^{(0)} = 0 \quad , \quad p_{1r}^{(0)} = \pm i\left[x^2\Delta - (z+z')\,\epsilon_1^2\right]^{\frac{1}{2}} \tag{3.4.6}$$

where the saddle points p_{1L} and $p_{1r}(+)$ correspond to the lateral and reflected waves found in the half space problem. The superscript is used to denote the order of approximation. The first approximation is obtained by evaluating the perturbing term in (3.4.4) with the unperturbed values given in (3.4.6) and then assuming $p_1^{(1)} = p_1^{(0)} + \delta p_1$ with $\delta p_1 \ll 1$. The first order saddle points are:

$$p_{1L}^{(1)} = (\epsilon_1)^{\frac{1}{2}}(k_o L_p)^{-1}(d\psi/dp_1)\Big|_{p_1 = 0}, \quad L_p = x - (\epsilon_1/\Delta)^{\frac{1}{2}}(z + z') \qquad (3.4.7)$$

$$p_{1r}^{(1)} = p_{1r}^{(0)} - \left\{ \left[(\Delta)^{\frac{1}{2}} k_o L_p (z/p_2^3 + x/p^3)(x(\Delta)^{\frac{1}{2}} + z(\epsilon_1)^{\frac{1}{2}}) \right]^{-1}(d\psi/dp_1) \right\}\Big|_{p_1 = p_{1r}^{(0)}} \qquad (3.4.8)$$

where L_p is the distance the lateral wave travels along the interface in the half space problem. The approximate method is only valid when $\delta p_1 \ll 1$. For this to be true it is sufficient to have

$$(k_o L_p)^{-1} \left| \frac{d\psi\left(p_1, \tau(\Delta)^{\frac{1}{2}}\right)}{dp_1} \right| \ll 1, \quad 0 \le \tau < \infty, \quad \mathrm{Re}\, p_1 = 0, \quad 0 \le \mathrm{Im}\, p_1 < (\Delta)^{\frac{1}{2}}. \qquad (3.4.9)$$

One can show for small and moderate values of τ that $d\psi(p_1(\Delta)^{\frac{1}{2}}\tau)/dp_1$ is bounded except at $p_2 = 0$ and for large values of τ that $d\psi/dp_1 \sim i\pi\tau$. With the aid of the above information, we see the method of successive approximations is valid when

$$k_o L_p \gg 1 \quad , \quad L/L_p \ll 1, \quad 0 \le \tau < \infty. \qquad (3.4.10)$$

When the method of successive approximation is applied to (3.4.5), one saddle point is found on the negative imaginary axis near the origin.

The second method of finding the saddle points is to use the asymptotic approximations for the Gamma functions in (3.4.4) and (3.4.5). The resulting saddle point equations are
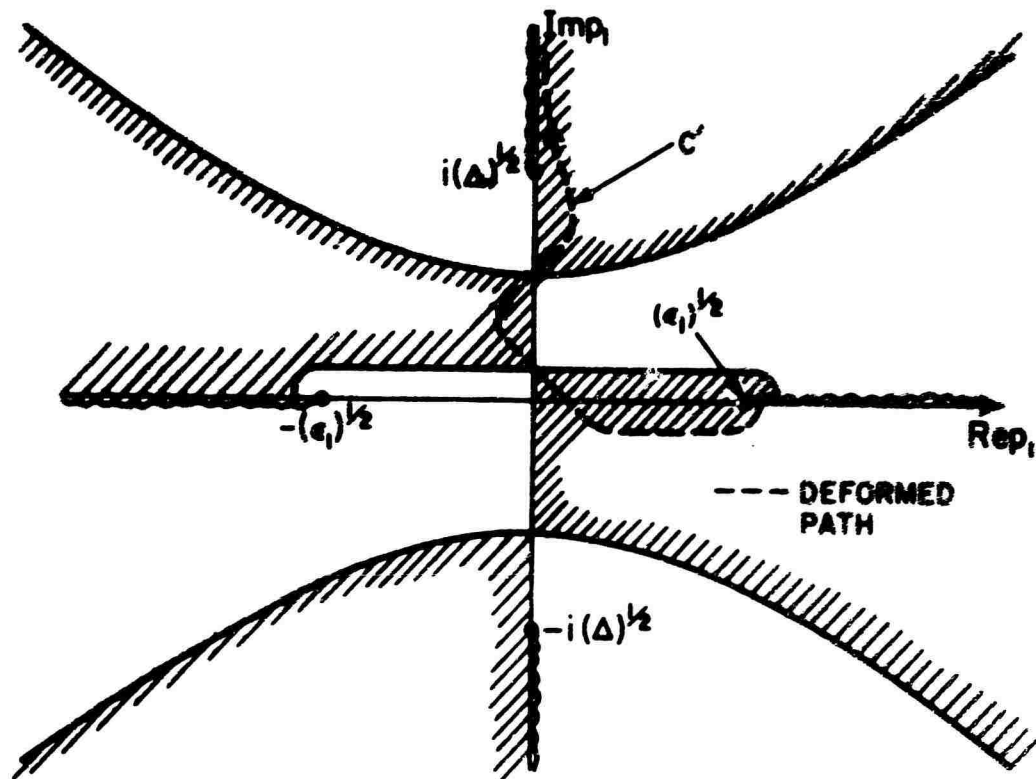
Fig. 3.3

Top Sheet of Riemann Surface-Decay Regions
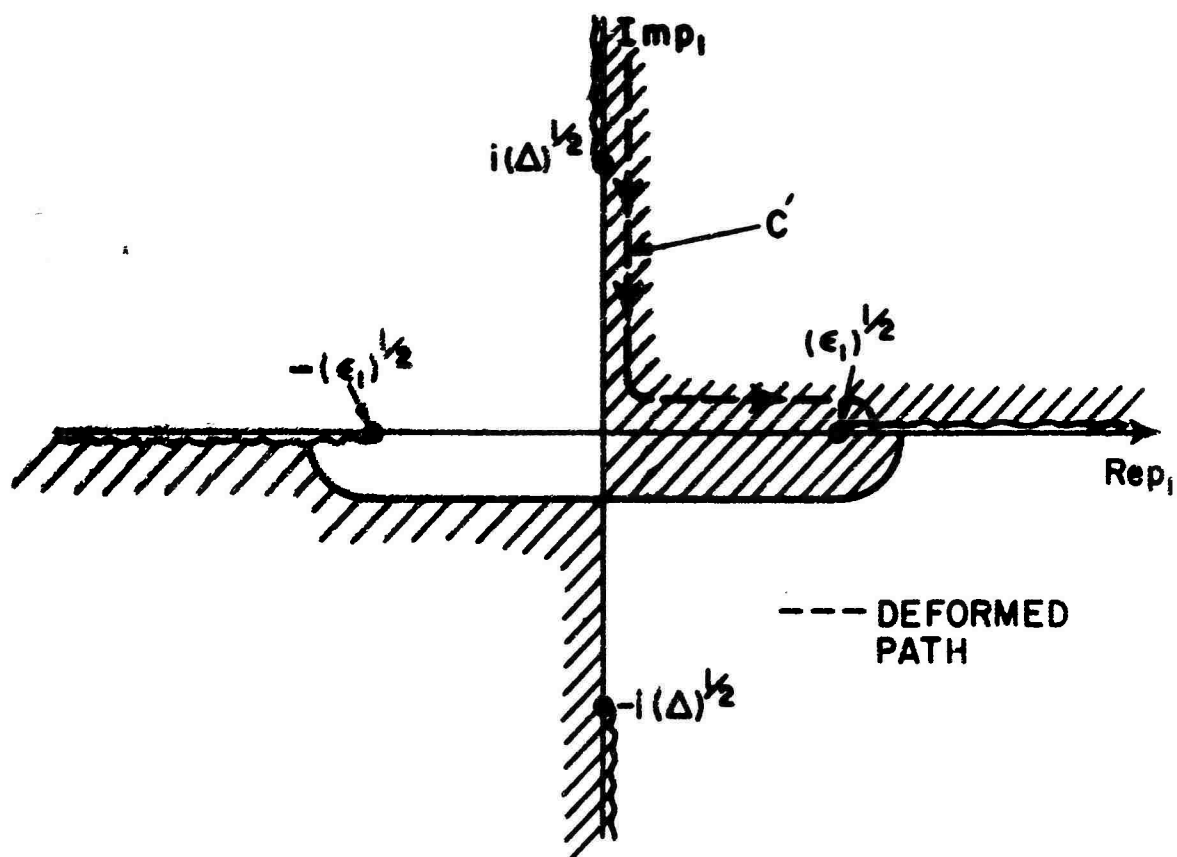
Fig. 3.4

Second Sheet of Riemann Surface-Decay Regions

$$p_1 \left(\frac{z + z'}{p_2} \mp \frac{x}{p} \right) + i n L = 0, \quad \begin{cases} - \text{ top sheet} \\ + \text{ second sheet} \end{cases} . \qquad (3.4.11)$$

Here again, we obtain a similar arrangement of saddle points to those obtained by the method of successive approximation. Three saddle points appear on the imaginary axis of the top sheet. Two occur for $0 < \text{Im} \, p_1 < (\Delta)^{\frac{1}{2}}$ and one occurs for $-(\Delta)^{\frac{1}{2}} < \text{Im} \, p_1 < 0$. On the bottom sheet we find only one saddle point on the imaginary axis for $-(\Delta)^{\frac{1}{2}} < \text{Im} \, p_1 < 0$. Solutions to (3.4.11) give a good approximation to saddle point location for arbitrary L/L_p and $\tau \gg 1$. The two approximate methods have a common region of validity when $\tau \gg 1$ and $L/L_p \ll 1$.

The decay regions relative to the saddle points have been investigated in Appendix C.[*] They are shown in Figs. 3.3 and 3.4. The shaded areas correspond to decay regions of the integrand. The integration path, C, will now be deformed into the path C′ as shown in Figs. 3.3 and 3.4. The deformed path has been chosen to go through the two saddle points which lie on the integration path, and everywhere else to lie in a decay region. In Appendix B, an investigation of the singularities of the integrand that lie between the original and deformed path is made. There, it is found that those singularities give rise to residue contributions which are, at most, an exponentially small order, and can be neglected. As a result, the integrals over the two paths are asymptotically equivalent.

Since the deformed path, C′, lies in a decay region except at the two saddle points, the integral

---

[*] The saddle points and decaying regions are for the dominant term of the asymptotic expansion of the integrand. Other terms in the integrand's asymptotic expansion will not affect our results.

$$E_R = \frac{1}{4\pi i} \int_{C'} \frac{P_1}{PP_2} e^{ik_o\left[P_2(z-z') + px + \frac{1}{k_o}\phi(p_1, \Delta^{\frac{1}{2}}\tau)\right]} \qquad (3.4.12)$$

is asymptotically equal to the two saddle point contributions. The method of steepest descent can be used to evaluate this integral if we generalize the method to include saddle points which depend on the large parameter k_o[26].

The dominant term of the asymptotic expansion of the integral

$$I = \int_{S.D.\,o.} \frac{P_1}{PP_2} e^{ik_o\phi(p_1, k_o)} dp_1 \qquad (3.4.13)$$

where

$$\phi(p_1, k_o) = P_2(z+z') + px + \frac{1}{k_o}\phi(p_1, (\Delta)^{\frac{1}{2}}\tau) \qquad (3.4.14)$$

and the path of integration is the steepest descent path, S.D.P. is given by

$$I \sim i\,k_o^{-\frac{1}{2}} G(0) e^{ik_o\phi(p_{1s}, k_o)} \qquad (3.4.15)$$

where

$$G(0) = \pm\left[P_{1s}/(p_s P_{2s})\right]\left[2\pi/|\phi''(p_{1s})|\right]^{\frac{1}{2}} e^{\pm i\pi/4}. \qquad (3.4.16)$$

Here we denoted the second derivative of $\phi(p, k_o)$ with respect to p_1 as $\phi''(p_{1s})$ and have assumed there is only one saddle point, p_{1s}, on the S.D.P. The choice of the + or - sign depends on the direction of the path and sign of $\phi''(p_{1s})$. The above evaluation is good only if no singularities of the integrand approach the saddle point as k_o becomes large. For the saddle points treated in this paper this is the case as is shown in Appendix B.

The asymptotic evaluation of (3.4.12) is now performed. For L going to zero, we can identify the contribution of the lower saddle point as the lateral wave, while that of the upper saddle point is the reflected wave. This

identification will be retained for arbitrary values of L, i.e.;

$$E_{yr} \sim E_L + E_r \tag{3.4.17}$$

where

$$E_L = \frac{P_{1L} \, e^{i k_o \left[p_{2L}(z+z') + p_L x + k_o^{-1} \psi\left(p_{1L}, (\Delta)^{\frac{1}{2}}\tau\right)\right] + i\pi/4}}{2(2\pi)^{\frac{1}{2}} P_L P_{2L} \left[\frac{x}{p_L} - \frac{z+z'}{p_{2L}} + p_{1L}^2 \left(\frac{z+z'}{p_{2L}^3} + \frac{x}{p_L^3}\right) - \frac{1}{k_o} \psi''\left(p_{1L}, (\Delta)^{\frac{1}{2}}\tau\right)\right]^{\frac{1}{2}} k_o^{\frac{1}{2}}} \tag{3.4.18}$$

and

$$E_r = \frac{P_{1r} \, e^{i k_o \left[p_{2r}(z+z') + p_r x + k_o^{-1} \psi\left(p_{1r}, (\Delta)^{\frac{1}{2}}\tau\right)\right] + i\,3\pi/4}}{2(2\pi)^{\frac{1}{2}} P_r P_{2r} \left[\frac{z+z'}{p_{2r}} - \frac{x}{p_r} - p_{1r}^2 \left(\frac{z+z'}{p_{2r}^3} + \frac{x}{p_r^3}\right) + \frac{1}{k_o} \psi''\left(p_{1r}, (\Delta)^{\frac{1}{2}}\tau\right)\right]^{\frac{1}{2}} k_o^{\frac{1}{2}}} \tag{3.4.19}$$

with ψ'' being the second derivative of ψ with respect to p_1. The positive sign has been chosen for p_{1r} in (3.4.6) and

$$p_{1L} = p_{1L}^{(1)} \quad , \quad p_{2L} = (\Delta + p_{1L}^2)^{\frac{1}{2}} \quad , \quad p_L = (\epsilon_1 - p_{1L}^2)^{\frac{1}{2}}$$

$$p_{1r} = p_{1r}^{(1)} \quad , \quad p_{2r} = (\Delta + p_{1r}^2)^{\frac{1}{2}} \quad , \quad p_r = (\epsilon_1 - p_{1r}^2)^{\frac{1}{2}} \ .$$

Since $\psi''(p_{1r}, (\Delta)^{\frac{1}{2}}\tau)/k_o \sim O(k_o^{-1})$ for all τ, it can be neglected in (3.4.18) and (3.4.19) if only the dominant term of the asymptotic approximation is desired.

It is interesting to see how these integrals reduce when τ is in the range where the saddle points can be obtained by the method of successive approximations, i.e., (3.4.7) and (3.4.8). The contribution from the reflected wave part of the integral is

$$E_r \sim \frac{|P_{1r}| e^{ik_o\left[P_{2r}(z+z')+px+k_o^{-1}\psi\left(P_{1r}, (\Delta)^{\frac{1}{2}}\tau\right)\right]+i\pi/4}}{2(2\pi)^{\frac{1}{2}}P_r P_{2r}\left[\frac{z+z'}{P_{2r}}-\frac{x}{P_r}-P_{1r}^2\left(\frac{z+z'}{P_{2r}^3}+\frac{x}{P_r^3}\right)\right]^{\frac{1}{2}}k_o^{\frac{1}{2}}} \qquad (3.4.20)$$

where

$$P_{1r} = \left\{x^2\Delta-(z+z')^2\epsilon_1\right\}^{\frac{1}{2}} .$$

This is the same contribution one would obtain from a sharply bounded half space problem except for the additional phase term. When the method of successive approximations is applied to E_L, we find

$$E_L \sim \frac{\epsilon_1^{1/4} A\left[(\Delta)^{\frac{1}{2}}\tau\right] e^{ik_o\left[\Delta^{\frac{1}{2}}(z+z')+(\epsilon_1)^{\frac{1}{2}}x+k_o^{-1}\psi\left[(\Delta)^{\frac{1}{2}}\tau\right]\right]+i3\pi/4}}{(2\pi)^{\frac{1}{2}}\Delta\left(k_o L_p\right)^{3/2}} \qquad (3.4.21)$$

where

$$\psi\left[(\Delta)^{\frac{1}{2}}\tau\right] = \psi(0, (\Delta)^{\frac{1}{2}}\tau) = 2\tan^{-1}\left|\frac{2\Gamma^2(\nu/2+1)}{\tau(\Delta)^{\frac{1}{2}}\Gamma^2(\nu/2+1/2)}\tan(\pi\nu/2)\right| \qquad (3.4.22)$$

and

$$A\left[(\Delta)^{\frac{1}{2}}\tau\right] = (\Delta/4)^{\frac{1}{2}}(d\psi/dp_1)\Big|_{P_1=0} = \frac{\pi\tau^2\Delta\sec^2(\pi\nu/2)\Gamma^2(\nu/2+1)\Gamma^2(\nu/2+1/2)}{4\tan^2(\pi\nu/2)\Gamma^4(\nu/2+1)+\tau^2\Delta\Gamma^4(\nu/2+1/2)} . \qquad (3.4.23)$$

Equation (3.4.21) in the limit of small τ reduces to

$$E_L \sim \frac{\epsilon_1^{1/4}}{(2\pi)^{\frac{1}{2}}\Delta(k_o L_p)^{3/2}}e^{ik_o\left(\Delta^{\frac{1}{2}}(z+z')+\epsilon_1^{\frac{1}{2}}x\right)+i3\pi/4} , \tau \ll 1 . \qquad (3.4.24)$$

This is the same as a lateral wave on a dielectric half space. On the other hand, if we assume τ is large enough, the asymptotic approximation for the
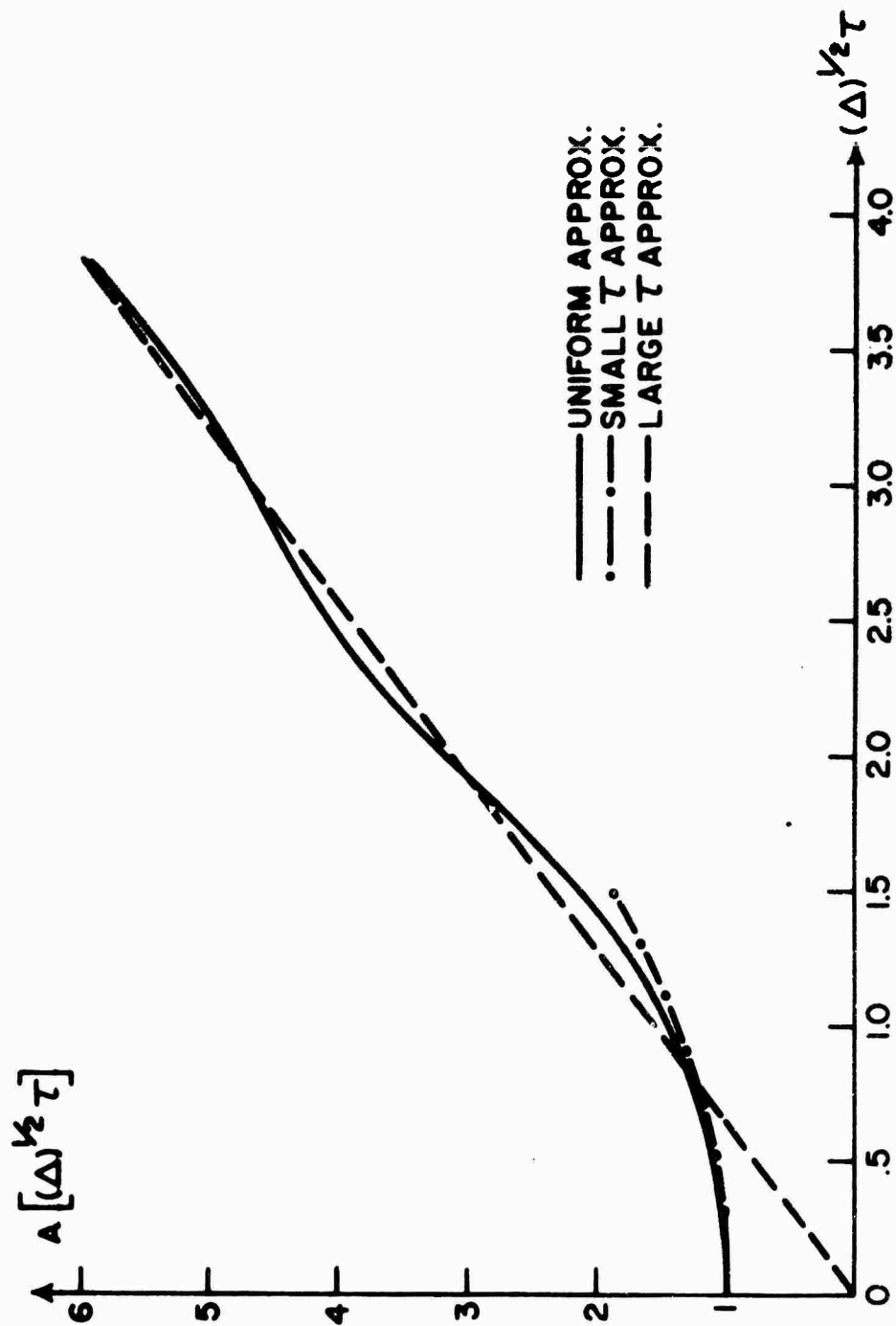
Fig. 3.5

Lateral Wave Amplitude vs. Normalized Transition Thickness
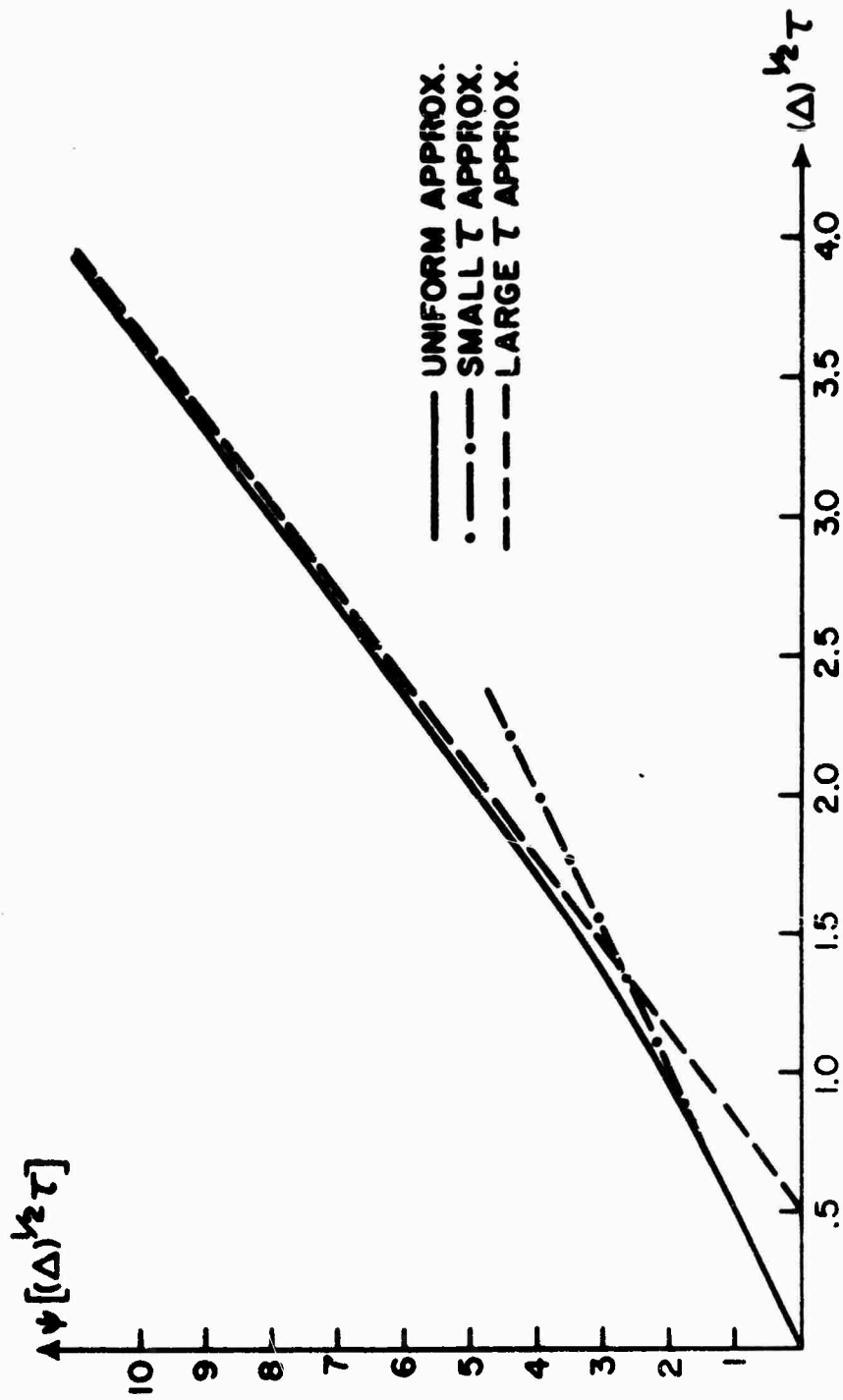
Fig. 3.6

Lateral Wave Phase vs. Normalized Transition Thickness

Gamma functions can be used and we obtain the geometric optical result.
It is

$$E_L \sim \frac{\pi^{\frac{1}{2}} c_1^{1/4} L}{2(2\Delta)^{\frac{1}{2}} L_p (k_o L_p)^{\frac{1}{2}}} e^{ik_o\left[\Delta^{\frac{1}{2}}(z+z') + (c_1)^{\frac{1}{2}}x + \pi L (\Delta)^{\frac{1}{2}}\right] + i\pi/4} \qquad (3.4.25)$$

The lateral wave amplitude, $A\left[(\Delta)^{\frac{1}{2}}\tau\right]$ and phase, $\psi\left[(\Delta)^{\frac{1}{2}}\tau\right]$, have been
plotted in Figs. 3.5 and 3.6 respectively. The straight line (shown dotted)
appearing in both graphs is the approximate solution when the transition is
slowly varying with respect to wavelength. The dash-dot line is the approximate
solution when the transition region is small compared with wavelength. In this
case the reflection coefficient has been approximated by the first few terms
of the Taylor series expansion of $\bar{\Gamma}$ about $\tau = 0$, i.e.

$$\bar{\Gamma} = \frac{P_2 - P_1}{P_2 + P_1} + \frac{2i\Delta P_2}{\left(P_2 + P_1\right)^2} \tau - 2\frac{P_1 P_2 \left(P_2 + P_1\right)\gamma + \Delta^2 P_2}{\left(P_2 + P_1\right)^3} \tau^2, \quad \tau \ll 1 \qquad (3.4.26)$$

where

$$\gamma = 2\Delta\ln 2 + O(P_1^2) .$$

The lateral wave contribution to each term in (3.4.26) was found and then these
three lateral wave contributions were cast in the form of (3.4.21) to give an
approximate lateral wave amplitude $A\left[(\Delta)^{\frac{1}{2}}\tau\right]$ and phase $\psi\left[(\Delta)^{\frac{1}{2}}\tau\right]$.

3.5 CONCLUSION

For purposes of investigating the high frequency reflected field from
the symmetrical Epstein layer the homogeneous half-space, $z \geqslant 0$, divides
naturally into two regions: first, the region between the z axis and the

caustic(Fig. 3.2) where the reflected field is exponentially small and , second, the region to the right of the caustic where there are two major contirubtions to the field at each point. The first of these contributions is the reflected ray contribution , (3.4.20) , whose amplitude variation with frequency is $k_o^{\frac{1}{2}}$. The frequency dependence does not change as τ is varied. The second field contribution to the right of the caustic (3.4.21) has an ampli - tude which is dependent on τ . For small τ the contribution approximates a lateral wave on a sharp interface whose amplitude dependence is $(k_o L_p)^{-3/2}$. The caustic in Fig. 3.2 provides the natural boundary for this contribution since for small τ it coincides with the critically reflected ray in the sharp interface problem. When τ becomes large, this second field contribution changes character from a lateral ray to a reflected ray contribution. The amplitude dependence now has a $(k_o L_p)^{\frac{1}{2}}$ variation. Approximate forms of the second contribution are given in (3.4.24) and (3.4.25) for small and large τ respectively. An examination of these two expressions shows that the lateral distance dependence $L_p^{-3/2}$ remains unchanged as τ is varied.

The two field contributions to the right of the caustic correspond to the rays through each point in this region. In the homogeneous region the rays that make up the caustic are the rays that correspond to the contribution E_L , given in (3.4.21) . The rays that form the caustic which approaches the $z = 0$ line asymptotically correspond to the contribution E_r , or (3.4.20) . Identifi- cation of contributions corresponding to rays that pass near the focus is more difficult and must be considered when L is small.

In Chapters 1 and 2 we found that a lateral wave was excited on the layer for all values of τ . This lateral wave changed its amplitude dependence on frequency from $(k_o L_p)^{-3/2}$ to $(k_o L_p)^{-7/6}$ for the linear layer and from $(k_o L_p)^{-3/2}$ to $(k_o L_p)^{-1}$ for the parabolic layer as τ went from small to large values. This contribution, however, always remained a diffraction effect, not predictable by

classical geometric - optics. In the Epstein transition treated in this chapter the lateral wave is excited for small τ but as τ becomes large this contribution becomes a reflected wave, which can be predictable solely on the basis of geometrical optics. This shows that the added continuity of the dielectric transition has a marked effect on the behavior of the lateral wave. The transition chosen in this chapter has the drawback that it has an infinite width. This has the effect that a ray which emerges from the inhomogeneous medium, having traveled a large distance along the interface, penetrates deeply into the stratified medium. It would be of interest to investigate transitions with a finite width but more continuity than the layers treated in Chapters 1 and 2 .

CHAPTER 4.

THE DOUBLE EXPONENTIAL TRANSITION LAYER

4.1 Introduction

In the last chapter the reflected fields from half of a symmetrical
Epstein layer were investigated for arbitrary layer thickness. When the
layer thickness was large in comparison to wavelength, the reflected field
was composed of geometrical-optic rays forming a two branched caustic
which met in a cusp. As the layer thickness decreased, a portion of these
reflected waves changed character and formed a lateral wave.

As the next step in our investigation of the reflected field from
transition layers, it would be ideal for us to study a dielectric profile that
is completely continuous, i. e., one having all derivatives of $\epsilon(z)$ continuous
for $-\infty < z < \infty$. The Epstein[4] transition layer is an example of such a profile
but the asymptotic properties of the wave functions have not been investi-
gated in enough detail to make the problem manageable.

Since this is not possible at present, we will study the double exponential
medium instead. This transition is composed of an exponential function which
approaches ϵ_1 as $z \to -\infty$ for $z < 0$ and an exponential function which approaches
1 as $z \to \infty$ for $z > 0$. At $z = 0$ the profile and its derivative are continuous. The
double exponential profile is similar to the Epstein profile since they are both
composed of inhomogeneous medium for all z. The two are different since
the double exponential medium is not completely continuous for all z. In fact,
the double exponential medium has a discontinuous second derivative of $\epsilon(z)$;
this was the case for the symmetrical Epstein layer considered in Chapter 3.

In this chapter we shall: first, evaluate the reflected fields when the
transition is thick compared to wavelength, and second, evaluate the reflected

fields for arbitrary transition thickness where the source and observation points are many transition thicknesses from the layer. We will determine if the lateral wave in this medium changes its character as observed in Chapter 3 and note what effects occur from the placement of the source in an inhomogeneous medium.

4.2 Statement of Problem and Formal Integral Representations

Consider a dielectric profile given by

$$\epsilon(z) = \begin{cases} 1 - [\Delta/2] \, e^{-2z/L} & , \quad z \geq 0 \\ \epsilon_1 + [\Delta/2] e^{+2z/L} & , \quad z < 0 \end{cases} \qquad \Delta = 1 - \epsilon_1 \qquad (4.2.1)$$

where an electric line current source is located at $x = 0$, $z = z'$, $z' > 0$ and parallel to the y axis. It is assumed, as before, that the $e^{-i\omega t}$ time dependence is understood. Because of the source location only the y component of the electric field, E_y, is excited and it obeys the equation

$$\left[\frac{d^2}{dx^2} + \frac{d^2}{dz^2} + k_o^2 \, \epsilon(z) \right] E_y = -\delta(x) \, \delta(z-z') \qquad (4.2.2)$$

The source magnitude has been adjusted to make the coefficient of the delta function -1 and is given by Eq. (1.2.2). Since the medium is uniform in the x direction, it becomes convenient to introduce the transformation

$$E_y = \frac{k_o}{2\pi} \int_{-\infty}^{+\infty} \psi(z,p) \, e^{ik_o p} \, dp \qquad (4.2.3)$$

into Eq. (4.2.2). The resulting equation for $\psi(z,p)$ is given by

$$\left[\frac{d^2}{dz^2} + k_o^2 \left(\epsilon(z) - p^2 \right) \right] \psi(z,p) = -\delta(z-z') \qquad (4.2.4)$$

where $\psi(z,p)$ must obey the radiation condition as $z \to \pm\infty$. The above

equation is a one dimensional Green's function problem. The Green's function $\psi(z,p)$ is given by Friedman[27] as

$$\psi(z,p) = \frac{\psi_1(z_<)\,\psi_2(z_>)}{W(\psi_2,\psi_1)} \qquad (4.2.5)$$

where ψ_2 and ψ_1 are homogeneous solutions of Eq. (4.2.4) which satisfy the radiation condition at plus and minus infinity respectively. The notation $z_<$ means that $z_<$ is equal to the lesser of z or z' while $z_>$ means that $z_>$ is greater of z or z'. The denominator of Eq. (4.2.5) is the Wronskian of ψ_2 and ψ_1 which is defined by

$$W(\psi_2,\psi_1) = \psi_2(z)\,d\psi_1(z)/dz - \psi_1(z)\,d\psi_2(z)/dz \ . \qquad (4.2.6)$$

We will now restrict ourselves to finding $\psi(z,p)$ in the region $z \geq 0$. Upon introducing the dielectric profile $\epsilon(z)$ for $z > 0$ into Eq. (4.2.4) and using Abromowitz[28], we find that the homogeneous solution $\psi_2(z)$ is given by

$$\psi_2(z) = J_{\nu_2}(-i\lambda\,e^{-z/L}) \ , \quad z \geq 0 \qquad (4.2.7)$$

where $J_\nu(z)$ is the Bessel function of order ν and argument z. The symbols ν_2 and λ are defined by

$$\nu_2 = -i\tau\sqrt{\epsilon_2 - p^2} \ , \quad \lambda = \tau\sqrt{\frac{\Delta}{2}} \quad , \quad \tau = k_o L \ . \qquad (4.2.8)$$

The solution $\psi_1(z)$ is given by

$$\psi_1(z) = \begin{cases} A\,J_{\nu_1}(\lambda\,e^{z/L}) & , z \leq 0 \\[12pt] J_{-\nu_2}(-i\lambda\,e^{-z/L}) + \overline{\Gamma}\,J_{\nu_2}(-i\lambda\,e^{-z/L}) \ , & z \geq 0 \end{cases} \qquad (4.2.9)$$

where A is constant independent of z, $\nu_1 = -i\tau\sqrt{\epsilon_1 - p^2}$ and

$$\bar{\Gamma} = - \frac{J_{-\nu_2}(-i\lambda) J'_{\nu_1}(\lambda) - i J_{\nu_1}(\lambda) J'_{-\nu_2}(-i\lambda)}{J_{\nu_2}(-i\lambda) J'_{\nu_1}(\lambda) - i J_{\nu_1}(\lambda) J'_{\nu_2}(-i\lambda)} \quad . \tag{4.2.10}$$

The prime over the Bessel function indicates differentiation with respect to the argument. The solution $J_{\nu_1}(\lambda e^{z/L})$ satisfies the radiation condition as $z \to -\infty$ while the functions $J_{\nu_2}(-i\lambda e^{-z/L})$ and $J_{-\nu_2}(-i\lambda e^{-z/L})$ are two independent homogeneous solutions of Eq. (4.2.4) for $z > 0$. A linear combination of these solutions is used for $\psi_1(z)$ in such a way as to make $\psi_1(z)$ and $d\psi_1(z)/dz$ continuous at $z = 0$. The Wronskian $W(\psi_2, \psi_1)$ is found to be

$$W(\psi_2, \psi_1) = (2/\pi L) \sin \nu_2 \pi \tag{4.2.11}$$

by using Abramowitz[29]. By substituting $\psi_1(z)$, $\psi_2(z)$ and $W(\psi_2, \psi_1)$ in Eq. (4.2.5) and then using the resulting expression for $\psi(z, p)$ in Eq. (4.2.3), the formal integral representation for E_y is obtained. It is

$$E_y = \frac{\tau}{4} \int_{-\infty}^{+\infty} [\sin(\pi\nu_2)]^{-1} J_{-\nu_2}\left[-i\lambda \exp(-z_< /L)\right] J_{\nu_2}\left[-i\lambda \exp(-z_> /L)\right] e^{ik_o px} dp$$

$$\tag{4.2.12}$$

$$+ \frac{\tau}{4} \int_{-\infty}^{+\infty} \frac{\bar{\Gamma}}{\sin(\nu_2\pi)} J_{\nu_2}\left[-i\lambda \exp(-z_< /L)\right] J_{\nu_2}\left[-i\lambda \exp(-z_> /L)\right] e^{ik_o px} dp \quad .$$

For these integrals to be completely defined, the square roots

$$p_1 = \sqrt{\epsilon_1 - p^2} \quad , \qquad p_2 = \sqrt{\epsilon_2 - p^2}$$

must be properly defined on a four sheeted Riemann surface which is shown in Fig. 1.4 . The multivalued character of the Bessel function need not concern us since the integration variable is not contained in the argument of any of the Bessel functions in Eq. (4.2.12) .

If we allow $\tau \to 0$, Eq. (4.2.12) reduces to

$$E_y = -\frac{1}{4\pi i} \int_{-\infty}^{+\infty} \frac{e^{ik_o(p_2|z-z'| + px)}}{p_2} \, dp$$

$$-\frac{1}{4\pi i} \int_{-\infty}^{+\infty} \frac{\bar{\Gamma}}{p_2} e^{ik_o[p_2(z+z') + px]} \, dp \quad , \quad \bar{\Gamma} = \frac{p_2 - p_1}{p_2 + p_1} \quad . \tag{4.2.13}$$

We see from the last equation that as $\tau \to 0$, or as the layer becomes thin compard to wave length, the formal integral representation, given in Eq. (4.2.12), reduces to the half space integral representation.

As in Chapter 1, the branch points at $p = \pm\sqrt{\epsilon_1}$ are now removed by means of the transformation

$$p = \sqrt{\epsilon_1 - p_1^2} \quad , \quad p_1 = \sqrt{\Delta + p_1^2} \quad .$$

This transforms the integral in Eq. (4.2.12) to

$$E_y = -\frac{\tau}{4} \int_C \frac{p_1}{p \sin(\pi\nu_2)} \, J_{-\nu_2}\left[-i\lambda \exp(-z_</L)\right] J_{\nu_2}\left[-i\lambda \exp(-z_>/L)\right] e^{ik_o px} \, dp_1$$

$$-\frac{\tau}{4} \int_C \frac{p_1 \, \bar{\Gamma}}{p \sin(\pi\nu_2)} \, J_{\nu_2}\left[-i\lambda \exp(-z_</L)\right] J_{\nu_2}\left[-i\lambda \exp(-z_>/L)\right] e^{ik_o px} \, dp_1 \quad . \tag{4.2.14}$$

where the multivalued functions p, p_2 are defined on a four sheeted Riemann surface. The first two sheets of this surface are shown in Fig. 1.5 and 1.6.

For reasons that will become obvious at a later point, it would be advantageous to obtain a different form of Eq. (4.2.14). This can be done by using the relation

$$J_{-\nu}(z) = e^{\nu\pi i} J_\nu(z) - i\sin(\pi\nu) H_\nu^{(2)}(z) \tag{4.2.15}$$

in Eq. (4.2.14). The resulting integral representation is

$$E_y = \frac{i\tau}{4} \int_C \frac{P_1}{P} H^{(2)}_{\nu_2}\left[-i\lambda \exp(-z_</L)\right] J_{\nu_2}\left[-i\lambda \exp(-z_>/L)\right] e^{ik_o px} dp_1$$

$$+ \frac{i\tau}{4} \int_C \frac{P_1}{P} \tilde{\Gamma} J_{\nu_2}\left[-i\lambda \exp(-z_</L)\right] J_{\nu_2}\left[-i\lambda \exp(-z_>/L)\right] e^{ik_o px} dp_1 \tag{4.2.16}$$

where

$$\tilde{\Gamma} = \frac{H^{(2)}_{\nu_2}(-i\lambda) J'_{\nu_1}(\lambda) - i J_{\nu_1}(\lambda) H'_{\nu_2}(-i\lambda)}{J_{\nu_2}(-i\lambda) J'_{\nu_1}(\lambda) - i J_{\nu_1}(\lambda) J'_{\nu_2}(-i\lambda)} . \tag{4.2.17}$$

4.3 Asymptotic Evaluation of Integral Representation for Large $k_o L$

4.3.1. General Considerations

Since the integral representations for E_y which have been presented in the last section are too complicated to be integrated directly, approximate procedures must be used to simplify the integrals further. If we assume that the medium is slowly varying with respect to a wave-length and that the observation point is not near the source, we can asymptotically approximate the integral representation. To be more specific : if the medium is slowly varying, i.e., $k_o L \gg 1$, the uniform asymptotic approximations to the Bessel functions can be used to simplify the integrand of Eqs. (4.2.14) and (4.2.16). By using this simplified form of the integrand, the integrals in Eqs. (4.2.14) and (4.2.16) can by asymptotically approximated by the method of steepest descents for large $k_o r$ where $r = \sqrt{x^2 + z^2}$.

Before proceeding with the asymptotic evaluation of the exact solution, the methods of geometric-optics will be applied to the problem in the next section, 4.3.2. This will allow us to represent the field as a sum of ray contributions. The ray family will be investigated in detail with its associated caustics and foci. A comparison of the field contributions, obtained

from the asymptotic evaluation, will be performed in section 4.3.3., and
the method of geometric-optics will clearly distinguish the geometric-optic
from the diffraction effects.

4.3.2   Rays in a Double Exponential Medium

a.   Description of Ray Regions

As stated in the last section, the methods of geometric-optics will now
be applied to the double exponential medium. We will assume $k_o L \gg 1$ since
the method requires the medium to be slowly varying with respect to wave-
length. By using this method, the field can be characterized by a family of
rays emanating from the source. In this section the structure of this ray
family will be studied including its associated caustics and foci. Also a
detailed investigation of this ray family will be made as $L \to 0$ while keeping
$k_o L$ large. This limiting ray family is important since a comparison, with
the ray family for a sharp interface problem, gives important clues to the
changing nature of the lateral wave a L increases.

The ray trajectories can be obtained by an integration of the ray
equation i.e.,

$$x = \pm \int_{z'}^{z} \frac{p d\tau}{[\epsilon(\tau) - p^2]^{\frac{1}{2}}}$$ (4.3.1)

where the plus and minus signs are used for rays with positive and
negative slope respectively. The symbol p, used above, is the ray para-
meter and is related to the initial ray angle θ_o by $p = \sqrt{\epsilon(z')} \sin\theta_o$; the angle
θ_o is measured between the tangent to the ray emerging from the source and
the line $z = z'$, $x > 0$, and is considered positive in the clockwise direction.

The rays divide naturally into three types : direct, reflected and trans-
mitted rays. The direct rays are restricted to three regions of the x - z
plane as shown by the Roman numerals in Fig. 4.1. Region I is bounded by

a portion of the z axis and the glancing ray, i.e., the ray emitted from the source at $\theta = 0$. The name, "glancing ray", stems from the fact that the ray just glances along the interface in the limiting case of an abrupt interface $(L \to 0)$. The glancing ray's trajectory is given by

$$x/L = \frac{(1-\Delta/2 \, e^{-2z'/L})^{\frac{1}{2}}}{\sqrt{\Delta/2} \, e^{-z'/L}} \cosh^{-1}\left(e^{(z-z')/L}\right) \, . \qquad (4.3.2)$$

Region II is bounded by the locus of turning points and the critical ray. The equations, describing the locus of turning points, are given in Eqs. (4.3.4) and (4.3.8) and will be discussed in detail at a later point. The critical ray is emitted from the source at the angle θ_c where θ_c is the critical angle given by $\theta_c = \sin^{-1}\sqrt{\epsilon_1/\epsilon(z')}$. This ray is found by integrating Eq. (4.3.1) with $p = \sqrt{\epsilon_1}$. Its ray trajectory is

$$x/L = \begin{cases} \sqrt{\dfrac{\epsilon_1}{\Delta}}\left[\cosh^{-1}\left(\sqrt{2}e^{z'/L}\right) - \cosh^{-1}\left(\sqrt{2}e^{z/L}\right)\right] \, , \quad z \geq 0 \\[4mm] \sqrt{\dfrac{\epsilon_1}{\Delta}}\left[\cosh^{-1}\left(\sqrt{2}e^{z'/L}\right) + \sqrt{2}e^{-z/L} - \sqrt{2} - \cosh^{-1}\sqrt{2}\right] \, , \quad z < 0 \, . \end{cases} \qquad (4.3.3)$$

The direct rays are not the only rays existing in regions I and II. They are, however, the only rays emitted directly by the source into regions I and II. Region III is bounded by a portion of the x axis, the z axis and the critical ray.

Direct rays emitted in the angular sector $0 < \theta < \theta_c$ are called returning rays after they pass through the locus of turning points. These returning rays have z coordinates that tend toward plus infinity as the observation point becomes far from the source. Direct rays which have been emitted in the angular sector $\theta_c < \theta \leq \pi/2$ and have passed through the interface $(z = 0)$ are called transmitted rays. These rays have z coordinates that tend toward minus infinity when the observation point is far from the source.

Because of the monotonic character of the dielectric profile, the direct
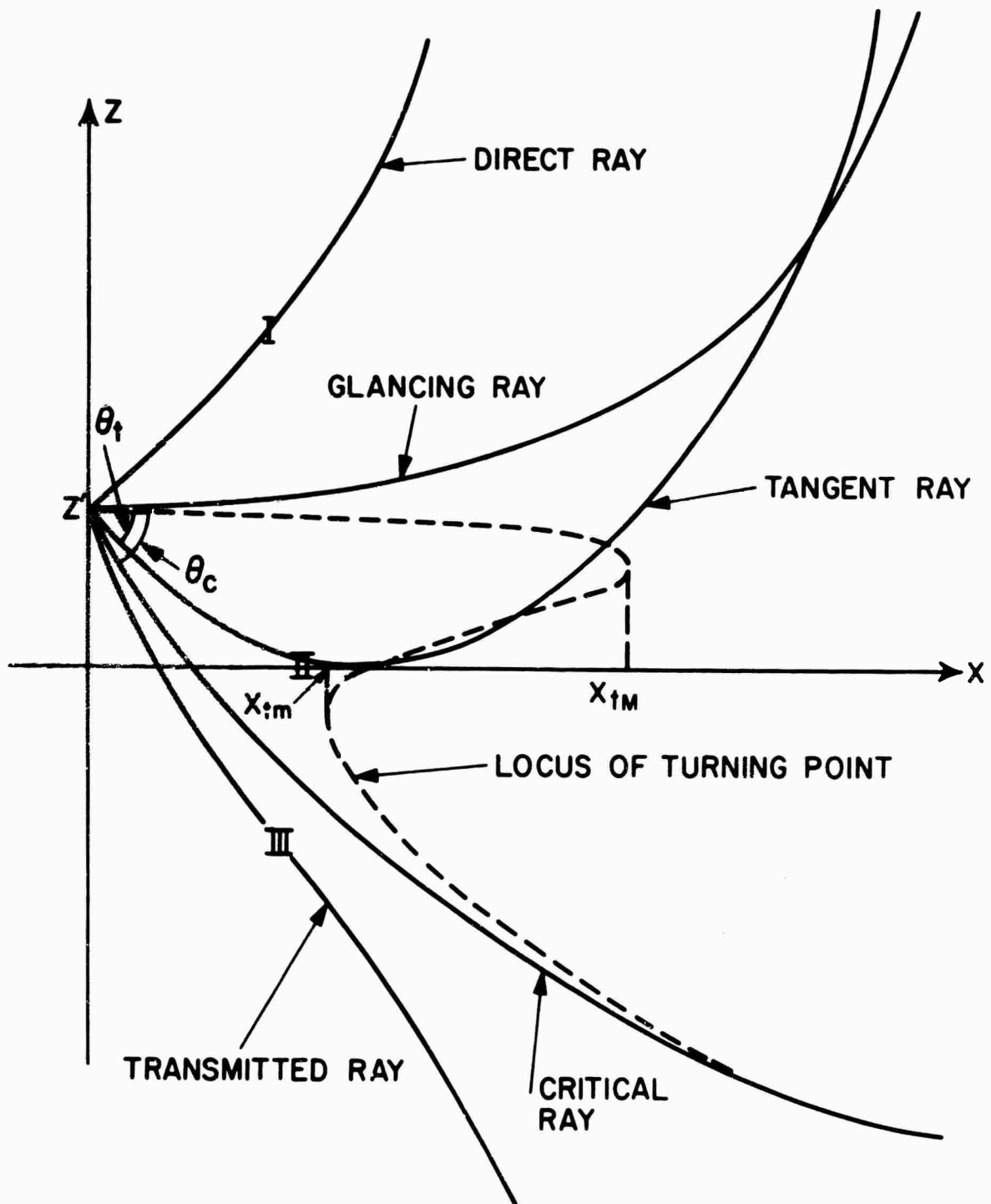
Fig. 4.1

Sketch of Typical Ray Trajectories for the Double Exponential Medium

rays never cross one another; the same is true for transmitted rays. As a result, these two ray types can never generate caustics or foci, therefore making further analysis of these rays unnecessary. The returning rays, on the other hand, do cross one another and must be studied further.

The returning rays can be subdivided into two ray types: those rays with turning points in the upper half space and those rays with turning points in the lower half space. The two ray types are divided by the tangent ray which has an initial angle denoted by θ_t as shown in Fig. 4.1.

b. Turning Points

Before considering the caustics formed by the returning rays, an investigation of the locus of turning points will be useful. The locus points, $z_t \geq 0$, are found by integrating Eq. (4.3.1) and noting that $p = \sqrt{\epsilon(z_t)}$. The resultant equation is

$$x_t/L = \sqrt{2/\Delta} \left[1-(\Delta/2) e^{-2z_t/L} \right]^{\frac{1}{2}} e^{z_t/L} \cosh^{-1} \left[e^{(z'-z_t)/L} \right] , \quad z_t \geq 0 . \qquad (4.3.4)$$

Some interesting features of this curve, as illustrated in Fig. 4.1, are: first, the locus intersects the source point and has a zero slope at this point; second, the curve has one maximum $(dx_t/dz_t = 0)$ when

$$\sqrt{1- e^{-2z'/L}} \cosh^{-1} e^{z'/L} > 1-\Delta/2 \qquad (4.3.5)$$

and is monotonically decreasing when inequality (4.3.5) is not fulfilled. The location of the maximum will be denoted by (x_{tM}, z_{tM}) .

If $(z'-z_t)/L \ll 1$ or $(z'-z_t)/L \gg 1$, Eq. (4.3.4) can be simplified. By use of the former approximation, the locus of the turning point reduces to

$$x_t \approx 2\sqrt{(z'-z_t) L/\Delta} \; e^{z'/L} . \qquad (4.3.6)$$

This describes the section of the locus of turning points near the $z = z'$ line. When $(z' - z_t)/L \gg 1$, on the other hand, we obtain the approximate form of the locus of turning points in the region $z' > z_t \geq 0$ but not including those points close to z'. This approximation is

$$x_t = \sqrt{2/\Delta} \left[1 - (\Delta/2) \, e^{-2z_t/L} \right]^{\frac{1}{2}} (z' - z_t) \, e^{z_t/L} \quad . \tag{4.3.7}$$

If we now assume that L is small, we see from inequality (4.3.5) that the locus of turning points has a maximum. As $L \to 0$ the x_t coordinate of this maximum tends toward infinity. The approximate forms of the locus above and below the maximum are described by Eqs. (4.3.6) and (4.3.7) respectively. As $L \to 0$ we see from Eq. (4.3.6) that the portion of the locus above z_{tM} tends toward the straight line $z = z'$ with $x > 0$, while we see from Eq. (4.3.7) that the portion of the locus below z_{tM} tends toward the straight line $z = 0$ with $\sqrt{2/\Delta} \, (1 - \Delta/2)^{\frac{1}{2}} \, z' < x < \infty$. A sketch of the locus for small L is shown in Fig. 4.2.

The turning points when $z_t < 0$, are obtained in a similar manner as those for $z_t > 0$, i.e., by integrating Eq. (4.3.1) but now z_t must be considered as negative. The resultant equation is

$$x_t/L = (p/p_2) \left\{ \cosh^{-1} \left[\sqrt{2/\Delta} \, p_2 \, e^{z'/L} \right] - \cosh^{-1} \left[\sqrt{2/\Delta} \, p_2 \right] \right\}$$

$$+ (p/|p_1|) \cosh^{-1} \left[|p_1| \sqrt{2/\Delta} \right] \tag{4.3.8}$$

with

$$|p_1| = \sqrt{\Delta/2} \; e^{+z_t/L} . \tag{4.3.9}$$

As would be expected from the continuity of the dielectric constant and its derivative at $z = 0$, the locus of turning points and its derivative are also continuous there. As we approach the critical angle, i.e., $|p_1| \to 0$, we find from Eq. (4.3.9) that $z_t \to -\infty$. Using this limit in Eq. (4.3.8) show
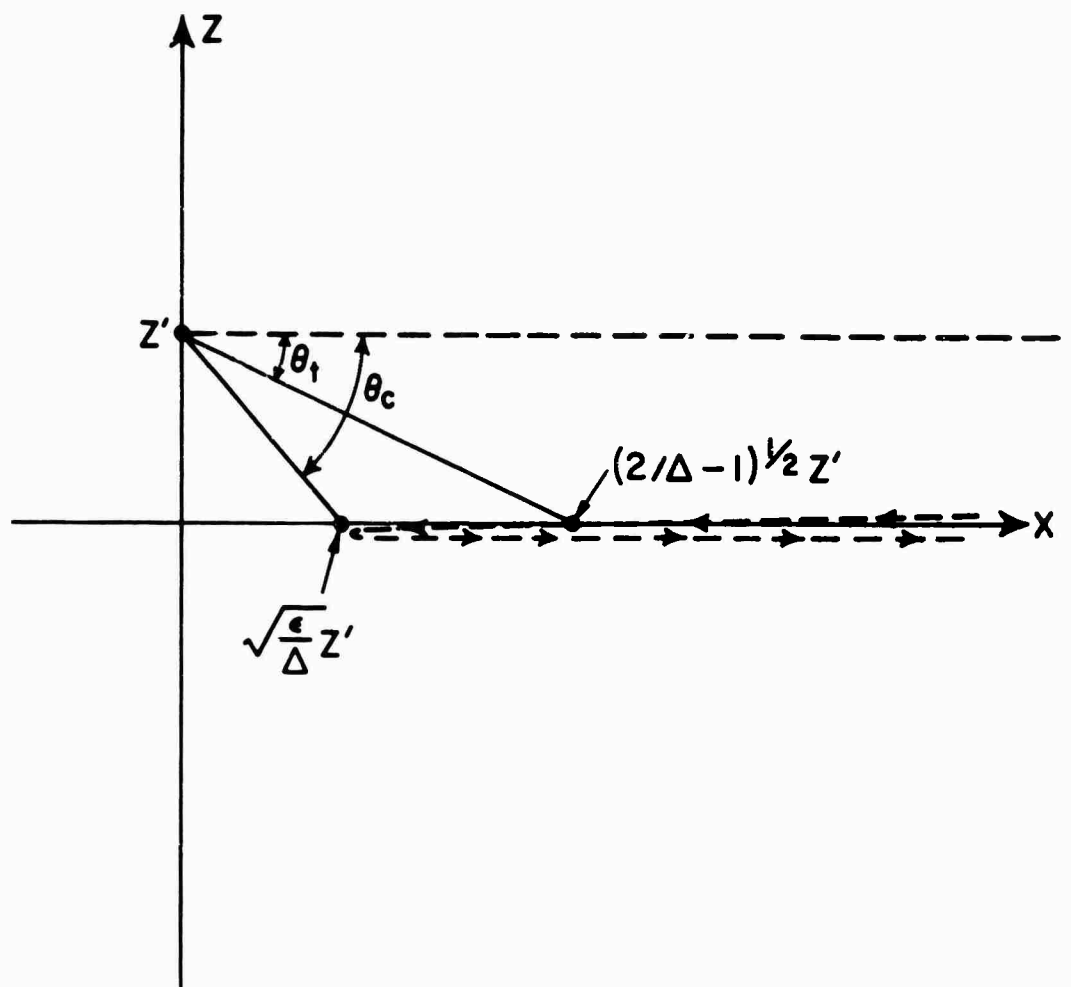
Fig. 4.2

Sketch of the Locus of Turning Points for Small L

that the locus of turning points approaches the critical ray, Eq.(4.3.3), as $z_t \to -\infty$. The locus in the region $z_t < 0$ has one extremum when inequality (4.3.5) is satisfied, and it has no extremum when it is not satisfied.

For small L inequality (4.3.5) is satisfied, and the locus of turning points has one minimum which is given asymptotically by

$$x_{tm} = \sqrt{\epsilon_1/\Delta}\, z' + O(L^{2/3}) \quad , \quad z_{tm} \sim O(L \ln L^{1/3}) \ . \tag{4.3.10}$$

In the limit of $L \to 0$, we see $x_{tm} \to \sqrt{\epsilon_1/\Delta}\, z'$ and $z_{tm} \to 0$. If we assume $|z_t|/L \gg 1$, the portion of the locus, that approaches the critical ray, can be approximated by

$$x_t \approx \sqrt{\epsilon_1/\Delta}\, z' + \pi \sqrt{\epsilon_1/2\Delta}\ L e^{|z_t|/L} \quad , \quad L \ll 1. \tag{4.3.11}$$

If we let $|z_t| \sim L \ln(\beta/L)$, then x_t becomes

$$x_t \sim \sqrt{\epsilon_1/\Delta}\, z' + \pi \sqrt{\epsilon_1/2\Delta}\ \beta. \tag{4.3.12}$$

If β is varied, all values of x_t in the interval $\sqrt{\epsilon_1/\Delta}\, z' < x_t < \infty$ are obtained with the exception of the region close to the point $x = \sqrt{\epsilon_1/\Delta}\, z'$. In the limit of small L, this section of the locus of turning points tends towards the interface. All z_t of order larger than $L \ln(\beta/L)$ lead to x_t which approach infinity as $L \to 0$.

The only section of the curve not investigated as yet, is the section between the minimum and the $z_t = 0$ crossing point. Since $|p_1|$ is non zero from Eq. (4.3.9) we see $z_t \to 0$ as $L \to 0$, and as a result, this section of the curve also approaches the interface as $L \to 0$. To summarize, all portions of the locus of turning points, which lie in the finite x - z plane as $L \to 0$, approach the interface and the $z = z'$ line.

c.   Returning Rays, $z_t \geq 0$

As mentioned previously, those rays, that are turned by the medium, cross one another after they have turned. This leads, as shall be seen, to the formation of a caustic. In this section we shall investigate the section of the caustic formed by those returning rays with turning points, $z_t \geq 0$.

The ray equation for returning rays is found by choosing the minus sign in Eq. (4. 3. 1) and integrating from z' to z_t and then, choosing the plus sign and integrating from z_t to z . The resultant ray equation is

$$x/L = (p/p_2)\left\{\cosh^{-1}\left[p_2 \sqrt{2/\Delta} \; e^{z'/L}\right] + \cosh^{-1}\left[p_2\sqrt{2/\Delta} \; e^{z/L}\right]\right\}. \qquad (4.3.13)$$

To find the caustic, the constraint equation will be needed. This equation, found by taking the derivative of the above equation with respect to p, is

$$\cosh^{-1}\left[p_2\sqrt{2/\Delta} \; e^{z'/L}\right] + \cosh^{-1}\left[p_2\sqrt{2/\Delta} \; e^{z/L}\right] = p^2 p_2\left[1/p_2(z') + 1/p_2(z)\right]$$

$$(4.3.14)$$

where

$$p_2(z) = \left[p_2^2 - (\Delta/2)e^{-2z/L}\right]^{\frac{1}{2}} , \quad p_2 = \lim_{z \to \infty} p_2(z) . \qquad (4.3.15)$$

Since both Eq. (4. 3. 13) and Eq. (4. 3. 14) are transcendental in p_2, it appears impossible to eliminate the parameter directly between the two equations and obtain the caustic directly. However, it is possible to obtain an asymptote to the caustic in the region where $(z-z')/L \gg 1$ and $p_2(z') e^{z'/L} \ll 1$. By using these relations to simplify the constraint equation, a relation is obtained between z and $p_2(z')$. When this relation is substituted in the ray equation, the asymptote obtained is

$$z \approx x\left[(2/\Delta) e^{2z'/L} -1\right]^{\frac{1}{2}} + z' - L\ln 2 . \qquad (4.3.16)$$

This asymptote is a straight line which is valid when $z > z'$.

Another general feature of the caustic is its intersection with the line $z = z'$. It is shown in Appendix D that the ray passing through an extremum of the turning point locus also passes through the caustic at $z = z'$. Thus, if the rays forming a caustic have a locus of turning points with an extremum, the caustic must cross the line $z = z'$. The condition that the locus of turning points has an extremum for $z_t \geq 0$, as expressed in Eq. (4.3.5), is

$$\sqrt{1 - e^{-2z'/L}} \ \cosh^{-1}\left(e^{z'/L}\right) > 1 - \Delta/2 \tag{4.3.17}$$

and, if satisfied, the section of the caustic for $z_t \geq 0$ crosses the $z' = z$ line once.

Because of the complex analytic character of the ray and constraint equations, a GE 235 computer was used to plot the caustic for several different transition thicknesses, L. The basic procedure for doing this was to pick a particular value of p_2, and then solve the constraint equation for z. Since this equation is transcendental in z, a Newton Raphson method was used to find z. The complete caustic has been plotted for L = 10, 1, .1 and is shown in Figs. 4.3, 4.4 and 4.5 respectively.

For L = 10, 1 the caustic consists of two branches meeting in a cusp. The cusp, having the ray with $z_t = 0$ passing through its tip, is not actually a regular cusp since the focal condition* is not satisfied at its tip. The cusped nature of the caustic is instead formed because of the discontinuous character of the dielectric distribution at z = 0. The lower branch of this caustic, having $z_t \geq 0$, is the caustic described in this section.

---

* The focal condition states that the second partial derivative of the ray equation with respect to the ray parameter must be zero at the focal point.
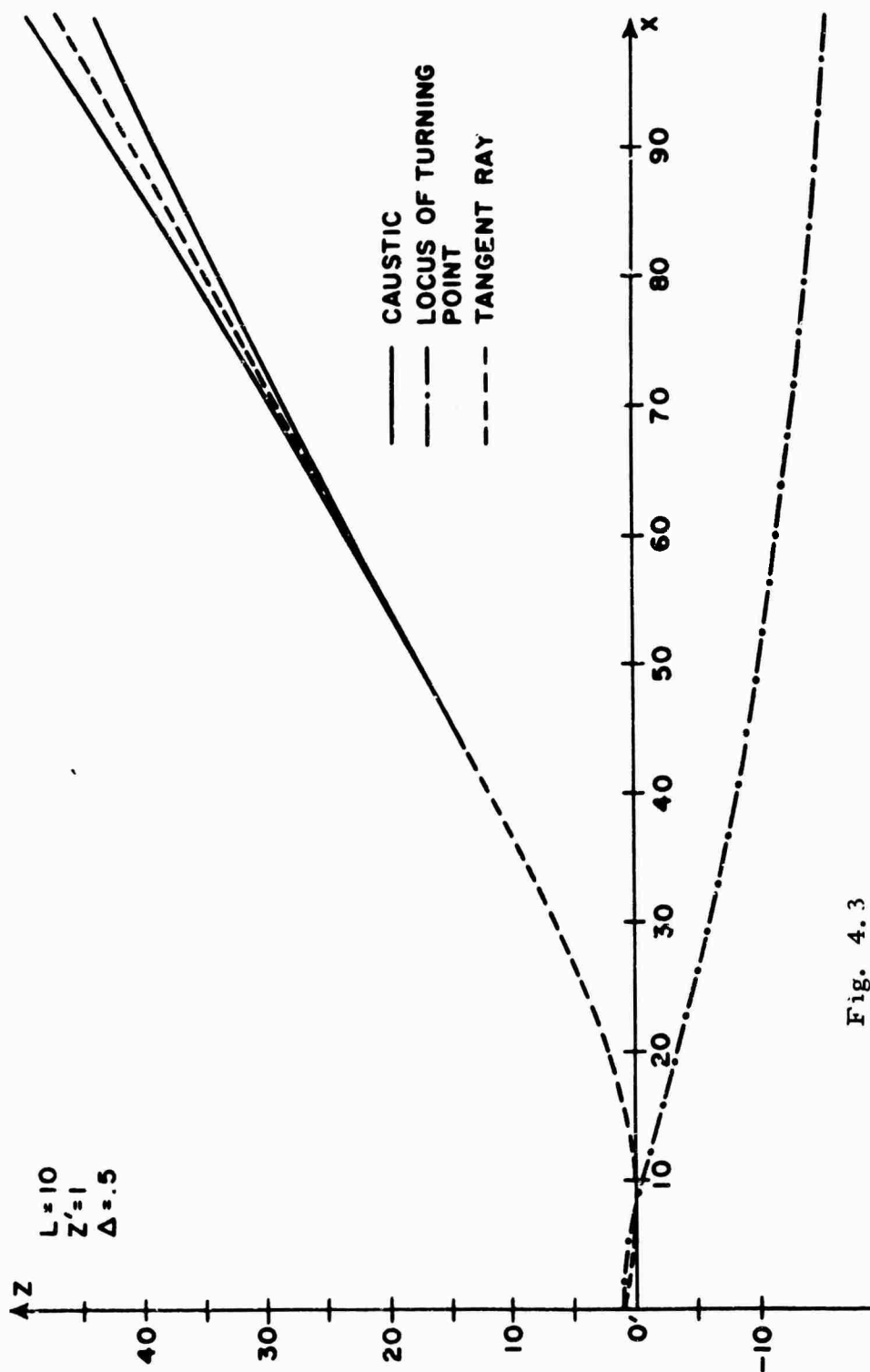
Fig. 4.3

Locus of Turning Points and Caustic for Double Exponential Medium, L = 10.
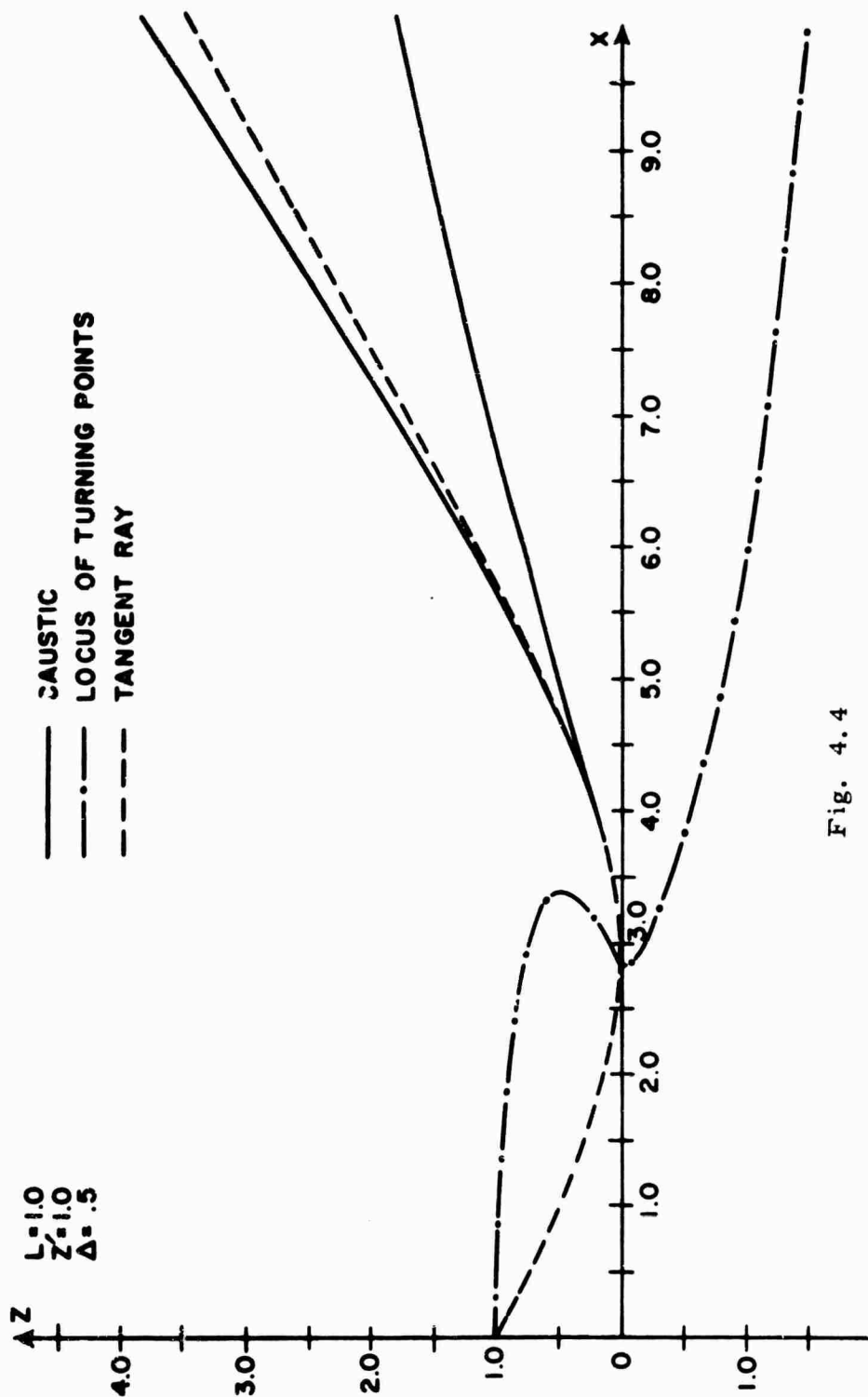
Fig. 4.4

Locus of Turning Points and Caustic for Double Exponential Medium, $L = 1$.
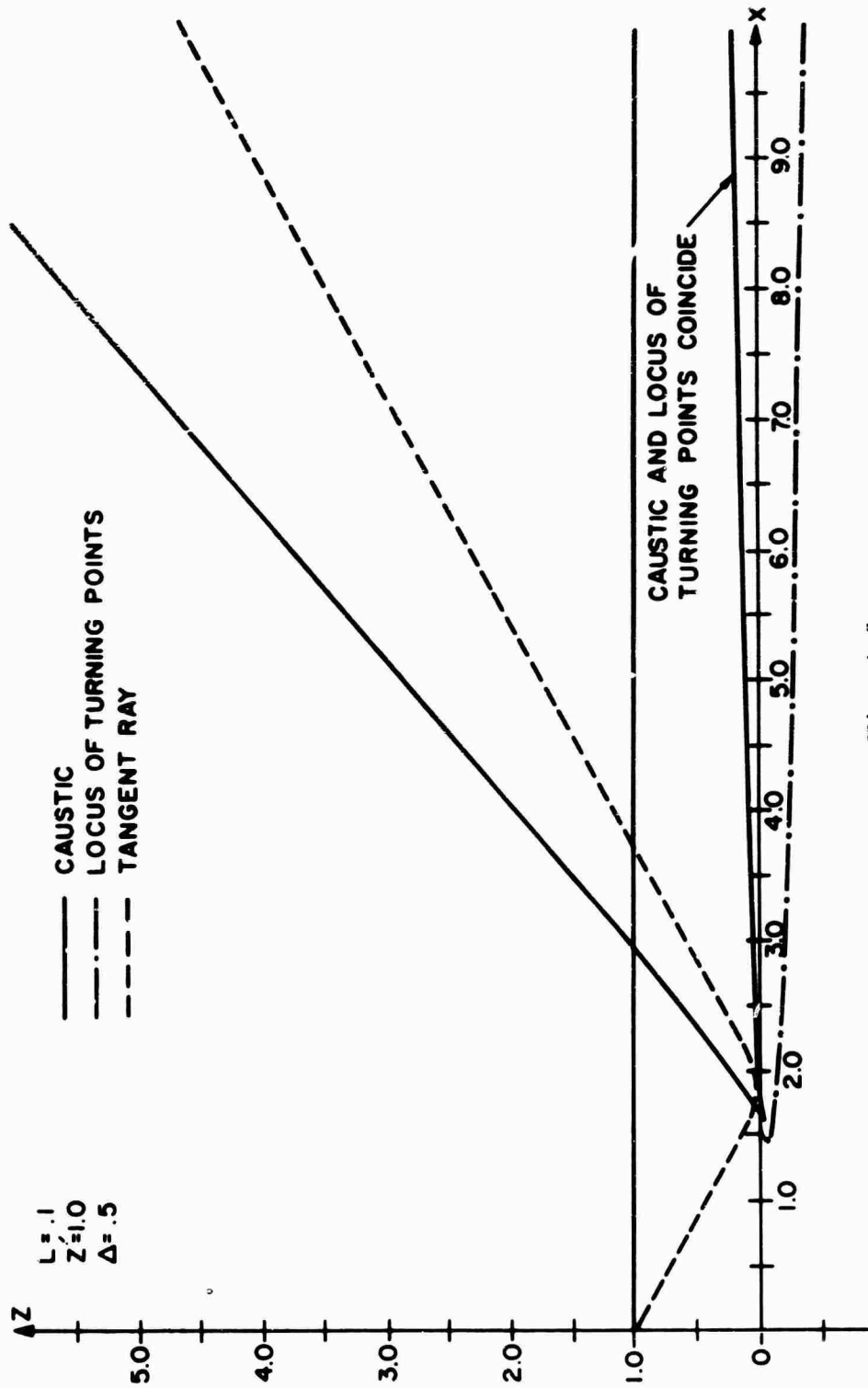
Fig. 4.5

Locus of Turning Points and Caustic for Double Exponential Medium, L = .1

In Fig. 4.5 the structure of the caustic changes because of the appearance of two new cusps : one below the x axis and one above. Both of these new cusps satisfy the focal condition at their tip. An enlargement of Fig. 4.5 in the area of the cusps is shown in Fig. 4.6. We note the regular cusp below the x axis is shown clearly in this figure, while the two cusps appearing above the x axis occur too close to one another to be distinguishable. To rectify this situation a detail of Fig. 4.6 has been plotted in the region of these two cusps. This detail is shown in Fig. 4.7. The coordinates used in this figure are RT and DL. The quantity DL is the distance measured along a straight line passing through the tip of the irregular cusp ; DL is equal to zero at the point the straight line passes through the cusp's tip. The slope of this line is the same as the slope of the caustic at the irregular cusp's tip[*]. The quantity RT is measured perpendicular to DL as shown in Fig. 4.7. The coordinates of the irregular cusp's tip, (x_F, z_F), and the angle, θ, that the DL axis makes with the x axis are given at the bottom of Fig. 4.7.

An examination of Fig. 4.7 shows that the caustic forms a bow tie configuration similar to that observed in the linear layer (Chapter I). The portion of the caustic tending toward the lower part of the graph is composed of rays with turning points $z_t < 0$, and, if extended, it would connect to the cusp shown in Fig. 4.6. On the other hand, the portion of the caustic that appears to coincide with the DL axis corresponds to rays with turning points $z_t > 0$, if extended, it would produce the lower branch of the caustic shown in Fig. 4.5. We also note that the irregular cusp occurs at $DL = 0 = RT$ as would be expected from the definition of the coordinates.

---

[*] The slope of the caustic exits at the cusp's tip and is unique.
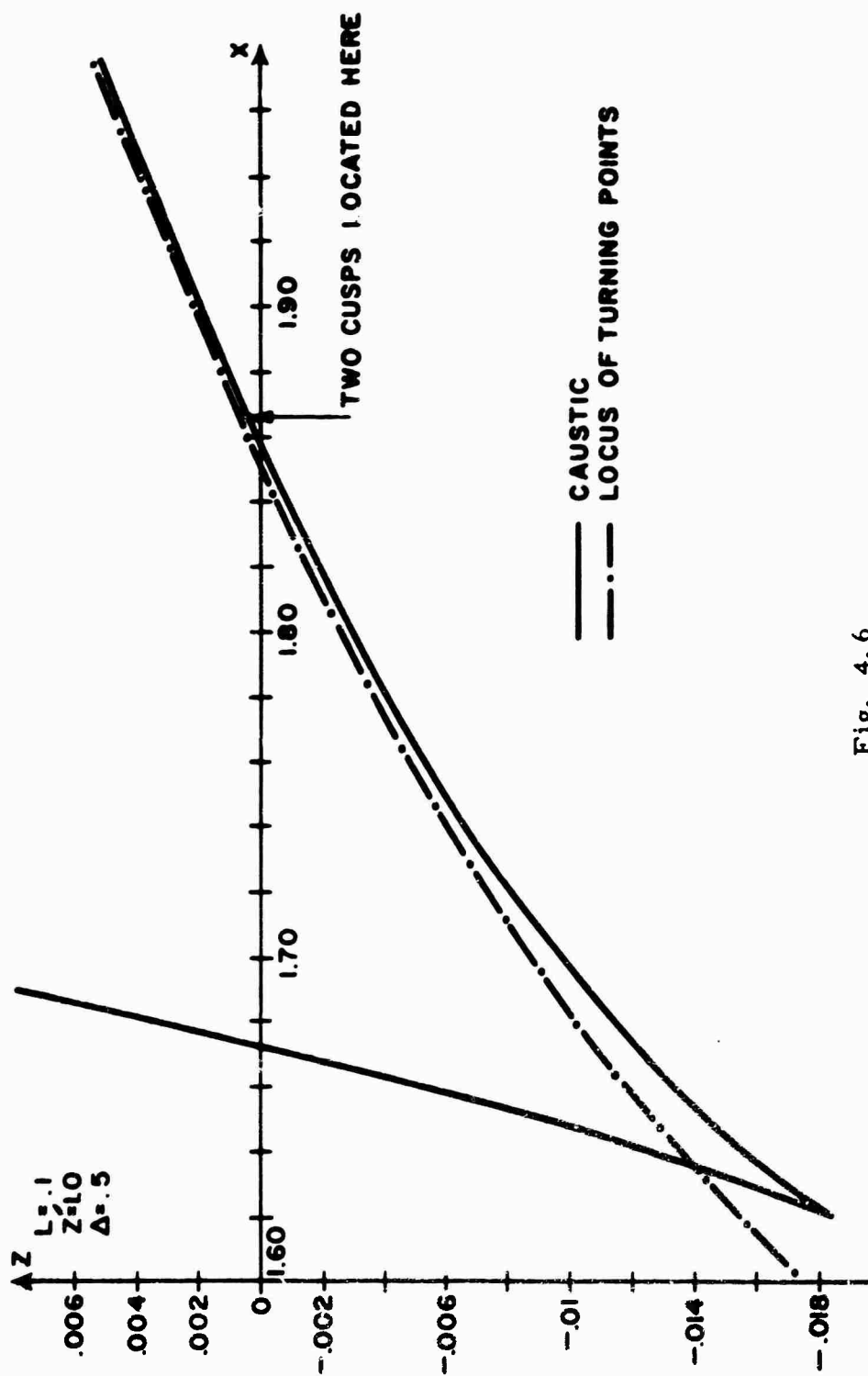
Fig. 4.6

Detail of Caustic for Double Exponential Medium, L = .1

CAUSTIC FOR $Z_f > 0$
AND DL AXIS COINCIDE

CAUSTIC

$X_F = 1.865098$

$Z_F = .0002810199$

$\theta = 2.48°$

$RT \times 10^9$

$DL \times 10^5$

(X_F, Z_F)
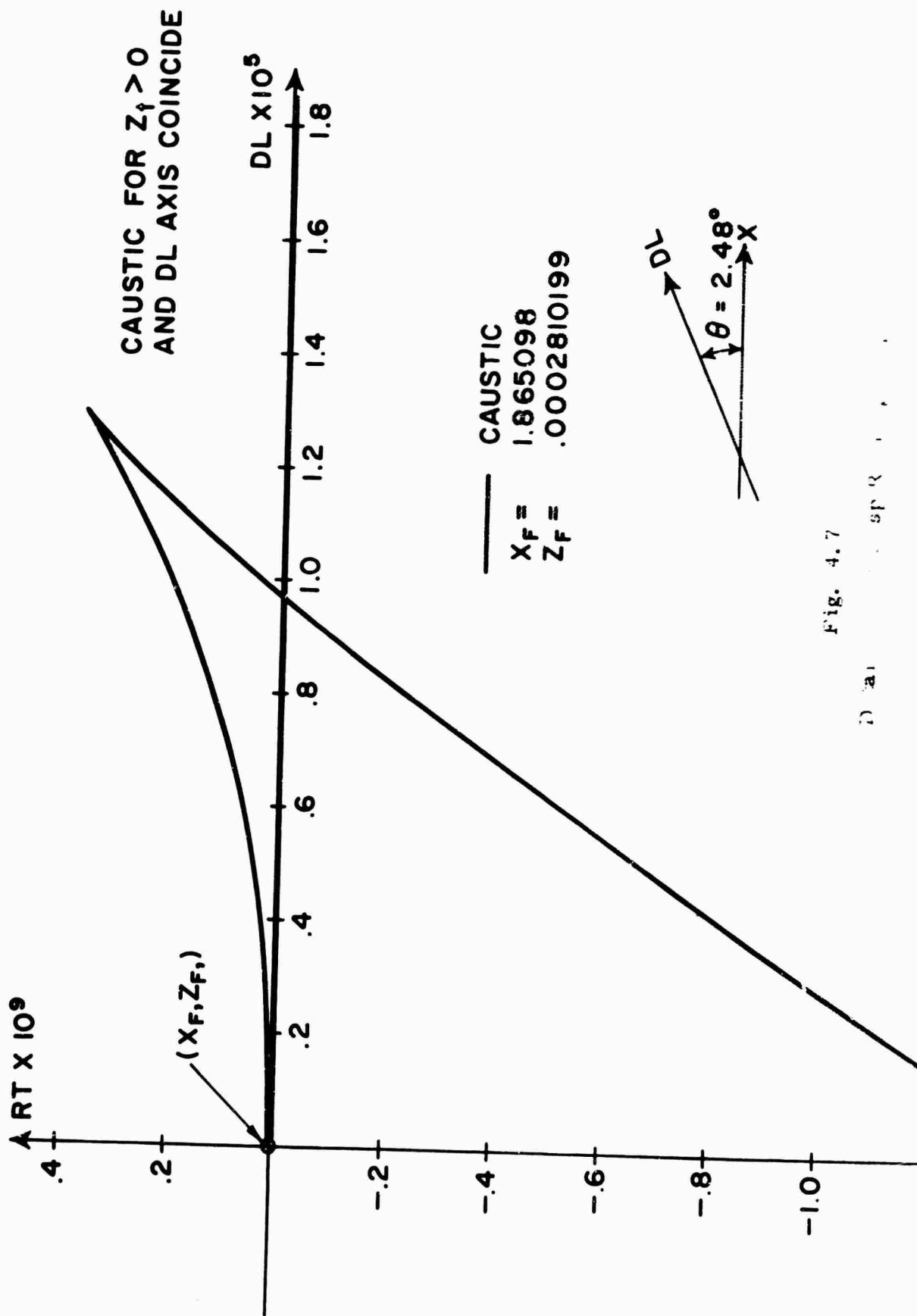
Fig. 4.7

As L becomes increasingly small, various approximations can be made which enable us to simplify Eqs. (4.3.13) and (4.3.14) that represent the lower branch of the caustic. First, we note from section 4.3.1b that for $z_t > 0$ and L small, a maximum of the locus of turning points always exists and as a result, the caustic crosses the line $z = z'$. An asymptotic approximation to the caustic can be obtained below this line. If we assume $(z' - z)/L \gg 1$ and $(z' - z_t)/L \gg 1$, the constraint equation, 4.3.14, reduces to

$$z - z_t \approx L^3 \left[1 - (\Delta/2) e^{-2z_t/L} \right]^2 / 2(z' - z_t)^2. \qquad (4.3.18)$$

By using the above approximation in the ray equation, we find

$$x = \left[(2/\Delta) e^{2z_t/L} - 1 \right]^{\frac{1}{2}} (z' - z_t), \qquad (4.3.19)$$

An examination of Eq. (4.3.18) as $L \to 0$ shows us that $z \to z_t$. Equation 4.3.19 divides naturally into two cases: first, those $z_t \approx \alpha L$ which lead to $(2/\Delta - 1)^{\frac{1}{2}} z' < x_t < \infty$ while z_t with a weaker dependence on L have x_t coordinates which tend toward infinity as $L \to 0$. With the above information and with the previous knowledge that $z_t \to 0$ for finite x_t, we conclude that this portion of the caustic coincides with the $z = 0$ line for $(2/\Delta - 1)^{\frac{1}{2}} z' < x < \infty$. A comparison of Figs. 4.3, 4.4 and 4.5 will show how this limit is approached as $L \to 0$.

The original asymptote, Eq. (4.3.16), still holds when L is small. From Eq. (4.3.16) we see that any $z > z'$ has a corresponding x coordinate which tends towards infinity as $L \to 0$. To summarize in the limit of $L \to 0$, a portion of the caustic lies along the x axis, while other points on the caustic, corresponding to non-zero z values, have x coordinates that lie at infinity.

The focal condition for this section of the caustic is

$$3 \left[1/p_2(z') + 1/p_2(z) \right] + p^2 \left[1/p_2^3(z') + 1/p_2^3(z) \right] = 0 \qquad (4.3.20)$$

where $p_2(z)$ is defined in Eq. (4.3.15). As can be seen this equation is never satisfied for real ray parameters and thus no foci exist on this section of the caustic. In particular this equation is not satisfied at $z_t = 0$ which corresponds to the ray that passes through the tip of the irregular cusp.

d. Returning Rays, $z_t \leq 0$, $z \geq 0$

The rays with turning points, $z_t \leq 0$, penetrate into the medium $z \geq 0$. Their ray equation, as in previous cases, is obtained by an integration of Eq. (4.3.1). The ray equation is

$$x/L = (p/p_2)\left\{-2\cosh^{-1}\left[\sqrt{2/\Delta}\, p_2\right] + \cosh^{-1}\left[\sqrt{2/\Delta}\, p_2\, e^{z'/L}\right]\right. \tag{4.3.21}$$

$$\left. + \cosh^{-1}\left[\sqrt{2/\Delta}\, p_2\, e^{z/L}\right]\right\} + (2p/|p_1|)\cos^{-1}\left[|p_1|\sqrt{2/\Delta}\right], \quad z_t \leq 0, \quad z \geq 0.$$

These rays form another section of the caustic found in the previous section 4.3.c. The constraint equation for this caustic,

$$0 = 2\cosh^{-1}\left[\sqrt{2/\Delta}\, p_2\right] - \cosh^{-1}\left[\sqrt{2/\Delta}\, p_2\, e^{z'/L}\right] - \cosh^{-1}\left[\sqrt{2/\Delta}\, p_2\, e^{z/L}\right]$$

$$+ \left(2\epsilon_1 p_2^3/|p_1|^3\right)\cos^{-1}\left[\sqrt{2/\Delta}\, |p_1|\right] + \left(4p^2 p_2/|p_1|^2\right)\left[p_2^2 - \Delta/2\right]^{-\frac{1}{2}} \tag{4.3.22}$$

$$+ p^2 p_2\left\{\left[p_2^2 - (\Delta/2)\, e^{-2z'/L}\right]^{-\frac{1}{2}} + \left[p_2^2 - (\Delta/2)\, e^{-2z/L}\right]^{-\frac{1}{2}}\right\}$$

was obtained by taking the derivative of the ray equation with respect to p_2. Since elimination of the parameter, p_2, between Eqs. (4.3.21) and (4.3.22) seems impossible, the caustic was plotted on the computer by a similar procedure to that described in the previous section.

The upper branch of the caustic shown in Figs. 4.3 and 4.4 is the section of the caustic whose rays have $z_t \leq 0$, i.e., the part of the caustic described in this section. In Figs. 4.5 and 4.6, the part of the caustic, resulting from rays with $z_t \leq 0$, $z \geq 0$, is more complicated. It consists of the upper branch, starting at the x axis, as shown in Fig. 4.5 and the section between the tip of the irregular cusp and the x axis, as shown in Figs. 4.5 and 4.6. Since the section of the caustic between the irregular cusp and the x axis is very small, an enlargement has been made in Fig. 4.6.

As can be seen from an examination of Figs. 4.3 - 4.6, the general structure of the caustic changes as L decreases; however, the irregular cusp always remains. The analytic behavior of this irregular cusp can be understood better by noting; first, the caustic and its first derivative, dx/dz, are continuous at the tip of the cusp, $z_t = 0$; second, as $z_t \to 0$ from the negative side, z increases for all values of Δ and L. This behavior gives the caustic in this region a cusp-like appearance.

As the transition thickness gets smaller, the irregular cusp approaches the x axis, and two additional regular cusps appear. One of these cusps is formed from rays with $z_t \leq 0$, $z \geq 0$ which are being considered in this section. The exact location of the focus is difficult to find because of the complicated analytical character of the focal condition. As L becomes small, the focal condition simplifies and an approximate location of the focus can be found.

The general focal condition is

$$0 = (6\epsilon_1 \Delta / |p_1|^5) \cos^{-1}\left[|p_1| \sqrt{2/\Delta}\right] + \frac{4\left[2|p_1|^2 p^2 + 3\epsilon_1 (p_2^2 - \Delta/2)\right]}{|p_1|^4 (p_2^2 - \Delta/2)^{\frac{1}{2}}}$$

$$-3\left[1/p_2(z') + 1/p_2(z)\right] - p^2\left[1/p_2^3(z') + 1/p_2^3(z)\right]$$

(4.3.23)

where $p_2(z)$ is defined in Eq. (4.3.15). If we assume L is small and $z_t \to 0$, the constraint equation, (4.3.22), reduces approximately to

$$z'/L = (1 - \Delta/2) \left[p_2^2 - (\Delta/2) e^{-2z/L} \right]^{\frac{1}{2}} . \tag{4.3.24}$$

We now let $p_2 = \sqrt{\Delta/2} + \delta$ where $\delta \ll 1$ since z_t is small and use this with Eq. (4.3.24) in the focal condition Eq. (4.3.23). We obtain

$$\delta = 32 \sqrt{\Delta/2} (1 - \Delta/2)^6 (z')^{-6} L^6 . \tag{4.3.25}$$

We now see that our assumption of small z_t was valid when L is assumed to be small. By using this value of δ in Eq. (4.3.24) we find the approximate focus location is given by

$$z = 2(1 - \Delta/2)^2 (z')^{-2} L^3 . \tag{4.3.26}$$

When L is small, an approximate equation for the upper branch of the caustic can be obtained by using $z/L \gg 1$ and $z'/L \gg 1$ in Eqs. (4.3.21) and (4.3.22). The equation obtained is

$$x/L = \sqrt{\epsilon_1/\Delta} \, (z+z')/L + \pi^{2/3} \epsilon_1^{1/6} \Delta^{-1/2} (z+z')^{1/3} L^{2/3} . \tag{4.3.27}$$

The use of Eq. (4.3.27) in conjunction with Eq. (4.3.23) shows that there are no focal points on the upper branch of the caustic for small L.

If we now consider the limiting case as $L \to 0$ we find: first, the section of the caustic between the irregular cusp and the x axis shrinks to zero as $L \to 0$; second, the upper branch of the caustic approaches the line $x = \sqrt{\epsilon_1/\Delta} \, (z + z')$ which is the critically reflected ray from a sharply bounded interface of height Δ.

e.   **Returning Rays $z_t \leq 0$, $z \leq 0$**

The returning rays with $z \leq 0$ are given via Eq. (4.3.1) by

$$x/L = (p/p_2) \left\{ -\cosh^{-1}\left[\sqrt{2/\Delta}\, p_2\right] + \cosh^{-1}\left[\sqrt{2/\Delta}\, p_2\, e^{z'/L}\right] \right\}$$

$$+ (p/|p_1|)\left\{\cos^{-1}\left[|p_1|\sqrt{2/\Delta}\right] + \cos^{-1}\left[|p_1|\sqrt{2/\Delta}\, e^{-z/L}\right]\right\}. \tag{4.3.28}$$

The constraint equation is obtained by taking the derivative with respect to p_2 of Eq. (4.3.28). The result is

$$0 = \cosh^{-1}\left[\sqrt{2/\Delta}\, p_2\right] - \cosh^{-1}\left[\sqrt{2/\Delta}\, p_2\, e^{z'/L}\right] + 2 p^2 p_2 \,(p_2^2 - \Delta/2)^{\frac{1}{2}}\, |p_1|^{-2}$$

$$+ (\epsilon_1 p_2^3/|p_1|^3)\left\{\cos^{-1}\left[|p_1|\sqrt{2/\Delta}\right] + \cos^{-1}\left[|p_1|\sqrt{2/\Delta}\, e^{-z/L}\right]\right\} \tag{4.3.29}$$

$$+ p^2 p_2 \left[p_2^2 - (\Delta/2)e^{-2z'/L}\right]^{-\frac{1}{2}} + p^2 p_2^3\, |p_1|^{-2}\left[(\Delta/2)e^{2z/L} - |p_1|^2\right]^{-\frac{1}{2}}.$$

A computer calculation of this sector of the caustic was made. An examination of these results shown in Figs. 4.3. - 4.6, seems to indicate that if a focal point does not exist below the x axis, then there exists no caustic below the x axis. Applying the focal condition to Eq. (4.3.28), gives us the second constraint equation. This equation, in conjunction with Eqs. (4.3.28) and (4.3.29), enables us to find the focal points. Nothing in general can be said because of the complication of the focal condition.

When L is small, Eqs. (4.3.28), (4.3.29) and the focal condition simplify substantially, enabling us to locate the foci if they exist. We find that one focus exists which tends towards the interface as $L \to 0$, i.e., $z \to 0$, $x \to \sqrt{\epsilon_1/\Delta}\, z'$ as $L \to 0$. The two branches of this cusp tend towards the interface also, as $L \to 0$.

f. Summary

The investigation of the rays emitted from a point source in a double exponential layer has led us to conclude : first, all rays, except the returning rays, have a simple character; second, the returning rays form a caustic with an irregular cusp resulting from the discontinuity in the dielectric; third, as L becomes small, two additional regular cusps appear one below the x axis and one above; fourth, as $L \to 0$, one portion of the caustic tends toward the interface while the other portion tends toward the critically reflected ray; fifth, the focus below the x axis tends toward the reflection point of the critically reflected ray; and sixth, the two focii above the x axis tend toward the turning point of the tangent ray as $L \to 0$.

4.3.3 Asymptotic Evaluation of the Formal Solution

a. Introduction

The asymptotic evaluation of the formal solution will now be carried out. As has been mentioned previously, the integrands of Eq. (4.2.14) or Eq. (4.2.16) will be asymptotically evaluated for large $k_o L$ and then the resulting integrals will be asymptotically approximated for large $k_o r$.

b. Asymptotic Approximations for Large $k_o L$

The integrands of the integrals appearing in Eqs. (4.2.14) and (4.2.16) contain the following Bessel functions : $J_{\nu_2}(-i\lambda e^{-z/L})$, $J_{-\nu_2}(-i\lambda e^{-z/L})$, $H_{\nu_2}^{(1)}(-i\lambda e^{-z/L})$, $H_{\nu_2}^{(2)}(-i\lambda e^{-z/L})$, $J_{\nu_2}(\lambda)$ and the derivatives of these functions with respect to their arguments. A significant simplification of the integrands will occur if the above functions are replaced by their asymptotic approximations for $k_o L$ large. These asymptotic approximations need only be known in a strip-like region centered around the integration path, C.

(30)
Olver has derived uniform asymptotic expansions for $J_\nu(\nu z)$, $H_\nu^{(1)}(\nu z)$ and $H_\nu^{(2)}(\nu z)$ and for their derivatives when ν is large and $|\arg \nu| < \pi/2$. These expansions are valid in the whole z plane when a branch cut introduced along a curve in the second quadrant, as described in Appendix E. Since the asymptotic expansions will be required when $\arg \nu = -\frac{\pi}{2}$, Olver's results have been extended in Appendix E to include this end point. The extension shows that the same expansions, which are valid when $|\arg \nu| < \pi/2$, are also valid when $\arg \nu = -\pi/2$. These uniform asymptotic expansions are

$$J_{\nu_2}(-i\lambda e^{-z/L}) \sim \frac{1}{\nu_2^{\frac{1}{3}}} \left[\frac{4|\nu|^{2/3} \zeta}{1 - w_2^2} \right]^{1/4} A_i(|\nu|^{2/3} \zeta) \tag{4.3.30}$$

$$H_{\nu_2}^{(1)}(-i\lambda e^{-z/L}) \sim \frac{2 e^{\mp i\pi/3}}{\nu_2^{\frac{1}{3}}} \left[\frac{4|\nu|^{2/3} \zeta}{1 - w_2^2} \right]^{1/4} A_i(e^{-2\pi i/3} |\nu|^{2/3} \zeta) \tag{4.3.31}$$

$$J_{\nu_2}'(-i\lambda e^{-z/L}) \sim -\frac{2}{w_2 \nu_2^{\frac{1}{3}}} \left[\frac{1 - w_2^2}{4|\nu|^{2/3} \zeta} \right]^{1/4} A_i'(|\nu|^{2/3} \zeta) \tag{4.3.32}$$

$$H_{\nu_2}^{(1)'}(-i\lambda e^{-z/L}) \sim \frac{4}{w_2 \nu_2^{\frac{1}{3}}} e^{\pm 4\pi i/3} \left[\frac{1 - w_2^2}{4|\nu|^{2/?}} \right]^{-1/4} A_i'(e^{\pm 2\pi i/3} |\nu|^{2/3} \zeta) \tag{4.3.33}$$

where

$$\frac{2}{3} \zeta^{3/2} = \left| \frac{\nu_2}{\nu_2} \right| \int_{w_2}^{1} \frac{\sqrt{1-t^2}}{t} dt \quad , \quad w_2(z) = \frac{\sqrt{\Delta/2} \, e^{-z/L}}{p_2} \quad . \tag{4.3.34}$$

The branch cuts which define the correspondence between the ζ and w_2 planes are defined in Appendix E. By using the definition for ν_2 given in Eq. (4.2.8), and the fact that the above asymptotic approximations are valid for $\text{Re} \, \nu_2 \geq 0$, we find that these approximations are valid in the first and third quadrants of the p_1 plane including the real and imaginary axes.

In Fig. 4.8, the regions of validity are shown by shaded regions composed of slanted lines. No branch cuts due to the square root $p = \sqrt{\epsilon_1 + |p_1|^2}$ are shown in this figure since these particular Bessel functions are independent of p.

The Bessel functions, given in Eqs. (4.3.30) - (4.3.33), have turning points which are located at $w_2 = \pm 1$. The turning point corresponding to $w_2 = 1$ appears in two places on the top sheet of the p_1 plane as shown in Fig. 4.8. These two points are located at $p_1 = \pm v_1(z)$ where $v_1(z) = (\epsilon - v_2^2(z))^{\frac{1}{2}}$ $v_2(z) = \sqrt{\Delta/2} \exp(-z/L)$. The two points corresponding to the turning point located at $w = -1$, are located on the bottom sheet.

To obtain the asymptotic approximation of $J_{-v_2}(-i\lambda e^{-z/L})$ in the same region of validity as described above, we will use the connection formula

$$J_{-v_2}(-i\lambda e^{-z/L}) = \left[e^{v_2 \pi i} H_{v_2}^{(1)}(-i\lambda e^{-z/L}) + e^{-v_2 \pi i} H_{v_2}^{(2)}(-i\lambda e^{-z/L}) \right] / 2 \qquad (4.3.35)$$

where the asymptotic approximations given by Eq. (4.3.31) are used for $H_{v_2}^{(1)}(-i\lambda e^{-z/L})$. Since it can be shown that in a region close to the integration path, C, the second term of Eq. (4.3.35) is exponentially small. The asymptotic approximation to $J_{-v_2}(-i\lambda e^{-z/L})$ is given by

$$J_{-v_2}(-i\lambda e^{-z/L}) \sim e^{|v_2|\pi + i\pi/3} \left[\frac{4|v_2|^{2/3}\xi}{1 - w_2^2} \right] \frac{A_i(e^{2\pi i/3}|v_2|^{2/3}\xi)}{v_2^{\frac{1}{3}}} . \qquad (4.3.36)$$

By a similar procedure, the asymptotic approximation for the derivative of J_{v_2} can be obtained. It is

$$J'_{-v_2}(-i\lambda e^{-z/L}) \sim \frac{2 e^{|v_2|\pi + 4\pi i/3}}{w_2} \left[\frac{1 - w_2^2}{4|v|^{2/3}\xi} \right]^{1/4} \frac{A'_i(e^{2\pi i/3}|v_2|^{2/3}\xi)}{v_2^{1/3}} . \qquad (4.3.37)$$

Fig. 4. 9
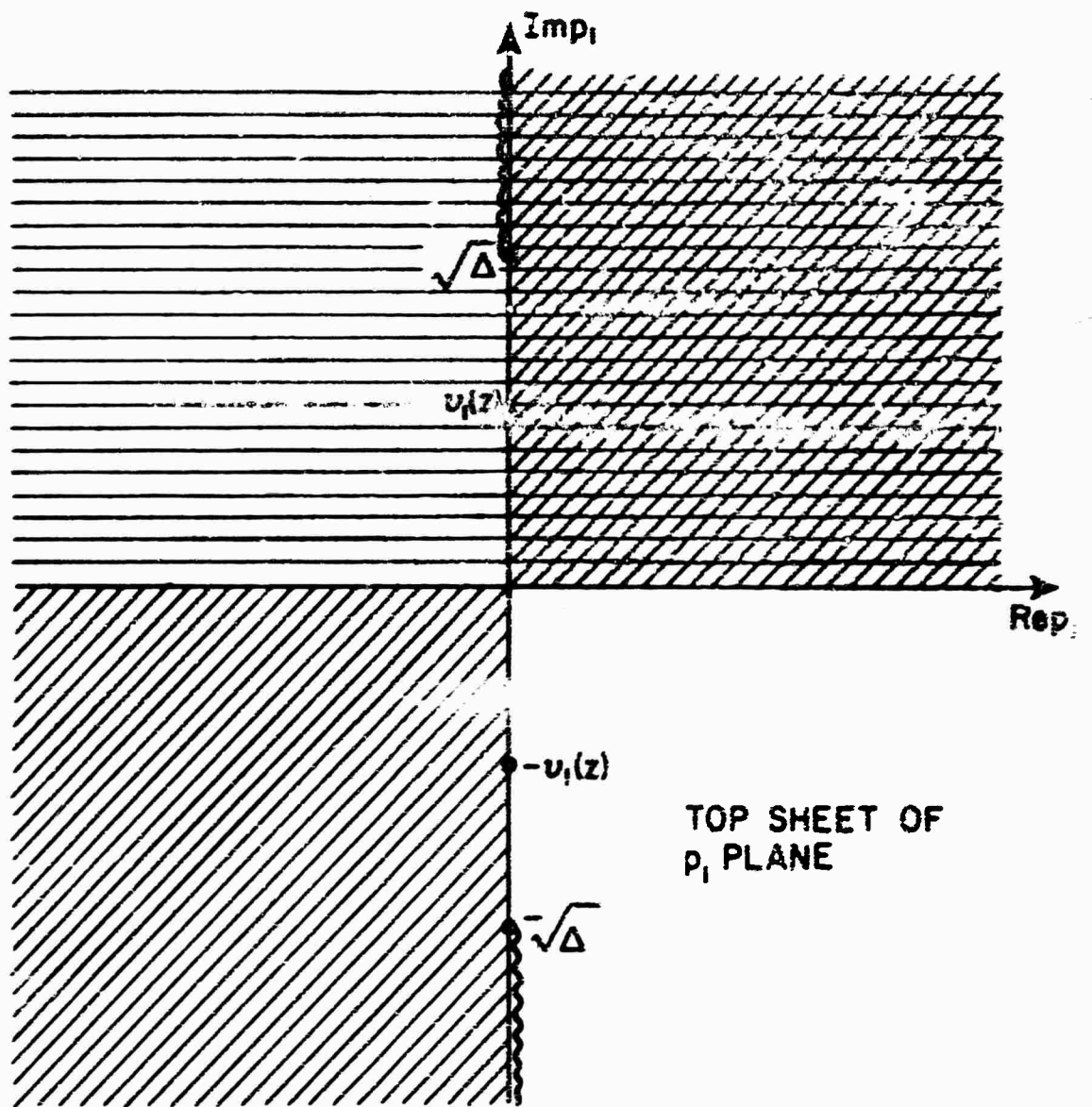
Regions of Validity for Asymptotic Approximations

The asymptotic approximation for $J_{\nu_1}(\lambda)$ and its derivative can be found by using Olver's results as were used before.

The resultant asymptotic approximations are

$$J_{\nu_1}(\lambda) \sim \left[\frac{4|\nu_1|^{2/3}\xi}{1-w_1^2}\right]^{1/4} \frac{A_i(|\nu_1|^{2/3}\xi)}{\nu_1^{\frac{1}{2}}} \tag{4.3.38}$$

and

$$J'_{\nu_1}(\lambda) \sim -\frac{2}{w_1}\left[\frac{1-w_1^2}{|\nu_1|^{2/3}\xi}\right] \frac{A'_i(|\nu_1|^{2/3}\xi)}{\nu_1^{\frac{1}{2}}} \tag{4.3.39}$$

where ξ is defined as in Eq. (4.3.34) with w_2 being replaced by w_1, $w_1 = -\sqrt{\xi/2}/ip_1$. The region of validity for these asymptotic approximations is the upper half of the p_1 plane including the $\text{Re}\,p_1$ axis as shown by the horizontal lines in Fig. 4.8. The turning point of J_{ν_1} corresponding to $w_1 = 1$, is located on the $\text{Im}\,p_1$ axis in the interval $0 < \text{Im}\,p_1 < \sqrt{\Delta}$ while the turning point corresponding to $w = -1$ is in the conjugate position.

The asymptotic approximation to the Bessel functions J_{ν_2}, $J_{-\nu_2}$ and $H_{\nu_2}^{(1)}$ will be needed in a narrow strip just to the left of the integration path, C, where $0 < \text{Im}\,p_1 < \sqrt{\Delta}$. By making use of the formula relating different types of Bessel functions given by Watson[31] we can show that the asymptotic expansions, which are valid on the $\text{Im}\,p_1$ axis, are also valid in a small strip to the right of it. These asymptotic expansions are not valid near the branch points, $p_1 = \pm i\sqrt{\Delta}$ since the large asymptotic parameter, ν_2 tends to zero there.

By applying these same ideas, the asymptotic approximations for J_{ν_2}, $J_{-\nu_2}$, and J_{ν_1} are analytically continued to a narrow strip below the positive real p_1 axis. As in the case of the Bessel functions of order $\pm\nu_2$, the asymptotic approximations of Bessel functions of order ν_1, are not valid in a small

circular region about the origin of tne p_1 plane.

The approximate forms of the Bessel functions previously mentioned, can be simplified further by using the asymptotic formula for the Airy functions . This is only possible when the integration variable p_1 is not too close to a turning point of the particular Bessel function under consideration. This has been done in Tables 4.1A and 4.1B for values of p_1 along the integration path C . These formulae, however, can be analytically continued, so that they will be valid in a narrow strip, centered around the integration path. The asymptotic approximations presented in Table 4.1A and 4.1B are valid in the neighborhood of $p_1 = 0$ and $p_2 = 0$. Although Olver's uniform expansions break down at these points, the Debye approximations[32], which utilize the large parameter λ , can be used to extend the range of validity of the approximations appearing in the tables to include the neighborhood of $p_1 = 0$ and $p_2 = 0$.

c. Approximation of Formal Solution

The asymptotic evaluation of Eq. (4.2.14) or its alternate, Eq. (4.2.16) , will now be performed with the a of the asymptotic approximations obtained in the last section. Before proceeding with this evaluation, we would like to note some important characteristics of the integrands.

The integrands as expressed in section 4.2, are completely defined. There is no need to consider the multivalued nature of the cylinder functions contained in these integrands, since the cylinder functions are only multi-valued with respect to their arguments which are a constant along the path of integration. These cylinder functions have turning points located on the $\mathrm{Im}\, p_1$ axis at $\mathrm{Im}\, p_1 = \pm v_1(z_<) , \pm v_1(z_>) , \pm v_1(0)$ where $v_1(z_<) \geq v_1(z_>) \geq v_1(0)$. The asymptotic formulae, used to approximate the cylinder functions, change characteristics upon the passage of the integration path through a turning point

	$J_{\nu_2}(-i\lambda e^{-\frac{z}{L}}) \sim$	$J'_{\nu_2}(-i\lambda e^{-\frac{z}{L}}) \sim$	$J_{-\nu_2}(-i\lambda e^{-\frac{z}{L}}) \sim$	$J'_{-\nu_2}(-i\lambda e^{-\frac{z}{L}}) \sim$
$0 < \text{Re}\,p_1 < \sqrt{\epsilon_1}$ $\text{Im}\,p_1 = 0$	$\dfrac{e^{+ik_0\phi_{2+}(z,p_2)+i\frac{\pi}{4}}}{\sqrt{2\pi\tau}\left[p_2^2 - \nu_2^2(z)\right]^{\frac{1}{4}}}$	$\dfrac{e^{ik_0\phi_{2+}(z,p_2)+i\frac{\pi}{4}}}{\sqrt{2\pi\tau}\,\nu_2(z)\left[p_2^2 - \nu_2^2(z)\right]^{-\frac{1}{4}}}$	$\dfrac{e^{|\nu_2|\pi\, -ik_0\phi_{2+}(z,p_2)-i\frac{\pi}{4}}}{\sqrt{2\pi\tau}\left[p_2^2 - \nu_2^2(z)\right]^{\frac{1}{4}}}$	$\dfrac{e^{|\nu_2|\pi\, -ik_0\phi_{2+}(z,p_2)-i\frac{\pi}{4}}}{\sqrt{2\pi\tau}\,\nu_2(z)\left[p_2^2 - \nu_2^2(z)\right]^{-\frac{1}{4}}}$
$\text{Re}\,p_1 = 0$ $0 < \text{Im}\,p_1 < \nu_1(z)$	SAME AS ABOVE	SAME AS ABOVE	SAME AS ABOVE	SAME AS ABOVE
$\text{Re}\,p_1 = 0$ $\nu_1(z) < \text{Im}\,p_1 < \sqrt{\Delta}$	$\dfrac{e^{k_0\phi_{2-}(z,p_2)}}{\sqrt{2\pi\tau}\left[\nu_2^2(z) - p_2^2\right]^{\frac{1}{4}}}$	$\dfrac{e^{k_0\phi_{2-}(z,p_2)+i\frac{\pi}{2}}}{\sqrt{2\pi\tau}\,\nu_2(z)\left[\nu_2^2(z) - p_2^2\right]^{-\frac{1}{4}}}$	$\dfrac{e^{|\nu_2|\pi\, k_0\phi_{2-}(z,p_2)}}{\sqrt{2\pi\tau}\left[\nu_2^2(z) - p_2^2\right]^{\frac{1}{4}}}$	$\dfrac{e^{|\nu_2|\pi\, k_0\phi_{2-}(z,p_2)-i\frac{\pi}{2}}}{\sqrt{2\pi\tau}\,\nu_2(z)\left[\nu_2^2(z) - p_2^2\right]^{-\frac{1}{4}}}$
$\text{Re}\,p_1 = 0$ $\sqrt{\Delta} < \text{Im}\,p_1 < \infty$	$\dfrac{e^{k_0\phi_{2-}(z,i|p_2|)}}{\sqrt{2\pi\tau}\left[\nu_2^2(z) + |p_2|^2\right]^{\frac{1}{4}}}$	$\dfrac{e^{k_0\phi_{2-}(z,i|p_2|)+i\frac{\pi}{2}}}{\sqrt{2\pi\tau}\,\nu_2(z)\left[\nu_2^2(z) + |p_2|^2\right]^{-\frac{1}{4}}}$		

$$\phi_{2+\underset{-}{}}(w,p_2) = \underset{-}{+}L \int_{\nu_2(z)}^{p_2} \frac{\underset{-}{+}(p_2^2 - t^2)^{\frac{1}{2}}}{t}\, dt$$

Table 3.1A Asymptotic approximations along integration path

	$J_{\nu_1}(\lambda) \sim$	$J'_{\nu_1}(\lambda) \sim$	$H^{(2)}_{\nu_2}(-i\lambda e^{-\frac{z}{L}}) \sim$	$H^{(2)'}_{\nu_2}(-i\lambda e^{-\frac{z}{L}}) \sim$
$\text{Re}\,P_1 = 0$ $\sqrt{\Delta} < \text{Im}\,P_1 < \infty$	$\dfrac{e^{-k_o\phi_{1+}(|P_1|)}}{\sqrt{2\pi\tau}\left[|P_1|^2 - v_1^2(0)\right]^{\frac14}}$	$\dfrac{e^{-k_o\phi_{1+}(|P_1|)}\sqrt{2\pi\tau}\,v_1(0)\left[|P_1|^2 - v_1^2(0)\right]^{-\frac14}}{}$	$\dfrac{e^{-k_o\phi_{2-}(x,i|P_2|)+i\frac{\pi}{2}}}{\sqrt{\pi\frac{\tau}{2}}\left[v_2^2(z)+|P_2|^2\right]^{\frac14}}$	$e^{-k_o\phi_{2-}(z,i|P_2|)}\sqrt{\pi\frac{\tau}{2}}\,v_2(z)\left[v_2^2(z)+|P_2|\right]^{-\frac14}$
$\text{Re}\,P_1 = 0$ $v_1(z) < \text{Im}\,P_1 < \sqrt{\Delta}$	*SAME AS ABOVE	*SAME AS ABOVE	$\dfrac{e^{-k_o\phi_{2-}(z,P_2)+i\frac{\pi}{4}}}{\sqrt{\pi\frac{\tau}{2}}\,v_2(z)\left[v_2^2(z)-P_2^2\right]^{\frac14}}$	$e^{-k_o\phi_{2-}(z,P_2)}\sqrt{\pi\frac{\tau}{2}}\,v_2(z)\left[v_2^2(z)-P_2^2\right]^{-\frac14}$
$\text{Re}\,P_1 = 0$ $0 < \text{Im}\,P_1 < v_1(z)$	$\dfrac{\sin\left[k_o\phi_{1-}(|P_1|)+\frac{\pi}{4}\right]}{\sqrt{\pi\frac{\tau}{2}}\left[v_1^2(0)-|P_1|^2\right]^{\frac14}}$	$\dfrac{\cos\left[k_o\phi_{1-}(|P_1|)+\frac{\pi}{4}\right]}{\sqrt{\pi\frac{\tau}{2}}\,v(0)\left[v_1^2(0)-|P_1|^2\right]^{-\frac14}}$	$\phi_{1\pm}(|P_1|)=\pm L\int_{v_1(0)}^{|P_1|}\dfrac{\left[\pm(|P_1|^2-t^2)\right]^{\frac12}}{t}\,dt$	
$0 < \text{Re}\,P_1 < \sqrt{\varepsilon_1}$ $\text{Im}\,P_1 = 0$	$\dfrac{ie^{-ik_o\phi_{-1}(-iP_1)-i\frac{\pi}{4}}}{\sqrt{2\pi\tau}\left[v_1^2(0)+P_1^2\right]^{\frac14}}$	$\dfrac{e^{-ik_o\phi_{1-}(-iP_1)-i\frac{\pi}{4}}}{\sqrt{2\pi\tau}\,v_1(0)\left[v_1^2(0)+P_1^2\right]^{-\frac14}}$	$\phi_{2\pm}(i\kappa,P_2)=\pm L\int_{v_2(z)}^{P_2}\dfrac{\left[\pm(P_2^2-t^2)\right]^{\frac12}}{t}\,dt$	

*For J_{ν_i} and J'_{ν_i} use z = 0

Table 3.1B - Asymptotic approximations along integration path

and, as a result, the turning points separate different regions of importance along the integration path.

The asymptotic approximation of the formal solution given in Eq. (4.2.14) along interval $\operatorname{Re} p_1 = 0$, $v_1(z_>) < \operatorname{Im} p_1 < \infty$ is carried out on the top sheet by introducing the approximate forms of the cylinder functions found in Tables 4.1A and 4.1B, into the two integrands and then integrating these integrands.

Because of the exponentially increasing nature of J_{v_2} and J_{-v_2} in this region, both integrals in Eq. (4.2.14) are large for large $k_o L$. Since the difference of the two integrals becomes indeterminate as $k_o L \to \infty$, the representation, given by Eq.(4.2.14), cannot be used over this portion of the integration path. To alleviate this difficulty, we use the alternative representation given in Eq. (4.2.16). Proceeding as before, we find that this portion of the integration path gives an exponentially small contribution to the field for all observation points with $z > 0$. The integration path was deformed a small amount around the branch cut in order to facilitate the evaluation of the integral. The same portion of the integration path, on the second sheet, gives a similar result since the asymptotic approximations used in the evaluation remain the same (they are independent of p).

The original representation for the field, i.e., Eq. (4.2.14), will be used to evaluate the contribution from the remaining portion of the integration path. The only motivation for introducing the alternate representation, 4.2.16, was to alleviate the difficulty encountered above. Before proceeding further we shall divide the field E_y, as represented in Eq. (4.2.14), in a sum of its individual integrals, i.e.,

$$E_y = E_{Dir} + E_{Ref} \tag{4.3.40}$$

where

$$E_{Dir} = \int_C \iota_D(z_<, z_>, p_1) dp_1 \ , \quad E_{Ref} = \int_C f_R(z_<, z_>, p_1) dp_1 \tag{4.3.41}$$

with

$$f_D(z_<, z_>, p_1) = - \frac{\tau p_1}{4p \sin(\pi \nu_2)} J_{-\nu_2}\left[-i\lambda e^{-z_</L}\right] J_{\nu_2}\left[-i\lambda e^{-z_>/L}\right] e^{ik_o px} \qquad (4.3.42)$$

and

$$f_R(z_<, z_>, p_1) = - \frac{\tau p_1 \overline{\Gamma}}{4p \sin(\pi \nu_2)} J_{\nu_2}\left[-i\lambda e^{-z_</L}\right] J_{\nu_2}\left[-i\lambda e^{-z_>/L}\right] e^{ik_o px} \qquad (4.3.43)$$

The choice of symbols E_{Dir} and E_{Ref} was motivated by the fact that the evaluation of E_{Dir} yields the direct ray contribution, while the evaluation of E_{Ref} yields the returning ray contributions.

The asymptotic approximations for J_{ν_2} and $J_{-\nu_2}$, listed in Table 4.1A, are now used to approximate $f_D(z_<, z_>, p_1)$ along the section of the integration path from $p_1 = \sqrt{\Delta}$ on the top sheet to $p_1 = \sqrt{\Delta}$ on the second sheet. The integrand is approximately given by

$$f_D(z_<, z_>, p_1) \sim - \frac{i}{4\pi} \frac{p_1 e^{ik_o L_D(p_1)}}{p[p_2^2 - v_2^2(z_<)]^{1/4} [p_2^2 - v_2^2(z_>)]^{1/4}} \qquad (4.3.44)$$

where

$$L_D(p_1) = \phi_2(z_<, p_2) - \phi_2(z_>, p_2) \pm px \begin{cases} + \text{ upper sheet} \\ - \text{ lower sheet} \end{cases} \qquad (4.3.45)$$

For large k_o, the main contributions to E_{Dir} will be in the vicinity of the saddle points of the integrand, i.e., where $dL_D(p_1)/dp_1 = 0$. By performing the indicated differentiation on Eq. (4.3.45), the saddle point locations are given by

$$x = \pm L \int_{v_2(z_>)}^{v_2(z_<)} \frac{p \, dt}{t\sqrt{p_2^2 - t^2}} , \begin{cases} + \text{ upper sheet} \\ - \text{ lower sheet} \end{cases} \qquad (4.3.46)$$

The above saddle point equation is the equation for the direct rays when
the plus sign is chosen. A sketch of the different ray regions has been
drawn in Fig. 4. 9. The basic regions defined in this figure are valid when
L is not too small. We have drawn in the portion of regions B and C,
appearing below the $z = z'$ line, but these may not appear for some parameter
ranges. When L is small, as we have seen in the section on rays, an add-
itional cusp is introduced into the region just above the $z = 0$ line. The
sketch of Fig. 4. 9 cannot be used to find the ray regions in the immediate
vicinity of this cusp, but the other ray regions, with minor modifications,
remain essentially the same for small L.

By using the nomenclature of Fig. 4. 9, these rays are located in regions
A, B, and C of the x-z plane. Since the rays do not cross, only one solution
of Eq. (4. 3. 46) exists for each point in the above mentioned regions. The
saddle point equation, 4. 3. 46, has no solutions on the lower sheet for any
location in the x-z plane.

The method of steepest descent can now be used to evaluate the integral
$[E_{Dir}]$ asymptotically. Without going into detail, we find that the integral
is approximated by the contribution due to the direct ray saddle point, when
the observation point is located in regions A, B, or C. On the other hand, the
integral is exponentially small when the observation point is located in regions
other than A, B, or C.

The reflected field integrand, $f_R(z_<, z_>, p_1)$ will now be asymptotically
approximated along that portion of the integrand path from $p_1 = i\sqrt{\Delta}$ on the top
sheet to $p_1 = i\sqrt{\Delta}$ on the bottom sheet. The uniform asymptotic approximations
found in section b can be used for this purpose. However, an additional simp-
lification of the integrand can be obtained by using the approximations given
in Tables 4. 1A and 4. 1B, but portions of the integration path lying close to
turning points of cylinder functions must be omitted. We will use the later

asymptotic approximations, and then, deform the integration path around the turning points.

Before doing this, it will be advantageous to divide the portion of the integration path under consideration into six intervals : three on the top sheet and three on the bottom sheet. The intervals are : 1)$\mathrm{Re}\, p_1 = 0$, $\sqrt{\Delta/2} < \mathrm{Im}\, p_1 < v_1(z_>)$, 2)$\mathrm{Re}\, p_1 = 0$. $0 < \mathrm{Im}\, p_1 < \sqrt{\Delta/2}$ and 3) $0 < \mathrm{Re}\, p_1 < \sqrt{\epsilon_1}$, $\mathrm{Im}\, p_1 = 0$. The intervals on the top and bottom sheets are the same. If we recall that $v_1(z_<)$ and $\sqrt{\Delta/2}$ are the locations of turning points. Then the approximations to be used for $f_R(z_<, z_>, p_1)$ will not hold near these points.

By using the asymptotic approximations appearing in Tables 4.1A and 4.1B, the integrand for the first interval on the top sheet is given approximately by

$$f_R(z_<, z_>, p_1) \sim - \frac{p_1 e^{ik_o L_R >}}{4\pi p [p_2^2 - v_2^2(z_>)]^{1/4}[p_2^2 - v_2^2(z_<)]^{1/4}} \; , \; \sqrt{\Delta/2} < \mathrm{Im}\, p_1 < v_1(z_>)$$

(4.3.47)

where

$$L_R > = \Phi_{2+}(z_>, p_2) + \Phi_{2+}(z_<, p_2) + px$$

(4.3.48)

with Φ_{2+} being in Table 4.1B. The equation for saddle points of this integrand is given by $dL_{R>}/dp_1 = 0$. By performing the differentiation on Eq. (4.3.48), we find that the resultant equation is the equation for the returning ray with $z_t > 0$ given in Eq. (4.3.13). The returning rays are located in regions D, E and F of Fig. 4.9 .

Proceeding in a similar manner, the integrand for the second interval on the top sheet is given by

$$f_R(z_<, z_>, p_1) \sim \frac{p_1 e^{ik_o L_{R<}(p_1)} dp_1}{4\pi p [p_2^2 - v_2^2(z_<)]^{1/4}[p_2^2 - v_2^2(z_>)]^{1/4}} \; , \; 0 < \mathrm{Im}\, p_1 < \sqrt{\Delta/2}$$

(4.3.49)

where

$$L_{R<} = \phi_{2+}(z_<, p_2) + \phi_{2+}(z_>, p_2) - 2\phi_{2+}(o, p_2) + 2\phi_{1-}(|p_1|) + px , \quad (4.3.50)$$

The saddle points for the above integrand are given by $dL_{R<}/dp_1 = 0$. If we perform the indicated differentiation upon Eq. (4.3.50), we find it to be the same as the equation for the returning rays with $z_t < 0, z > 0$, Eq. (4.3.21). Therefore saddle points appearing in this region correspond to returning rays with $z_t < 0$. These returning rays are located in regions B, C, D, E, and G of Fig. 4.9.

To show the correspondence between the number of saddle points in a particular interval and their associated regions in the x-z plane, we have prepared Table 4.2. In the table, only saddle points of E_{Ref} have been considered, while saddle points of E_{Dir} have been omitted because of their simpler form.

By using the asymptotic formulae to approximate the integrand in the third interval, we obtain

Region in x-z plane	Number of Saddle Points	
	$0 < \text{Im } p_1 \sqrt{\Delta/2}$	$\sqrt{\Delta/2} < \text{Im } p_1 < \sqrt{\Delta}$
A	0	0
B	2	0
C	1	1
D	1	2
E	2	1
F	0	1
G	1	0

Table 4.2

Correspondence between Saddle Points and Ray Regions of

Integral E_{Ref}.

$$f_R(z_<, z_>, p_1) \sim \frac{p_1 A(\tau, p_1) e^{ik_o L_r(p_1)}}{4\pi p \left[p_2^2 - v_2^2(z_<)\right]^{1/4} \left[p_2^2 - v_2^2(z_>)\right]^{1/4}}, \quad 0 < \text{Re} p_1 < \sqrt{\epsilon_1}$$

(4.3.51)

where

$$L_r(p_1) = \psi_{2+}(z_<, p_2) + \psi_{2+}(z_>, p_2) - 2\psi_{2+}(o, p_2) \quad , \quad A(\tau, p_1) \sim O(\tau^{-2}) \quad . \quad (4.3.52)$$

We can show that the function $A(\tau, p_1)$ in the above integrand is of order k_o^{-2}. This means that any saddle points, occurring in this interval, will rot give a dominant asymptotic contribution to E_{Ref}; therefore, these contributions can be neglected.

It is, however, interesting to learn about the physical significance of these saddle points if they occur. The saddle points are given by $\frac{d L_r(p_1)}{dp_1} = 0$. An investigation of this saddle point equation shows that it represents the equation for direct rays which are reflected from the discontinuity at $z = 0$. Only those direct rays, to the left of the critically reflected ray, shown in Fig. 4.9, are obtained from integral 4.3.51. It is strongly suspected that direct rays, reflected from the interface and lying between the critically reflected ray and the tangent ray, would be found from a higher order asymptotic analysis of integral 4.3.49; however, this has not been done.

A similar asymptotic analysis of the integrand for the three intervals on the bottom sheet shows that no saddle points occur along this portion of this integration path.

Since we now know the location of all the saddle points occurring on the integration path, the field E_{Ref} can be evaluated by using the method of steepest descents. We deform the original integration path into the adjacent decay region and through the appropriate saddle points. The resultant field will then be given asymptotically as a sum of a relevant saddle point contributions
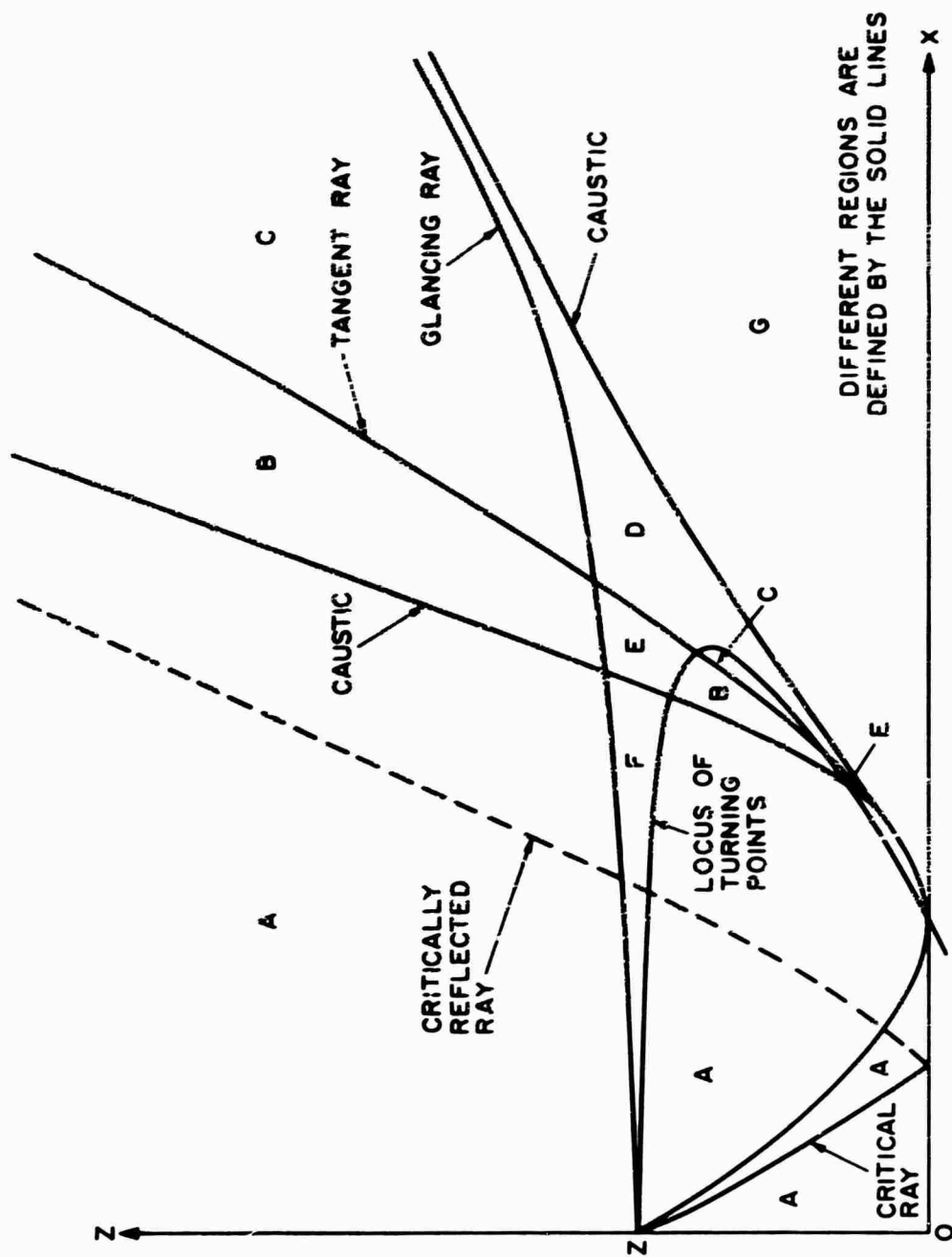
Fig. 4.9

Sketch of Ray Regions

plus any contributions that come from singularities between the original and deformed paths. At this point we will restrict our attention to cases where the observation point lies in regions B and C. The evaluation of the field in these two regions will illustrate the main features of the reflected field and will be useful for comparison purposes in a later section.

Two saddle points occur on the integration path when the observation point is located in either regions B or C. For region B both these saddle points lie in the second interval, i.e., $\text{Re}\,p_1 = 0$, $0 < \text{Im}\,p_1 < \sqrt{\Delta/2}$ and they are shown in Fig. 4.10 where the lower saddle point is denoted by p_{1L} and the upper one by $p_{1R<}$. The nomenclature has been motivated by the fact that for small L the rays corresponding to p_{1L} and $p_{1R<}$ look like the lateral and reflected rays on an abrupt interface respectively. For region C one saddle point, p_{1L}, lies in the second interval while the second saddle point, $p_{1R>}$, is located in the first interval, i.e., $\sqrt{\Delta/2} \le \text{Im}\,p_1 < v_1(z_>)$, $\text{Re}\,p_1 = 0$. The naming of saddle points in this region has a similar motivation to those saddle points associated with region B.

The decay regions which are adjacent to the integration path on the top sheet have been investigated by expanding $L_{R>}(p_1)$, $L_{R<}(p_1)$ and $L_r(p_1)$ about an arbitrary point in integration intervals one, two and three respectively. If p_1 is close to the integration path the appropriate phase function can be approximated by its first one or two terms. Use of the approximation in the integrands of Eqs. (4.3.47), (4.3.49) and (4.3.51) yields the decay regions for Band C, shown in Figs. 4.10, 4.11 and 4.12.

The original integration path is then deformed and evaluated along this deformed path. The portions of the integral passing through saddle points are evaluated by the method of steepest descents, while portions of the integration path in decay regions are exponentially small.
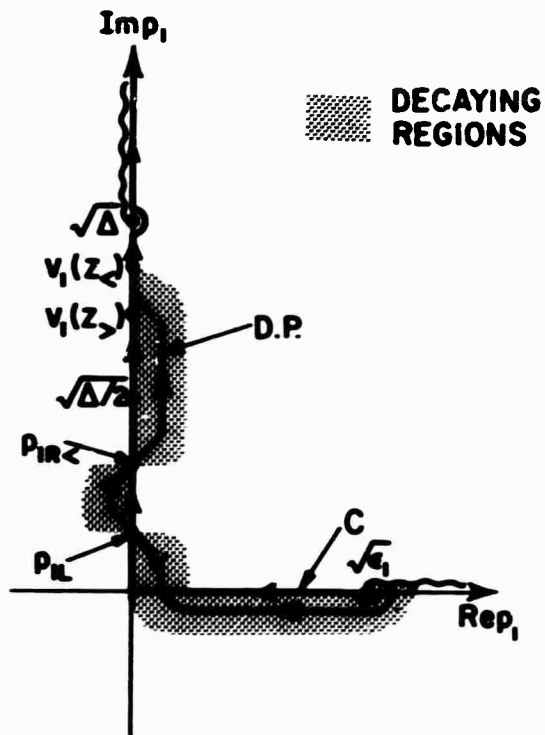
Fig. 4.10

Deformed Path on Top Sheet for
Region B
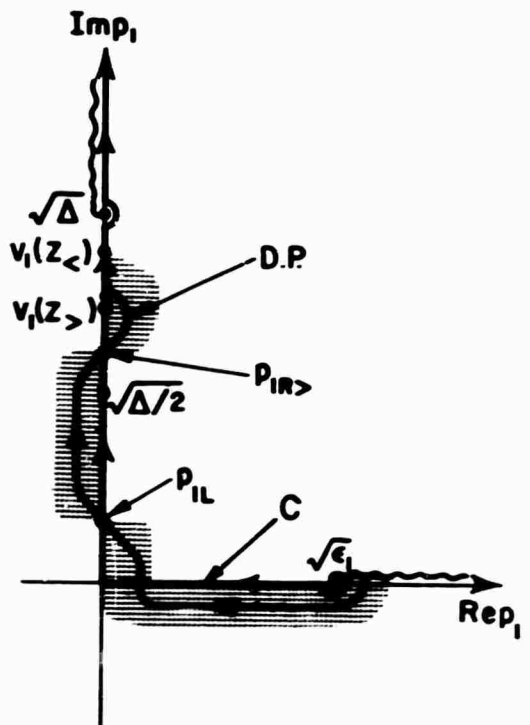
Fig. 4.11

Deformed Path on Top Sheet for
Region C
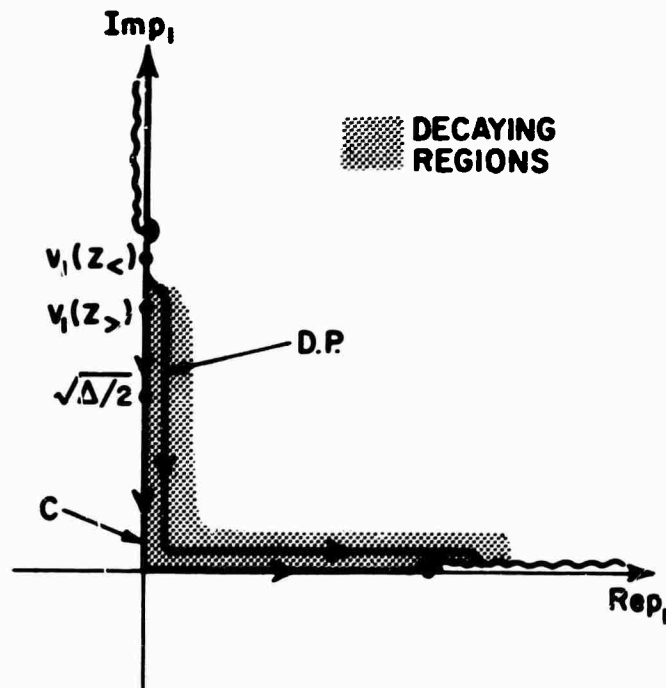
Fig. 4.12

Deformed Path on Second Sheet for Regions B and C

The singularities that can occur between the original and deformed paths are of two types : branch cuts and simple poles. There are no branch cuts intercepted by the deformed path as can be seen from Figs. 4.10, 4.11 and 4.12. The asymptotic form of the reflection coefficient has no poles located between the two paths except possibly in the turning point region, $p_1 = \sqrt{\Delta/2}$. Because of the complicated nature of the reflection coefficient in this region, the singularities have not been investigated here. We will assume that singularities, contributing other than exponentially small contributions, are not present.

Upon applying the method of steepest descent when the observation point is located in region B, we obtain

$$E_{Ref}\Big|_B \sim iI_1(p_1) + I_1(p_1)\Big|_{p_1 = p_{1R<}} \tag{4.3.53}$$

where

$$I_1(p_1) = \frac{p_1 e^{ik_o L_{R<}(p_1) + i\pi/4}}{2\sqrt{2\pi}\, p[p_2^2 - v_2^2(z_<)]^{1/4}\, [p_2^2 - v_2^2(z_>)]^{1/4}[k_o|L''_{R<}(p_1)|]^{1/2}} \tag{4.3.54}$$

and doing the same in region C, we obtain

$$E_{Ref}\Big|_C \sim iI_1(p_1)\Big|_{p_1 = p_{1L}} + I_2(p_1)\Big|_{p_1 = p_{1R>}} \tag{4.3.55}$$

where

$$I_2(p_1) = \frac{p_1 e^{ik_o L_{R>}(p_1) + i\pi/4}}{2\sqrt{2\pi}\, p[p_2^2 - v_2^2(z_<)]^{1/4}[p_2^2 - v_2^2(z_>)]^{1/4}[k_o L''_{R>}(p_1)]^{1/2}} \cdot \tag{4.3.56}$$

To find the total field for regions B and C, we shall have to add the contribution from the first integral in Eq. (4.2.14) due to the direct ray.

The asymptotic formulae obtained in Eqs. (4. 3. 54) and (4. 3. 55) break down as the observation approaches the tangent ray. Here a saddle point approaches the turning point at $p_1 = \sqrt{\Delta/2}$ and the simple asymptotic analysis used, can no longer be applied.

d. Conclusions

We have taken the exact solution, Eq. (4. 2. 14), and approximated it for large $k_o L$, i. e. , we have assumed that the medium is slowly varying with respect to wavelength. The asymptotic approximations developed by Olver have enabled us to show that the first integral in Eq. (3. 2. 14) corresponds to direct ray contributions while the second integral corresponds to returning ray contributions. In addition, contributions due to direct rays, reflected from the interface, were found in the second integral but were of order $1/k_o^2$ lower than the dominant contributions. The above finding again confirms the method of geometric-optics since all of the above results can be predicted without resorting to the asymptotic approximation of the exact solution; this was demonstrated in section 4. 3. 2. The reflected waves for the discontinuity were not mentioned in section 4. 3. 2, but Chester and Keller[33] have shown that, for a dielectric profile having a discontinuous second derivative, the reflected waves will be $1/k_o^2$ lower than the incident wave.

4. 4 Asymptotic Evaluation of the Field for Large $k_o Lp$

a. Introduction

In the last two sections, 4. 3. 2 and 4. 3. 3, the high frequency field has been investigated when the transition profile is slowly varying with respect to frequency. We shall now investigate the high frequency field for all transition thicknesses, $k_o L$, with special attention placed upon the changing character of the lateral wave, as the transition thickness increases. The method

used will essentially follow Chapter 3, i.e., we will write the reflection coefficient in an exponential form and then use the method of successive approximations to find the saddle points.

b.   Restriction of Field Evaluation to Homogeneous Regions

An examination of the field representation given in Eqs. (4.3.40), (4.3.41), (4.3.42) and (4.3.43) shows that both the integrals for the direct field, E_{Dir} and the reflected field E_{Ref} are of a different generic type than the integrals that were uniformly evaluated in Chapter 3. The basic difference is the presence of the Bessel functions $J_{\nu_2}(-i\lambda e^{-z/L})$ and $J_{-\nu_2}(-i\lambda e^{-z/L})$. In order to apply the methods of Chapter 3, the Bessel functions must be approximated and this will, in turn, limit the region in which the uniform asymptotic approximation is valid.

Since the integral evaluated in Chapter 3 resulted from an exact field representation in a homogeneous region, it would seem likely that placing the observation and source points far from the interface ($z = 0$) might put the integrals for E_{Dir} and E_{Ref} in a more tractable form. For large z and z' the arguments of the Bessel functions become small, and the Bessel functions can be represented approximately by the first term of their series representation.

To put this on a more rigorous basis, the Bessel function can be represented as [34]

$$J_{\nu_2}(-i\lambda e^{-z/L}) = \left(\frac{-i\lambda}{2}\right)^{\nu_2} e^{ik_o p_2 z} \sum_{m=0}^{\infty} \frac{\left(\frac{-i\lambda}{2}\right)^{2m} e^{-2m z/L}}{m! \; \Gamma(\nu_2+m+1)} \; . \qquad (4.4.1)$$

The rate of convergence of the series can be measured by the absolute value of the ratio of adjacent terms in the series. The ratio of the $(m+1)^{th}$ to the mth term is

$$R_m = \frac{\Delta \tau^2 e^{-2z/L}}{8m \left[(m+2+\tau p_{2i})^2 + \tau^2 p_{2r}^2 \right]^{\frac{1}{2}}} \qquad (4.4.2)$$

where p_{2r} and p_{2i} are the real and imaginary parts of p_2 respectively.
An examination of the above ratios shows that a sufficient condition for
the Bessel function to be approximately equal to the first term in the series
representation is $R_o \ll 1$. A slightly more restrictive condition than $R_o \ll 1$
is

$$\frac{\Delta \tau e^{-2z/L}}{|p_2|} \ll 1 \quad . \qquad (4.4.3)$$

This more restrictive condition can be expressed in a more physically
understandable form, i.e.,

$$\left(\tau / p_2 \right) \left(\frac{d \epsilon(z)}{dz} \Big/ \epsilon(z) \right) \ll 1 . \qquad (4.4.4)$$

As z becomes large, $\epsilon(z)$ tends toward unity, and the above condition
requires that $\epsilon'(z)$ must be small compared with p_2/τ .

This more accurately defines what is meant by assuming that the source
and observation points lie in the "homogeneous" region. We note that rays
close to the glancing angle will have to be excluded from our treatment since
these rays have $p_2 \simeq 0$.

It must be mentioned at this point that one representation for the field
will be sufficient for an asymptotic calculation along the whole integration
path. If we recall in section 4.3.3, two different representations are
necessary to calculate the field. The representation given by Eq. (4.2.14)
does not give an indeterminate asymptotic expression for the field if the
source and observation points are located in the "homogeneous" region.
As a result we will not need the alternative representation in Eq. 4.2.16
in this section.

By using the first term of the series representation for the Bessel function in the integral for E_{Dir} , Eq. (4.3.41), we have

$$E_{Dir} \approx + \frac{1}{4\pi i} \int_C \frac{P_1}{P P_2} e^{+ik_o[p_2|z-z'|+px]} dp_1 . \qquad (4.4.5)$$

We can recognize the above expression as the incident field emitted from a source located in a homogeneous medium having a dielectric constant of unity. The asymptotic evaluation of the above integral leads to an interpretation of the field as consisting of straight line rays. It can be shown that the "homogeneous" approximation, in general, limits us to the region where the rays are approximately straight lines.

By substituting the same approximation for the Bessel function in the expression for E_{Ref} , Eq. (4.3.42), we obtain

$$E_{Ref} \approx \frac{1}{4\pi i} \int_C \frac{P_1 \hat{\Gamma}}{P P_2} e^{ik_o[p_2(z+z'+px]} dp_1 \qquad (4.4.6)$$

where

$$\hat{\Gamma} = \frac{\Gamma(1-\nu_2) \overline{\Gamma}}{\Gamma(1+\nu_2)P_2} . \qquad (4.4.7)$$

In the above expression $\hat{\Gamma}$ is the plane wave reflection coefficient as $z \to \infty$. Here again the rays in the "homogeneous" region will be straight lines but will have a phase delay due to $\hat{\Gamma}$.

c. Asymptotic Evaluation of E_{Ref}

Following Chapter 3, we rewrite Eq. (4.4.6) as

$$E_{Ref} \approx \frac{1}{4\pi i} \int_C \frac{P_1}{P P_2} e^{ik_o[p_2(z+z')+px+1/k_o \psi(p_1,\sqrt{\Delta}\tau)]} dp_1 \qquad (4.4.8)$$

where $\hat{\Gamma}$ has been represented as

$$\hat{\Gamma} = e^{i\psi(p_1, \sqrt{\Delta}\tau)} \tag{4.4.9}$$

with

$$\psi(p_1, \sqrt{\Delta}\tau) = -i \ln\left\{\overline{\mp} \frac{\Gamma(1-\nu_2)}{\Gamma(1+\nu_2)} \left(\frac{i\lambda}{2}\right)^{2\nu_2}\right\} . \tag{4.4.10}$$

The multivaluedness of the logarithm does not appear in the integrand since the function $e^{\ln Q}$ is single valued.

The uniform asymptotic evaluation of the above integral will be performed by the method of steepest descents. As was the case in Chapter 3, the saddle points will be found by the method of successive approximations and will have a location in the p_1 plane that varies with the large parameter k_0.

The equation that describes the location of the saddle points is

$$p_1\left[(z+z')/p_2 \mp x/p\right] + (1/k_0)d\psi/dp_1 = 0 , \quad \begin{cases} -\text{top sheet} \\ +\text{second sheet} \end{cases} . \tag{4.4.11}$$

We shall solve this equation in the region to the right of the critically reflected ray. When τ is small or moderate in value, the position of the critical ray is closely approximated by the critically reflected ray from an equivalent abrupt interface problem. When τ is large, the position of this ray is shown in Fig. 4.9. For observation points in the "homogeneous" region, the critically reflected ray in Fig. 4.9 and the upper branch of the caustic almost coincide. Therefore, using the nomenclature of Fig. 4.9 for large τ, we are finding the saddle points in regions B and C.

By applying the method of successive approximations to Eq. (4.4.11) on the upper sheet when k_0 is large, the first corrected location for the saddle points is given by

$$p_{1L}^{(1)} = \frac{\sqrt{\epsilon_1}}{k_o L_p} \left. \frac{d\psi}{dp_1} \right|_{p_1 = 0} \quad , \quad L_p = x - \sqrt{\epsilon_1/\Delta}(z + z') \tag{4.4.12}$$

$$p_{1r}^{(1)} = p_{1r}^{(0)} - \frac{d\psi}{dp_1} \left/ \left\{ \sqrt{\Delta} k_o L_p \left((z+z')/p_2^3 + x/p^3 \right) \left(\sqrt{\Delta} x + \sqrt{\epsilon}(z+z') \right) \right\} \right|_{p_1 = p_{1r}^{(0)}}$$

$$\tag{4.4.13}$$

where the superscript is the order of approximation with $p_{1r}^{(0)} = i\sqrt{\Delta x^2 - (z+z')^2 \epsilon_1}$ and $d\psi/dp_1 = i|d\psi/dp_1|$ for $\text{Re } p_1 = 0$, $0 < \text{Im } p_1 < \sqrt{\Delta}$. For this approximation to be valid we must have

$$\left| \frac{d\psi(p_1, \sqrt{\Delta}\tau)}{dp_1} \left/ k_o L_p \right. \right| \ll 1 \quad , \quad 0 \le \tau < \infty \quad , \quad \text{Re } p_1 = 0 \quad , \quad 0 \le \text{Im } p_1 < \sqrt{\Delta} \quad . \tag{4.4.14}$$

We can show for small and for moderate values of τ that $d\psi/dp_1$ is bounded except at $v_2 = 0$ and for large values of τ that $d\psi/dp_1 \sim \tau f(p_1)$ where $f(p_1)$ is a bounded function of p except at $p_2 = 0$. This leads us to the conclusions that the method of successive approximations is valid when

$$k_o L_p > 1 \quad , \quad L/L_p \ll 1 \quad . \tag{4.4.15}$$

Since the critically reflected ray occurs at $L_p = 0$, these conditions essentially state that the observation point should be located a number of transition lengths L from the critically reflected ray, for the method of successive approximations to be valid. No other saddle points occur in the remaining portions of the integration path on the top sheet or along any portion of the integration path on the lower sheet.

The integration path will now be deformed in the adjacent decay regions and through the two saddle points just mentioned; it can be shown that the decay regions for small or for moderate τ are similar to those described in

Chapter 3 and also to those shown in Figs. 4.10, 4.11 and 4.12. For large τ, the decay regions have been calculated in the last section, 4.3.3., and are shown in the three figures mentioned above. No singularities of the branch type occur between the original and deformed paths. The nature of pole singularities have not been investigated in detail except in the case of large τ where a partial investigation shows that no singularities which have a substantial effect on the field are present. We will assume that any singularities which might occur between the two paths are unimportant and their residues can be neglected.

The integral is now evaluated along the deformed path. Portions of the path in the decay regions have exponentially small contributions while the dominant contributions come from the portions of the path near the two saddle points. The asymptotic approximation for the reflected field is

$$E_{Ref} = E_r + E_L \tag{4.4.16}$$

where

$$E_r \sim \frac{|p_1| \, e^{ik_o[p_2(z+z')+px+(1/k_o)\psi(p_1,\sqrt{\Delta}\tau)]+i\pi/4}}{2\sqrt{2\pi} \, p \, p_2 \left[\frac{(z+z')}{p_2} - \frac{x}{p} - p_1^2\left(\frac{z+z'}{p_2^3} + \frac{x}{p^3}\right)\right]^{\frac{1}{2}} k_o^{\frac{1}{2}}} \Bigg|_{p_1 = p_{1r}^{(0)}} \tag{4.4.17}$$

and

$$E_L \sim \frac{\epsilon_1^{1/4} \, A(\sqrt{\Delta}\tau) \, e^{ik_o[\sqrt{\Delta}(z+z')+\sqrt{\epsilon_1}\,x+(1/k_o)\psi(\sqrt{\Delta}\tau)]+3\pi/4}}{\sqrt{2\pi}\,\Delta\,(k_o L_p)^{3/2}} \tag{4.4.18}$$

with

$$\psi(\sqrt{\Delta}\tau) = \psi(0,\sqrt{\Delta}\tau) = 2\tan^{-1}\left(\frac{Im\,M}{Re\,M}\right) - 2\sqrt{\Delta}\,\tau\ln\left(\frac{\lambda}{2}\right) , \tag{4.4.19}$$

$$A(\sqrt{\Delta}\tau) = \frac{\sqrt{\Delta}}{2}\left|\frac{d\psi}{dp_1}\right|\Bigg|_{p_1=0} = \frac{1 - e^{-2\pi\sqrt{\Delta}\,\tau}}{\pi\sqrt{\Delta}\,\tau\,|M|^2} \tag{4.4.20}$$

and

$$M = [J_{i\sqrt{\Delta}\,\tau}(-i\lambda)\,J_0'(\lambda) - i\,J_0(\lambda)\,J_{i\sqrt{\Delta}\,\tau}'(-i\lambda)]\,\Gamma(1+i\sqrt{\Delta}\,\tau) \quad . \qquad (4.4.21)$$

The notation E_r and E_L has been adopted since, in the limit of small τ, these terms correspond respectively to the reflected and lateral wave contributions on an abrupt interface.

The contribution E_r has the form of a reflected wave for an abrupt interface except for the presence of the phase term, $\Psi(p_{ir}, \sqrt{\Delta}\,\tau)$. This phase term increases as the normalized transition thickness, $k_0 L$, increases. For large τ, the asymptotic approximations for the Bessel functions can be used in $\Psi(p_{1r}, \sqrt{\Delta}\,\tau)$. We obtain

$$\Psi(p_{1r}, \sqrt{\Delta}\,\tau) \sim \begin{cases} 2\,\Phi_{1-}(|p_{1r}|) - 2\Phi_{2+}(0, p_{2r}) - 2\,Lp_{2r}\ln(2\,p_{2r}\sqrt{2/\Delta}) - 2\,Lp_{2r} \quad , \\[4pt] \qquad\qquad\qquad 0 < |p_{1r}| < \sqrt{\Delta/2} \qquad\qquad\qquad (4.4.22a) \\[12pt] 2\,Lp_{2r}\ln(2\,p_{2r}\sqrt{2/\Delta}) - 2\,Lp_{2r} \quad , \qquad \sqrt{\Delta/2} < |p_{1r}| < v_1(z>) \qquad (4.4.22b) \end{cases}$$

where Φ_{1-} and Φ_{2+} have been defined in Table 4.1B and $p_{2r} = \sqrt{\Delta - |p_{1r}|^2}$. The use of these approximations in Eq. (4.4.17) gives us a portion of the reflected wave when the transition is slowly varying with respect to frequency. This portion of the reflected field corresponds to contributions from rays that make up the section of the caustic close to the interface as shown in Fig. 4.5.

The contribution E_L has the form

$$E_L \sim A(\sqrt{\Delta}\,\tau)\,e^{i\Psi(\sqrt{\Delta}\,\tau)}\,\{\text{conventional lateral wave contribution}\}.$$

$$(4.4.23)$$

Here $A(\sqrt{\Delta}\, \tau)$ and $\psi(\sqrt{\Delta}\, \tau)$ form a transition function which modifies the form
of the lateral wave. For small τ, E_L is approximately represented by the
conventional lateral wave contribution since $A(\sqrt{\Delta}\, \tau) \approx 1$ and $\psi(\sqrt{\Delta}\, \tau) \approx 0$. As τ
increases, $A(\sqrt{\Delta}\, \tau)$ and $\psi(\sqrt{\Delta}\, \tau)$ increase in such a way as to modify the lateral
wave term and change it into a geometric-optics contribution. For large τ,
the asymptotic forms of the Bessel functions can be used to approximate
$A(\sqrt{\Delta}\, \tau)$ and $\psi(\sqrt{\Delta}\, \tau)$. We obtain

$$
E_L \sim \frac{\sqrt{\pi}\, \epsilon_1^{1/4}\, L\, e^{ik_o\left\{\sqrt{\Delta}\,(z+z')+\sqrt{\epsilon_1}\, x + 2\sqrt{\Delta}\,\left[2/\sqrt{2}-1-\ln(\frac{1+\sqrt{2}}{2\sqrt{2}})\right]\right\}+i\pi/4}}{2\sqrt{2\Delta}\, L_p (k_o L_p)^2} \quad , \quad \tau \gg 1 \ .
$$

$$(4.4.24)$$

We note that the $k_o^{-3/2}$ dependence for small τ in Eq. (4.4.18) has now
been replaced by a $k_o^{-1/2}$ dependence. This signifies the change in the
contribution E_L from a diffraction effect to a geometric-optic effect. The
amplitude $A(\sqrt{\Delta}\, \tau)$ and the phase $\psi(\sqrt{\Delta}\, \tau)$ have been plotted in Figs. 4.13
and 4.14 respectively. The dash line in these figures represents the slowly
varying approximation, i.e., when $A(\sqrt{\Delta}\, \tau)$ and $\psi(\sqrt{\Delta}\, \tau)$ are asymptotically
approximated for large τ.

The approximate forms of E_r and E_L for large τ can also be obtained
from the results of section 4.3. There the field in region B is given by
Eq. (4.3.53) while the field for region C is given in Eq. (4.3.55). If we
simplify the expressions by placing the source and observation points in
the "homogeneous" region and assume $L/L_p \gg 1$, these reduce to the large
τ results of this section. To be more explicit, the term $i I_1(p_1)\big|_{p_1 = p_{1L}}$
reduces to Eq. (4.4.24); the term $I_1(p_1)\big|_{p_1 = p_{1R<}}$ reduces to (4.4.17)
with $\psi(p_{1r}, \sqrt{\Delta}\, \tau)$ approximated by Eq. (4.4.22a) and finally the term
$I_2(p_1)\big|_{p_1 = p_{1R>}}$ reduce to Eq. (4.4.17) where in Eq. (4.4.17) is approxi-
mated by Eq. (4.4.22b).
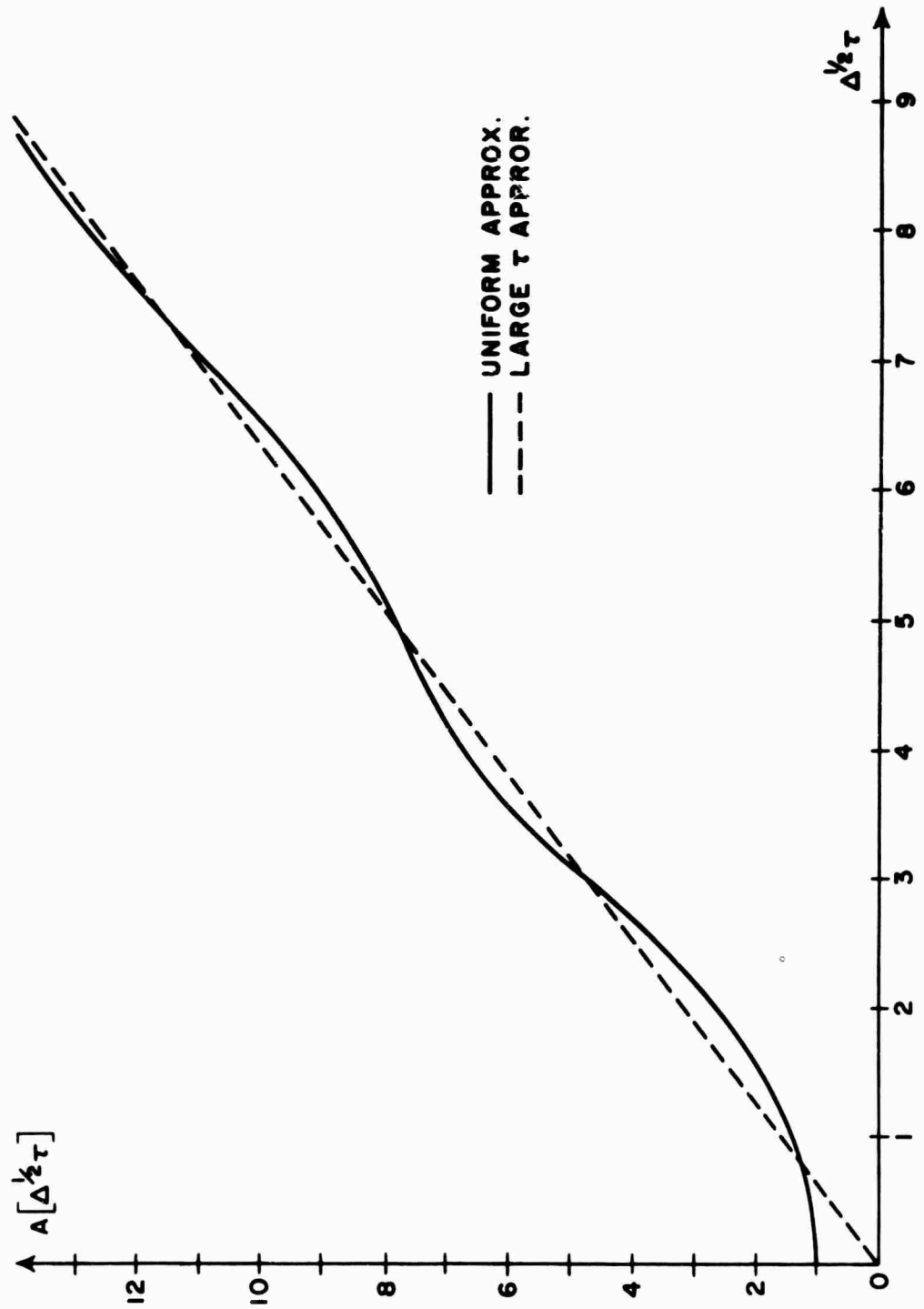
Fig. 4.13

Lateral Wave Amplitude vs. Normalized Transition Thickness
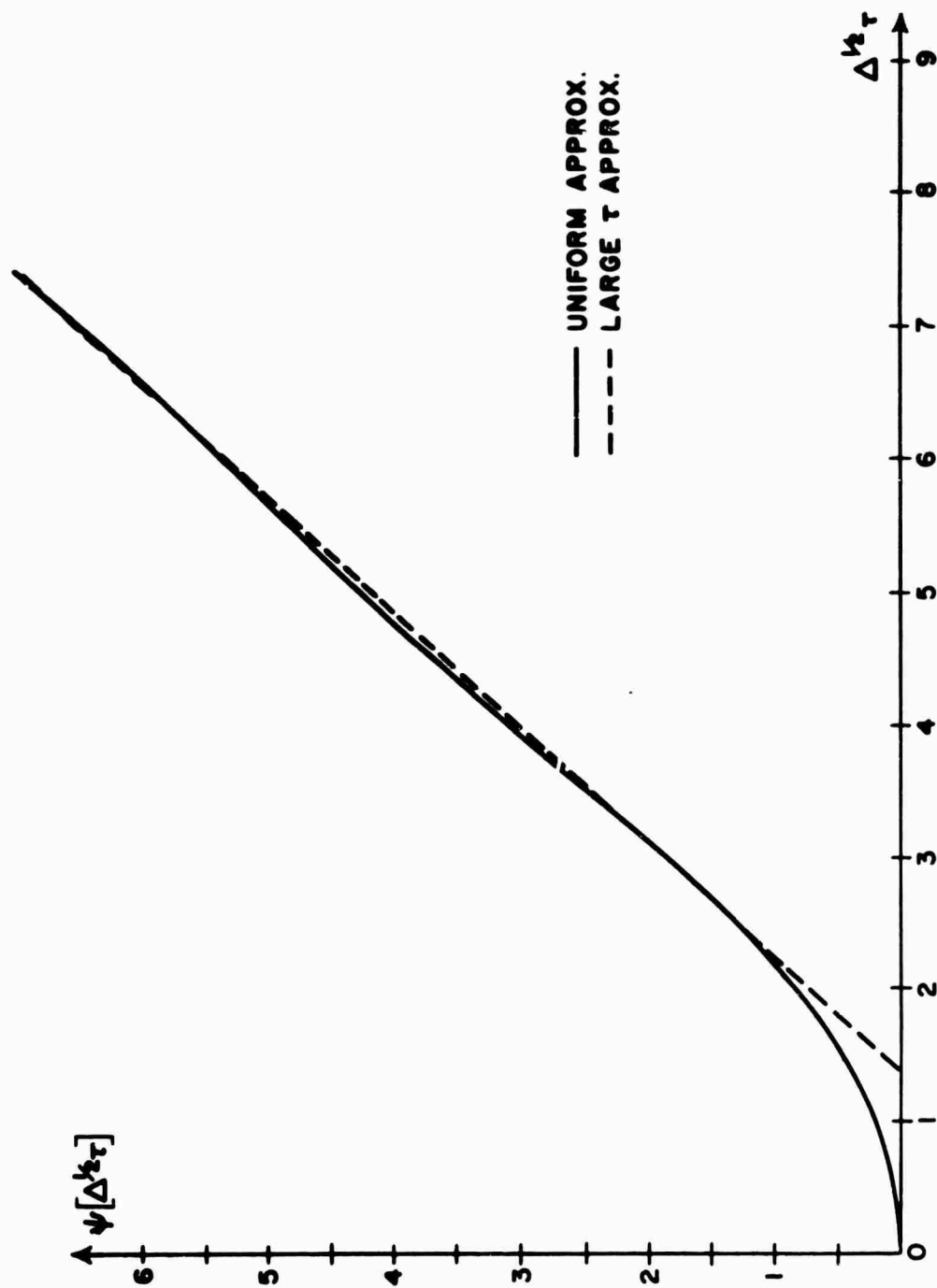
Fig. 4.14

Lateral Wave Phase vs. Normalized Transition Thickness

d. Conclusions

Our basic purposes for treating the double exponential medium were twofold: first, to see if the lateral wave behavior observed on the Epstein half space carried over to profiles where the source was located in the inhomogeneous medium, and second, to see the effect of relocating the second order discontinuity in the dielectric profile. We found that by restricting the source and observation point locations to the "homogeneous" region, results, similar to those in Chapter 3 were found. The lateral wave changed to a geometric-optics wave as the transition went from abrupt to slowly varying. It was also observed here and in Chapter 3 that the dependence on the lateral distance L_p remained $L_p^{-3/2}$, independently of the transition length. The discontinuity in the dielectric profile did not affect the basic nature of the lateral wave expression but it did introduce a difficulty in the reflected field, E_r. For large transition length, the field close to the tangent ray could not be treated by the classical methods of geometric-optics.

CHAPTER 5.

AN ARBITRARY TRANSITION LAYER

5.1 Introduction

To conclude our investigation of lateral waves which are excited on transition layers, we shall discuss and, in some cases, analytically formulate the dominant asymptotic contributions to the reflected field from an arbitrary monotonically increasing layer. The layers to be considered are divided into two basic classes : finite and infinite. The finite layers of width L will consist of a dielectric medium varying continuously between two half spaces, one being composed of vacuum ($z > 0$) and the other ($z < - L$) having a dielectric constant of $\epsilon_1 < 1$. The dielectric variation of the layer should be strictly increasing, i. e: $d\epsilon(z)/dz > 0$ except at the lower interface where (n-1) derivatives of $\epsilon(z)$ may be zero. To be more explicit, the dielectric profile $\epsilon(z)$ has a series expansion at the lower interface which is given by

$$\epsilon(z) = \epsilon_1 + \frac{d^n \epsilon(z)}{dz^n}\bigg|_{z = - L} \frac{(z+L)^n}{n!} \quad . \tag{5.1.1}$$

The infinite layer, on the other hand, will again consist of a vacuum half space for $z > 0$ and a strictly increasing dielectric profile ($z < 0$) which approaches ϵ_1 asymptotically as $z \to - \infty$. In addition, we will require that all derivatives of $\epsilon(z)$ approach zero $z \to - \infty$ and that $\epsilon(z) = \epsilon(z/L)$ where L is a parameter which is proportioned to the average thickness of the layer. Both classes of layers have this property: as L becomes small, the medium approaches an abrupt transition.

The line source, as in previous chapters, will be located parallel to the $z = 0$ interface in the vacuum medium . Sources placed in the inhomogeneous

portion of the layer will not be considered, since the results of Chapter 4 indicate that such a source location has little effect on the basic character of the lateral wave excited.

The structure of this chapter will be similar to previous chapters. First, the reflected field from a layer that is thick compared with wavelength will be discussed and then, an asymptotic evaluation of the reflected field representation will be carried out when $k_o L_p \gg 1$.

5.2   Reflected Field from an Arbitrary Layer for $k_o L \gg 1$

The reflected field from a layer that is thick compared with wavelength can be obtained asymptotically by the classical methods of geometrical-optics with the exception of those regions where diffraction effects are important. In this section we would like to locate those diffraction regions for an arbitrary layer and try to predict, by using the results of previous chapters, what type of diffraction effects we can expect.

Before doing this, however, the ray trajectories, as predicted by classical geometrical-optics, will be investigated. The rays emitted from the source toward the layer divide into two ray types : transmitted and returning ; the two ray types are separated by a critical ray. The returning ray equation, as given by Orlov[20], is

$$x = x_o + x_i z/z' \quad , \qquad z \geq 0 \qquad\qquad (5.2.1)$$

where x_i , the coordinate at which the ray enters the medium, can be related to the ray parameter p used in previous chapters. Their relationship is $x_o = p_2 z'/p$. The coordinate x_o is the point at which the returning ray leaves the layer, as shown in Fig. 5.1, and is related to x_i by

$$x_o = x_i + 2 x_t \quad . \qquad\qquad (5.2.2)$$
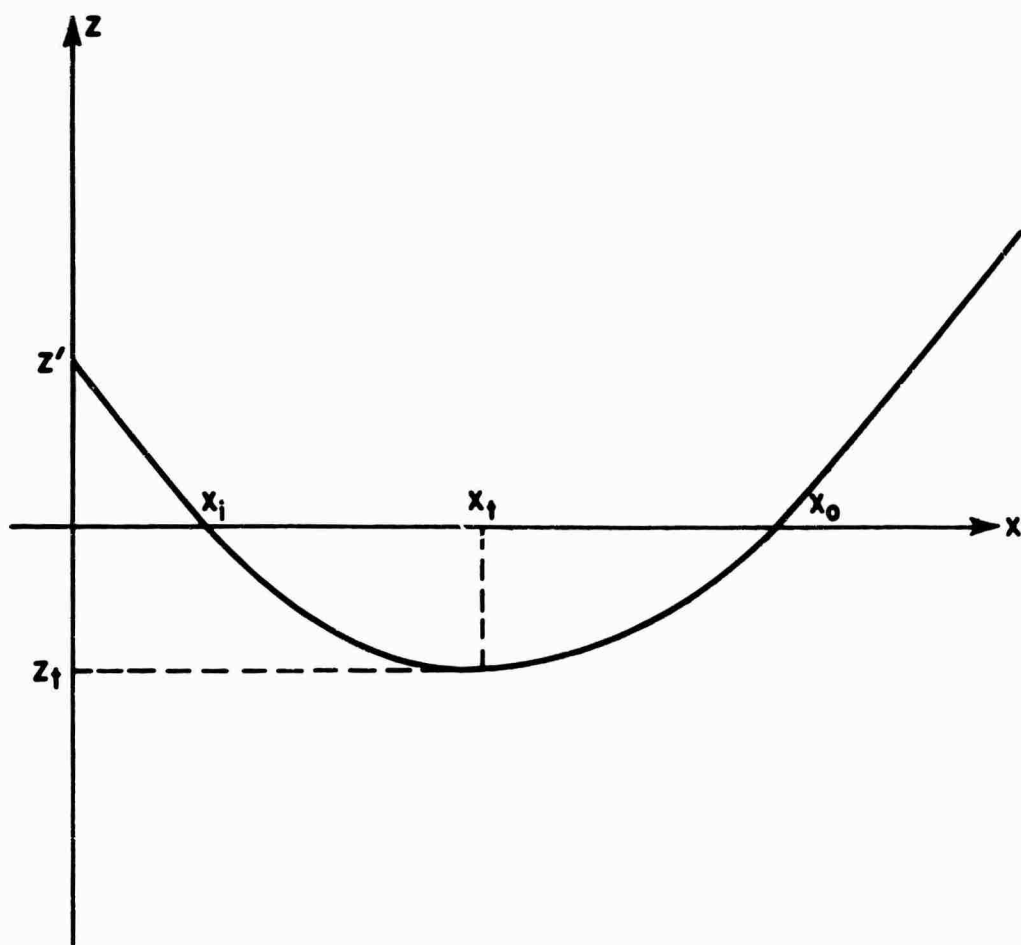
Fig. 5.1

Typical Returning Ray Trajectories

Here x_t is the x coordinate of the turning point which is given by

$$x_t = - \int_0^{z_t} \frac{p\,d\tau}{\sqrt{\epsilon(\tau) - p^2}} \qquad (5.2.3)$$

in terms of the ray parameter p.

The rays described by Eq. (5.2.1) usually cross one another in such a way as to form a caustic and foci. The constraint equation of this caustic can be found by taking the derivative of Eq. (5.2.1) with respect to x_i. The result is

$$d x_0 / d x_i = z/z' \qquad . \qquad (5.2.4)$$

We see, from this equation, that the caustic goes into the layer at points given by $dx_0/dx_i = 0$. An additional point or points on the caustic can be found by using the result of Appendix D where it has been shown that the maximum of the locus of turning points $(dx_t/dz_t = 0)$ corresponds to points at which the caustic crosses the line $z = z'$.

The locations of possible foci are given by the second constraint equation

$$d^2 x_0 / d x_i^2 = 0 \qquad (5.2.5)$$

when used in conjunction with Eqs. (5.2.4) and (5.2.1). The constraint equation was found by taking the derivative of Eq. (5.2.4) with respect to x_i.

Now that we have outlined the means by which we can obtain the structure of the reflected ray family, as predicted by classical geometrical-optics, we will discuss diffraction effects. To simplify the following discussion, it will be assumed that the profile of the arbitrary layer is completely continuous for $-L < z < 0$, i.e: all derivatives of $\epsilon(z)$ are continuous in the layer region.

This assumption eliminates diffraction regions occurring in the vicinity
of rays which have their turning points located at discontinuities of
$d^n \epsilon(z)/dz^n$.

Diffraction regions are those regions in which the classical theory of
geometrical-optics gives a poor approximation to the field. Typical regions
of this type are caustics, foci and ray regions composed of rays emitted close
to the critical angle. It is the latter of these diffraction effects that we wish to
discuss. The class of layers, under discussion, will be divided into three
parts : first, layers with a discontinuity in slope, $n = 1$; second, layers with
discontinuities in higher derivatives, $n \geq 2$; and third, infinite layers. Each
sub-class of layers will be discussed individually.

The layers with $n = 1$ have been singled out since these layers have
critical rays whose turning points have finite coordinates. The results of
Chapter 1 indicate that a lateral ray should be exicted at this turning point
and it should travel along the $z = -L$ interface while shedding energy into the
reflected field. The general form of this wave would be $A((k_o L)^{1/3}/(k_o L_s)^{3/2})e^{i\psi}$.
Here ψ is the phase from the source to the observation point along the lateral
ray; L_s is the distance that the ray travels along the $z = -L$ interface and A
is the excitation coefficient which will depend on the slope of the layer at
$z = -L$. We note that the k_o dependence is smaller than the returning ray
contribution, however, the lateral wave contribution might be important if
there were any loss in the layer. The results of Chapter 1 also seem to
indicate that the returning rays which lie close to the reflected critical ray
have field contributions that are not predictable by the theory of geometrical-
optics. The field in this region could be obtained by an asymptotic analysis of
the integral representation for the reflected field.

The next class of layers to be considered are those layers with $n \geq 2$.
An examination of the critical ray in this class of layers shows that it is

similar to the critical ray observed in Chapter 2. There the critical ray never becomes tangent to the lower interface but only approaches it asymptotically i.e., as $z_c \to -L$, $x_c \to +\infty$ where x_c and z_c are the coordinates of the critical ray. Because this ray never becomes tangent to the lower interface, the geometrical interpretation, rendered to the lateral wave in the $n = 1$ case, does not seem applicable here. However, it does appear that returning rays, emitted close to the critical angle, form a diffraction region.

To see the behavior of these returning rays for a special case, we have chosen

$$\varepsilon(z) = \varepsilon_1 + \Delta (z/L + 1)^n \quad , \quad n \geq 3 \quad . \tag{5.2.6}$$

We have not included $n = 2$ since an example of this case has been given in Chapter 2. The ray equation (5.2.1), when rewritten in terms of the ray parameter p, becomes

$$x = p(z + z')/p_2 + 2x_t \quad , \quad p_2 = \sqrt{1 - p^2} \tag{5.2.7}$$

where

$$x_t = - \int_0^{z_t} \frac{p \, d\tau}{\sqrt{\Delta(\tau/L + 1)^n - |p_1|^2}} \quad , \quad \varepsilon(z_t) = p^2 \tag{5.2.8}$$

and $|p_1| = \sqrt{p^2 - \varepsilon_1}$. For $|p_1|$ small, Eq. (5.2.8) can be written as

$$x_t = \frac{Lp}{\Delta^{1/n} |p_1|^{\frac{n-2}{n}}} \int_1^{\frac{\Delta^{1/n}}{|p_1|^{2/n}}} \frac{dw}{\sqrt{w^n - 1}} \tag{5.2.9}$$

where we have used the change of variable $w = \Delta^{1/n}(\tau/L+1) |p_1|^{-2/n}$.

The dominant asymptotic approximation for x_t as $|p_1| \to 0$ is then given by

$$x_t = \frac{L\sqrt{\epsilon_1}\, I_n}{\Delta^{1/n} |p_1|^{\frac{n-2}{n}}} + O(|p_1|^0) \quad , \quad n \geq 3 \qquad (5.2.10)$$

where I_n is a convergent integral given by

$$I_n = \int_1^\infty \frac{dw}{\sqrt{w^n - 1}} \quad .$$

We see as $|p_1| \to 0$, the slope of the ray tends toward $\sqrt{\Delta/\epsilon_1}$ while the intercept at the x axis tends toward infinity. As in the $n = 2$ case, these rays have trajectories similar to the lateral wave observed in the linear layer in Chapter 1.

We see that rays in this type of medium, which are emitted at angles close to the critical angle, contribute to the reflected field at large distances from the source. The results of Chapter 2 would also indicate that the methods of geometrical-optics are not generally successful in computing the amplitudes of these ray contributions.

The obvious step to take after considering profiles with $n \geq 2$, is to investigate an analytic layer. At present this has not been done for a finite layer, since no analytic profile could be found which has known wave functions associated with it. Recourse was taken to infinite layers, such as the symmetrical Epstein transition, for which the wave functions were known. An examination of the critical ray in an infinite layer shows that as $x_c \to \infty, z_c \to -\infty$. This differs from the finite layers where $z_c \to -L$. The results of Chapters 3 and 4 have indicated that returning rays emitted close to the critical angle tend to act in a similar manner as the returning rays from finite layers with $n \geq 2$, with one exception. This exception is that as

$|p_1| \to 0$, the turning point z_t tends toward infinity. The results of Chapters 3 and 4 also indicate that the method of geometrical-optics does not break down as the angle of ray emission from the source approaches the critical angle. Therefore no diffraction region is observed.

5.3   Evaluation of the Reflected Field for $k_o L_p \gg 1$

5.3.1   General Considerations

In this section we will investigate the reflected field from an arbitrary transition when $k_o L_p \gg 1$ and $L_p \gg L$. From this investigation we will determine the nature of the diffraction field at large distances from the source when $k_o L \gg 1$, and relate this diffraction field to the lateral wave contribution which is excited on an abrupt interface. The analytical treatment will be limited to finite layers; infinite layers will be discussed by using the results of Chapters 3 and 4.

5.3.2   Finite Layers

The integral representation for the reflected field from an arbitrary finite layer is given by

$$E_{yr} = \frac{1}{4\pi i} \int_C \frac{p_1 \bar{\Gamma}}{p p_2} e^{ik_o [p_2(z+z') + px]} \, dp_1 \quad , \quad z \ge 0 \qquad (5.3.1)$$

where

$$\bar{\Gamma} = - \Delta_t / \Delta_b \qquad (5.3.2)$$

with

$$
\Delta_{\substack{t \\ b}} = \begin{vmatrix} \left\{ \Phi'_2(-L) + i k_o p_1 \, \Phi_2(-L) \right\} & \left\{ \Phi'_1(-L) + i k_o p_1 \, \Phi_1(-L) \right\} \\ \left\{ \Phi'_2(o) \pm i k_o p_2 \, \Phi_2(o) \right\} & \left\{ \Phi'_1(o) \pm i k_o p_2 \, \Phi_1(o) \right\} \end{vmatrix}.
$$

The integral representation is the same as the integral representation appearing in Eq. (1.4.1) with one exception; their reflection coefficients are different. The reflection coefficient, appearing in Eq. (5.3.1), has been derived in Appendix A. In this Appendix, we have defined $\Phi_1(z)$ and $\Phi_2(z)$ as two independent solutions to the reduced wave equation in the layer region. The square roots $p = \sqrt{\epsilon_1 - p_1^2}$, $p_2 = \sqrt{\Delta + p_1^2}$ and the path C are defined in Figs. 1.5 and 1.6.

If we now use the assumption that $k_o L \ll k_o L_p$, then the reflection coefficient in Eq. (5.3.1) is slowly varying compared to the exponential in the integrand, and the standard steepest descents techniques can be used to asymptotically evaulate the integral representation for large $k_o L_p$. The asymptotic evaluation parallels the evaluation of the integral in Eq. (1.4.1) and, as a result, we will not present it here. The results of this asymptotic analysis are that two saddle point contributions make up the reflected field when $k_o L_p \gg 1$. The first of these is a contribution from a ray reflected from the $z = 0$ interface. The contribution has a $O(k_o^{-1/2})$ for all layer thicknesses. When $k_o L \gg 1$, the contribution can be predicted by the classical theory of geometrical-optics.

The second contribution to the reflected field comes from the saddle point occurring at $p_1 = 0$, as shown in Chapter 1. This contribution, which will be denoted by E_L is given by

$$E_L \sim \frac{\epsilon_1^{1/4} \frac{d\bar{\Gamma}}{dp_1}\Big|_{p_1 = 0}}{2\sqrt{2\pi\Delta}\,(k_o L_p)^{3/2}} \; e^{i k_o [\sqrt{\Delta}\,(z+z') + \sqrt{\epsilon_1}\,x] - i\pi/4} \qquad (5.3.3)$$

where

$$\frac{d\bar{\Gamma}}{dp_1}\Big|_{p_1 = 0} = \frac{2\,\tau\sqrt{\Delta}\,[\Phi_2(o)\,\Phi_1'(o) - \Phi_2'(o)\,\Phi_1(o)]^2}{\{[\Phi_2'(\cdot L)\,\Phi_1'(o) - \Phi_1'(-L)\,\Phi_2'(o)] - i k_o\sqrt{\Delta}\,[\Phi_2'(-L)\,\Phi_1(o) - \Phi_1'(-L)\,\Phi_2(o)]\}^2},$$

$$(5.3.4)$$

$\tau = k_o L$ and the prime indicates differentiation with respect to z/L. The above contribution can be written in the following form

$$E_L \sim T(\tau) \left\{ \begin{array}{l} \text{the lateral wave} \\ \text{contribution on} \\ \text{an abrupt interface.} \end{array} \right\} \qquad (5.3.5)$$

where

$$T(\tau) = -\frac{\sqrt{\Delta}}{2}\; \frac{d\bar{\Gamma}}{dp_1}\Big|_{p_1 = 0} \qquad (5.3.6)$$

In the above $T(\tau)$ is a transition function which is independent of the observation point if we keep within our original assumption that $k_o L \gg 1$ and $L_p \gg L$.

It would be interesting to learn what particular characteristics of the layer's profile affect the transition function $T(\tau)$, however the wave functions $\Phi_1(z)$ and $\Phi_2(z)$ are not known. As a result, we will limit our investigation of $T(\tau)$ to values of τ which are small or large compared with unity.

We will proceed first with an investigation of $T(\tau)$ for small τ. An approximate expression for $T(\tau)$ when τ is small can be obtained by expressing $\bar{\Gamma}$ in a power series in τ. We can obtain this power series by considering the generalized reflection coefficient $\bar{\Gamma}(z)$ in the layer. This reflection coefficient obeys the Ricatti equation as given by Brekhovskikh[1], i.e:

$$d\bar{\Gamma}/dz = 2ik_o p_z(z)\bar{\Gamma}(z) + \epsilon'(z)[1-\bar{\Gamma}^2(z)]/p_z^2(z) \qquad (5.3.7)$$

where $p_z(z) = \sqrt{\epsilon(z) - p^2}$. This reflection coefficient is the ratio of incident to reflection wave fields at any point z. As a result when z becomes less then $-L$, the reflected wave disappears and $\bar{\Gamma}(-L) = 0$. We use this condition as the one initial condition necessary to make the solution to Eq. (5.3.7) unique.

Actually the function $\bar{\Gamma}(z)$ defined by this equation has, in general, no physical meaning since incident and reflected waves are indistinguishable in an inhomogeneous medium. However, when the medium is slowly varying, compared to wavelength or z is located in an homogeneous region, this difficulty no longer occurs and the reflection coefficient takes on the meaning that we usually ascribe to it. In our particular case, $\bar{\Gamma}(z)$ will be evaluated at $z = 0^+$, a point where $\bar{\Gamma}(z)$ is physically meaningful. For a more complete discussion of Eq. (5.3.7) and its physical interpretation we refer the reader to Schelkunoff[35].

Brekhovskikh[2] and Wait[36] have developed a procedure for expressing $\bar{\Gamma}(z)$ in terms of an ascending power series in k_o which would be useful for our purposes. Unfortunately the above series does not converge for $p_1 = 0$ and it is at this point that we require the series development. To alleviate this difficulty we have slightly modified Brekhovskikh's method and developed a series which does converge at $p_1 = 0$.

At this point we will assume $\epsilon(z) = \epsilon(z/L)$. This assumption is not necessary but it will simplify the analysis to follow and, at the same time, allows for a sufficient amount of generality. The transformations

$$\bar{\Gamma}(\bar{z}) = \frac{\bar{p}_z(\bar{z}) \, v(\bar{z}) - u(\bar{z})}{p_z(\bar{z}) \, v(\bar{z}) + u(\bar{z})} \quad , \quad \bar{z} = z/L \tag{5.3.8}$$

where $p_z(\bar{z})$ will now be used in Eq. (5.3.7) and an equation for $v(\bar{z})$ and $u(\bar{z})$ will be obtained. It is

$$u'/u - v'/v = i\tau p_z(\bar{z}) \left[\frac{u}{p_z(\bar{z}) \, v} - \frac{p_z(\bar{z}) v}{u} \right] \tag{5.3.9}$$

where the prime indicates differentiation with respect to $\bar{z}$. This equation can be satisfied by subjecting u and v to the two equations

$$u' = - i\tau p_z^2(\bar{z}) \, v \tag{5.3.10}$$

$$v' = - i\tau u \quad . \tag{5.3.11}$$

The solutions of the above equations with the boundary conditions[*]

$$u(-1) = p_1 \quad , \quad v(-1) = 1$$

yields Eq. (5.3.7) with the boundary condition that $\left.\Gamma\right|_{z = -L} = 0$. Now combining the Eqs. (5.3.10) and (5.3.11) we obtain a second order equation for $v(z)$. It is

$$v'' = - \tau^2 p_z^2(\bar{z}) \, v \tag{5.3.12}$$

---

[*] The boundary conditions are imposed on the negative side of the discontinuity at $z = -L$.

with

$$v(-1) = 1 \quad , \quad v'(-1) = - i\tau p_1 \quad . \tag{5.3.13}$$

We will now convert Eq. (5.3.12) into an integral equation by considering the Green's function problem $v'' = -\delta(z-z')$ and by considering the right hand side of Eq. (5.3.12) as a source term. By using Friedman's[37] result for the Green's function, Eq. (5.3.12) becomes

$$v(\bar{z}) = 1 - i\tau p_1 \bar{z} - \tau^2 \int_{-1}^{\cdot} p_z^2(t)(\bar{z} - t) v(t) dt \quad . \tag{5.3.14}$$

With the aid of Tricomi[38] , it can be shown that the method of successive approximations with $1 - i\tau p_1 \bar{z}$, as the zeroth approximation, converges to the solution of Eq. (5.3.14). The only requirements are that $1 - i\tau p_1 \bar{z}$ and $\tau^2 p_z^2(t)(\bar{z}-t)$ be square integrable in the interval $-1 \leq \bar{z} \leq 0$. We take special note that this solution will converge at $p_1 = 0$.

By applying the method of successive approximations to find $v(\bar{z})$ and then by using Eq. (5.3.11) to find $u(\bar{z})$, we can obtain an approximation to $\bar{\Gamma}(0)$ for small τ . It is

$$\bar{\Gamma} = \bar{\Gamma}(0) = \frac{p_2 - p_1}{p_2 + p_1} + \frac{2i\tau p_2 \left[\int_{-1}^{0} (\epsilon(t) - \epsilon_1) dt - p_1^2 \right]}{(p_2 + p_1)^2} + O(\tau^2) \quad . \tag{5.3.15}$$

If we now take the derivative of $\bar{\Gamma}$ with respect to p_1 , we can obtain an approximate expression $T(\tau)$ when $\tau \ll 1$. This expression is

$$T(\tau) = 1 + \frac{2i\tau}{\sqrt{\Delta}} \left\{ \epsilon(\bar{z}) - \epsilon_1 \right\}_{av} + O(\tau^2) \tag{5.3.16}$$

where the term in the brackets is the average of $\epsilon(\bar{z}) - \epsilon_1$, i.e.,

$$\left\{ \epsilon(\bar{z}) - \epsilon_1 \right\}_{av} = \int_{-1}^{0} (\epsilon(t) - \epsilon_1)dt = \frac{1}{L} \int_{-L}^{0} (\epsilon(z/L) - \epsilon_1)dz \ . \tag{5.3.17}$$

If we refer to Eq. (5.3.5) we see that as $\tau \to 0$, the lateral wave contribution E_L tends toward the lateral wave excited on an abrupt interface. The first perturbing term, as can be seen from Eq. (5.3.16), is proportional to the average amount that the dielectric constant exceeds ϵ_1.

Since we have obtained the approximate form of $T(\tau)$ when $\tau \ll 1$, we will now investigate $T(\tau)$ when $\tau \gg 1$. The general procedure for doing this will be to asymptotically approximate the function $\Phi_1(z)$ and $\Phi_2(z)$ appearing in Eq. (5.3.4). The asymptotic approximations to these functions will be obtained by using Langer's[39] comparison method. This method allows us to find the asymptotic solution to one equation in terms of the solution of another. For the procedure to apply, the two equations must have turning points of equal order.

The unknown functions $\Phi_1(\bar{z})$ and $\Phi_2(\bar{z})$ obey a reduced wave equation

$$\left\{ \frac{d^2}{d\bar{z}^2} + \tau^2 \left[\epsilon(\bar{z}) - \epsilon_1 \right] \right\} \Phi_{\substack{1\\2}}(\bar{z}) = 0 \quad , \quad \bar{z} = z/L \tag{5.3.18}$$

with the boundary condition that $\Phi_1(\bar{z})$ and $\Phi_2(\bar{z})$ must be outgoing and incoming waves respectively, when $k_o L$ is large. We have assumed, as before, that $\epsilon(z) = \epsilon(\bar{z})$. Since Eq. (5.3.18) has one turning point of nth order, we choose as a comparison equation

$$\left\{ \frac{d^2}{d\xi^2} + \tau^2 \xi^n \right\} \psi_{\substack{1\\2}}(\xi) = 0 \tag{5.3.19}$$

where $\psi_{\substack{1\\2}}(z)$ must obey the same boundary conditions as $\Phi_{\substack{1\\2}}(z)$. The above equation can be transformed into a Bessel equation and has the following

solutions:

$$\psi_{\frac{1}{2}}(\xi) = \sqrt{\xi} \; H_{\frac{1}{n+2}}^{(\frac{1}{2})} \left[\frac{2}{n+2} \; \tau \, \xi^{\frac{n+2}{2}} \right] \; . \tag{5.3.20}$$

By applying Langer's method with Eq. (5.3.19) as the comparison equation, the asymptotic approximations $\Phi_{\frac{1}{2}}(z)$ are given by

$$\Phi_{\frac{1}{2}}(\bar{z}) \sim \frac{\left[\frac{n+2}{2} \int_{-1}^{\bar{z}} (\epsilon(\tau) - \epsilon_1)^{\frac{1}{2}} d\tau \right]^{\frac{1}{2}}}{\left[\epsilon(\bar{z}) - \epsilon_1 \right]^{1/4}} \; H_{\frac{1}{n+2}}^{(\frac{1}{2})} \left[\tau \int_{-1}^{\bar{z}} (\epsilon(\tau) - \epsilon_1)^{\frac{1}{2}} d\tau \right] . \tag{5.3.21}$$

We shall also require the asymptotic approximation for $d\Phi_{\frac{1}{2}}(\bar{z})/d\bar{z}$. This can be obtained by taking the formal derivations of Eq. (5.2.21) and retaining only the higher order term. The result is

$$\frac{d\Phi_{\frac{1}{2}}(\bar{z})}{d\bar{z}} \sim \tau \left[\epsilon(\bar{z}) - \epsilon_1 \right]^{1/4} \left[\frac{n+2}{2} \int_{-1}^{\bar{z}} (\epsilon(\tau) - \epsilon_1)^{\frac{1}{2}} d\tau \right]^{\frac{1}{2}} H_{\frac{-n+1}{n+2}}^{(\frac{1}{2})} \left[\tau \int_{-1}^{\bar{z}} (\epsilon(\tau) - \epsilon_1)^{\frac{1}{2}} d\tau \right] \; .$$

$$\tag{5.3.22}$$

An examination of Eq. (5.3.4) shows that we will require Φ_1 , Φ_2 and their derivative at $z = 0$. When τ is large, the argument of the Hankel functions in Eqs. (5.3.21) and (5.3.22) becomes large. By using the asymptotic expansion for Hankel functions with large argument and fixed orders, we obtain

$$\Phi_{\frac{1}{2}}(0) \sim \sqrt{\frac{n+2}{\pi \sqrt{\Delta \tau}}} \; e^{\pm i \left[\tau \int_{-1}^{0} (\epsilon(\tau) - \epsilon_1)^{\frac{1}{2}} d\tau - \frac{n+4}{4(n+2)} \pi \right]} \tag{5.3.23}$$

and

$$\phi'_{\frac{1}{2}}(o) \sim \pm i \tau \sqrt{\frac{(n+2)\Delta}{\pi\tau}} \ e^{\pm i \left[\tau \int_{-1}^{o} (\epsilon(\tau) - \epsilon_1)^{\frac{1}{2}} d\tau - \frac{n+4}{4(n+2)} \ \pi\right]} \ . \qquad (5.3.24)$$

The evaluation of Eq. (5.3.4) will also require knowledge of $\phi'_{\frac{1}{2}}(-L)$. This can be obtained by using

$$H_{-\nu}^{\binom{1}{2}}(z) \approx \mp \frac{i(z/2)^{-\nu}}{\pi} \ \Gamma(\nu) \ e^{\pm \pi \nu} \ , \quad z \ll 1 \ . \qquad (5.3.25)$$

in Eq. (5.3.22). The result is

$$\phi'_{\frac{1}{2}}(-L) \sim \mp \left[\tau(n+2) \left[\frac{\epsilon(n)}{n!}\right]^{\frac{1}{2}}\right]^{1/n+2} \ \Gamma\left(\frac{n+1}{n+2}\right) \ e^{\pm i\pi \ \frac{n+1}{n+2}} \qquad (5.3.26)$$

where $\epsilon(n) = d^n \epsilon(\bar{z})/d\bar{z}^n \big|_{\bar{z} = -1}$. If we now use Eqs. (5.3.23), (5.3.24) and (5.3.26) in Eq. (5.3.4) we find that $T(\tau)$ is given by

$$T(\tau) \sim A \tau^{\left[\frac{n}{n+2}\right]} e^{2i\tau \int_{-1}^{o} (\epsilon(\tau) - \epsilon_1)^{\frac{1}{2}} d\tau - \frac{in\pi}{2(n+2)}} \qquad (5.3.27)$$

when $\tau \gg 1$. The constant A is given by

$$A = \pi\sqrt{\Delta} \left[\frac{n!}{(n+2)^n \epsilon(n)}\right]^{\frac{1}{n+2}} \Big/ \Gamma^2\left(\frac{n+1}{n+2}\right) \ . \qquad (5.3.28)$$

An inspection of Eq. (5.3.27) shows that as n increases, the order of $T(\tau)$ rises. This means that the more continuous the dielectric profile is at $z = -L$, the stronger the lateral wave is excited. In fact, as n tends toward infinity, the lateral wave contribution approaches an $O(k_o^{1/2})$. This means that the lateral wave contribution will be as strong as the geometrical-optic contribution.

It is interesting to compare the lateral wave field with the
reflected field discussed in section 5.2. There, when $n = 1$, a lateral
wave is excited and has an $O(k_o^{7/6})$. As the lateral distance, L_p,
becomes great compared to wavelength, the lateral wave contribution
found in section 5.2 becomes identical with the lateral wave contribution
given by Eq. (5.2.3) with Eq. (5.3.27) and $n = 1$. We also note in section
5.2 that when $n \geq 2$, the reflected field is composed of two contributions.
One of these contributions can not be obtained by the methods of geomet-
rical-optics when L_p becomes large compared with wavelength. In this
section we see that the geometrical-optic contribution, observed in
section 5.2, makes a transition to a lateral wave type contribution as
$k_o L_p \gg 1$. We have made no attempt to find the transition function between
these two contributions.

5.3.3.   Infinite Layers

We will not treat the class of infinite layers analytically, as has been
done for finite layers in the last section, but instead, we will discuss the
contributions that we might expe t on the basis of the results of Chapters
3 and 4. The results of both of these chapters indicate that. as in the
finite case, the reflected field for $k_o L_p \gg 1$ consists of two contributions.
One of these contributions appears to come from a ray reflected from the
$z = 0$ interface while the other contribution has a ray trajectory similar to
a lateral ray. The latter contribution has an algebric decay factor of $L_p^{-3/2}$
which is independent of $k_o L$. This behavior is also observed in sections
5.3.2. The excitation coefficient of the contribution changes with τ . For
small τ the contribution appears to reduce to a lateral wave on an abrupt
interface while, for large τ , the contribution reduces to a geometrical-
optic ray. It is interesting to note that the lateral wave contribution,

investigated in the last section for arbitrary n, approaches a $O(k_r^{-1/2})$ as $n \to \infty$. This is the same order as a geometrical-optic contribution. The interesting contrast between the lateral type contributions on finite and infinite layers for $k_o L_p \gg k_o L \gg 1$ is that in the infinite case the methods of geometrical-optics can be used to obtain the lateral contribution while in the finite cases it cannot.

APPENDIX A.

ONE-DIMENSIONAL GREEN'S FUNCTION
PROBLEM FOR AN ARBITRARY LAYER

The function $\Phi(z, p)$ is a one-dimensional Green's function. It obeys the equation

$$\left\{ \frac{d^2}{dz^2} + k_o^2 \left[\epsilon(z) - p^2 \right] \right\} \Phi(z, p) = - \delta(z - z')$$ (A-1)

and must satisfy the radiation condition as $z \to \pm\infty$. We shall choose an $\epsilon(z)$ which is given by

$$\epsilon(z) = \begin{cases} \epsilon_2 & , \quad z \geq 0 \\ \overline{\epsilon}(z) & , \quad -L < z < 0 \\ \epsilon_1 & , \quad z \leq -L \end{cases}$$ (A-2)

where $\overline{\epsilon}(z)$ is an arbitrary function of z. The formal solution to Eq. (A-1) is well known[40] and is given by

$$\Phi(z, p) = \frac{\overleftarrow{\Phi}(z_<) \overrightarrow{\Phi}(z_>)}{W(\overleftarrow{\Phi}, \overrightarrow{\Phi})}$$ (A-3)

where $z_>$ is the greater of z or z'; $z_<$ is the lesser of z or z'; $\overrightarrow{\Phi}(z)$ and $\overleftarrow{\Phi}(z)$ are independent homogeneous solutions to Eq. (A-1) which satisfy the boudnary conditions at + and - infinity respectively; and the Wronskian $W(\overleftarrow{\Phi}, \overrightarrow{\Phi})$ is given by

$$W(\overleftarrow{\Phi}, \overrightarrow{\Phi}) = \overrightarrow{\Phi}(z) \frac{d\overleftarrow{\Phi}(z)}{dz} - \overleftarrow{\Phi}(z) \frac{d\overrightarrow{\Phi}(z)}{dz} \ .$$ (A-4)

At this point we will limit ourselves to finding the Green's function for $z > 0$ and $z' > 0$. In this region the function $\overrightarrow{\phi}(z)$ and $\overleftarrow{\phi}(z)$ are given by

$$\overrightarrow{\phi}(z) = e^{i k_o P_2 z} \quad , \quad z \geq 0 \tag{A-5}$$

$$\overleftarrow{\phi}(z) = e^{-i k_o P_2 z} + \overline{\Gamma} e^{i k_o P_2 z} \quad , \quad z \geq 0 \tag{A-6}$$

where $p_2 = \sqrt{\epsilon_2 - p^2}$. The coefficient $\overline{\Gamma}$ will be determined at a later point. By using Eqs. (A-5) and (A-6) we can calculate $\phi(z, p)$. It is given by

$$\phi(z, p) = -\frac{e^{i k_o p |z - z'|}}{2 i k_o P_2} - \frac{\overline{\Gamma}}{2 i k_o P_2} e^{i k_o P_2 (z + z')} . \tag{A-7}$$

All that remains to be done is to determine $\overline{\Gamma}$. This can be accomplished by imposing the boundary condition on $\overleftarrow{\phi}(z)$ that it must be outgoing at $-\infty$. This gives

$$\overleftarrow{\phi}(z) = \begin{cases} e^{-i k_o P_2 z} + \overline{\Gamma} e^{i k_o P_2 z} & , \quad z \geq 0 \\ \alpha \phi_1(z) + \beta \phi_2(z) & , \quad -L < z < 0 \\ \gamma e^{-i k_o P_1 z} & z \leq -L \end{cases} \tag{A-8}$$

where $\phi_1(z)$ and $\phi_2(z)$ are two independent homogeneous solutions of Eq. (A-1) for $-L < z < 0$ and $p_1 = \sqrt{\epsilon_1 - p^2}$. If we recall that the one-dimensional Green's function, $\phi(z, p)$ is related to the electric field via a Fourier transform, then we can conclude that $\phi(z, p)$ and $(d/dz)\phi(z, p)$ must be continuous across the discontinuities of $\epsilon(z)$ since the tangential fields E_y and H_x are continuous across these discontinuities. By applying these conditions at $z = 0$, we obtain

$$1 + \overline{\Gamma} = \alpha \phi_1(o) + \beta \phi_2(o) \tag{A-9}$$

$$-i k_o P_2 + i k_o P_2 \overline{\Gamma} = \alpha \phi_1'(o) + \beta \phi_2'(o) \quad . \tag{A-10}$$

By imposing the same conditions at $z = -L$, we also obtain

$$\gamma e^{i k_o P_1 L} = \alpha \phi_1(-L) + \beta \phi_2(-L) \tag{A-11}$$

$$-i k_o P_1 \gamma e^{i k_o P_1 L} = \alpha \phi_1'(-L) + \beta \phi_2'(-L) \tag{A-12}$$

where

$$\phi_i'(z) = d \phi_i(z)/dz \quad , \quad i = 1, 2 .$$

The solution of these four equations for $\overline{\Gamma}$ gives

$$\overline{\Gamma} = - \frac{\Delta_t}{\Delta_b} \tag{A-13}$$

with

$$\Delta_{\genfrac{}{}{0pt}{}{t}{b}} = \begin{vmatrix} \left\{ \phi_2'(-L) + i k_o P_1 \phi_2(-L) \right\} & \left\{ \phi_1'(-L) + i k_o P_1 \phi_1(-L) \right\} \\ \left\{ \phi_2'(o) \pm i k_o P_2 \phi_2(o) \right\} & \left\{ \phi_1'(o) \pm i k_o P_2 \phi_1(o) \right\} \end{vmatrix}$$

It must be emphasized at this point that $\phi_1(z)$ and $\phi_2(z)$ are any pair of independent solutions to the homogeneous equation. For each different pair of solutions we obtain a different representation for the reflection coefficient.

APPENDIX B.
INTEGRAND'S SINGULARITIES

The pole singularities of the integrand are the singularities of the reflection coefficient, (3.2.4) , or the roots of

$$i = - \frac{2 \Gamma (\nu/2 + \mu/2 + 1) \Gamma (\nu/2 - \mu/2 + 1)}{\tau p_2^{-} (\nu/2 + \mu/2 + 1/2) \Gamma (\nu/2 - \mu/2 + 1/2)} \tan \left[\pi(\nu+\mu)/2 \right]. \quad (1B)$$

Since the square root $(\varepsilon_1 - p_1^2)^{\frac{1}{2}}$ doesn't appear in the above equation, a root of (1B) will correspond to a pole on the first and second sheet of the Riemann surface.

The poles lying on the integration path, C, (Figs.(1.5) and (1.6)) will be examined first. Consider roots of (1B) in the range $\operatorname{Re} p_1 = 0$, $0 \le \operatorname{Im} p_1 \le (\Delta)^{\frac{1}{2}}$. The right-hand side of (1B) is real and, therefore, no roots exist in this range. In the range $0 \le \operatorname{Re} p_1 \le (\varepsilon_1)^{\frac{1}{2}}$, $\operatorname{Im} p_1 = 0$, (1B) can be simplified. Using the simplified form

$$1 = \frac{2}{\tau p_2} \left| \frac{\Gamma^2 (\nu/2+\mu/2+1)}{\Gamma^2 (\nu/2+\mu/2+1/2)} \right| \frac{-\sinh \pi |\mu| + i \sin \pi \nu}{\cos \pi \nu + \cosh \pi |\mu|} \quad (2B)$$

one sees the right hand side has an imaginary part when $\sin(\pi\nu) \ne 0$. When $\sin(\pi\nu) = 0$, the right hand side of the equation is less than zero. Therefore, no roots exist in the range $0 \le \operatorname{Re} p_1 \le (\varepsilon_1)^{\frac{1}{2}}$, $\operatorname{Im} p_1 = 0$. The final range to consider is $\operatorname{Re} p_1 = 0$, $(\Delta)^{\frac{1}{2}} < \operatorname{Im} p_1 < \infty$. Transform (1B) to

$$-1 = \frac{2 \Gamma(1/2 - \nu/2 - |\mu|/2) \Gamma (\nu/2 + |\mu|/2 + 1)}{\tau |p_2| \Gamma(-\nu/2 + |\mu|/2) \Gamma(\nu/2 + |\mu|/2 + 1/2)} \quad (3B)$$

where the gamma functions appearing in (3B) are greater than zero since $|\mu| - \nu > 0$ for the range of p_1 under consideration. As a result, (3B) has no solutions on the integration path C.

Since no poles lie on the integration path, the only other residue contributions lie between the original and deformed path. If τ has a small or moderate value, then for large k_o any residue contribution will be a rapidly exponentially decay function which can be neglected asymptotically. When τ is large enough, the asymptotic form of the reflection coefficient,

$$R \sim e^{i\pi\tau(\Delta^{\frac{1}{2}} + i\, p_1)} \, ,$$

can be used. Since the exponential function has no singularities in the finite p_1 plane, the reflection coefficient is analytic there. As a result, we see no residues contribute to the asymptotic reflected field solution. We also note that since the saddle points lie on the integration path C, no singularities approach the saddle points as k_o increases.

APPENDIX C.
DECAY REGIONS

The decay regions of the integrand appearing in (3.4.12) are those regions where $\text{Im } \xi(p_1) > 0$ with

$$\xi(p_1) = p_2 \bar{z} + p \bar{x} + k_o^{-1} \, v(p_1, \, (\Delta)^{\frac{1}{2}} \tau) \, . \tag{1C}$$

Since the integration path is on two sheets of a four-sheeted Riemann surface, the decay regions must be found for both of these sheets. The method of finding the decay regions will be: first, to find the location of the saddle points and; second, to find the constant level paths through these saddle points, i. e. paths on which $\text{Im } \xi(p_1) = 0$. Since the constant level paths separate the decay and growth regions, once these paths are found, the boundaries of the decay regions are known.

The location of the saddle point can be found in the main part of the text. On the top sheet of the Riemann surface three saddle points were found. Two were on the positive imaginary axis where $0 < \text{Im } p_1 < (\Delta)^{\frac{1}{2}}$ and one was on the negative imaginary axis where $-(\Lambda)^{\frac{1}{2}} < \text{Im } p_1 < 0$. On the second sheet there was only one saddle point. It was located on the negative imaginary axis where $-(\Lambda)^{\frac{1}{2}} < \text{Im } p_1 < 0$.

Two constant level paths pass through each saddle point at right angles to each other. The imaginary p_1 axis where $|\text{Im } p_1| < (\Lambda)^{\frac{1}{2}}$ is one of the constant level paths. The other paths cross the imaginary axis at the saddle point normal to the axis. Since their functional behavior is complicated, only approximate path locations can be found. The asymptotes of these paths as $|p_1| \to \infty$ are found to be

$$\psi(p_1, (\Delta)^{\frac{1}{2}} \tau) \approx i\pi \, p_1 \tau \, , \quad p_1 \gg 1 \, . \tag{2C}$$

The expansion is valid on both the upper and lower sheet. On the upper sheet the four asymptotes are:

$$P_{1i} = \left[(x - \pi L)/z\right] P_{1r} \qquad 1^{st} \text{ quadrant} \qquad (3C)$$

$$P_{1i} = -\left[(x - \pi L)/z\right] P_{1r} \qquad 2^{nd} \text{ quadrant} \qquad (4C)$$

$$P_{1i} = -\left[(x + \pi L)/z\right] P_{1r} \qquad 3^{rd} \text{ quadrant} \qquad (5C)$$

$$P_{1i} = -\left[(x + \pi L)/z\right] P_{1r} \qquad 4^{th} \text{ quadrant} \qquad (6C)$$

where $p_1 = p_{1r} + i p_{1i}$. An examination of $\Phi(p_1)$ for large k_o shows that a constant level path goes through the saddle point which is highest on the imaginary p_1 axis and the path is asymptotic to (3C) and (4C). Similarly, a constant level path goes through the saddle point which is lowest on the imaginary p_1 axis and the path is asymptotic to (5C) and (6C). There are no asymptotes on the second sheet. As a result, the constant level path always remains in the finite region of the plane.

There is one constant level path on each sheet still to be found. An investigation of $\Phi(p_1)$ along the real p_1 axis shows that $\text{Im } \Phi(p_1) > 0$ on both sheets for $0 \leq \text{Re } p_1 \leq (\epsilon_1)^{\frac{1}{2}}$ and $\text{Im } \Phi(p_1) < 0$ on both sheets for $(\epsilon_1)^{\frac{1}{2}} \leq \text{Re } p_1 \leq 0$. The equation for $\text{Im } \Phi(p_1)$ where $(\epsilon_1)^{\frac{1}{2}} < |\text{Re } p_1|$ is

$$\text{Im}\left[\Phi(p_1)\right] = -(p_1^2 - \epsilon_1)^{\frac{1}{2}} x + k_o^{-1} \text{ Im } \psi(p_1, (\Delta)^{\frac{1}{2}} \tau) \qquad (7C)$$

which is valid on both sheets. This equation has one zero for $\text{Re } p_1 > (\epsilon_1)^{\frac{1}{2}}$ and another for $\text{Re } p_1 < -(\epsilon_1)^{\frac{1}{2}}$ when τ small or moderate and k_o large. When τ becomes large (7C) becomes

$$\text{Im } \Phi(p_1) = -(p_1^2 - \epsilon_1)^{\frac{1}{2}} x + \pi p_1 L.$$

This equation has a similar arrangement of zeros, if $x > \pi L$. This restriction does not hinder us since the caustic lies in this region. With the above information, the trajectory of the remaining constant level paths becomes clear. The path forms a complete circle crossing the two saddle points, one on each sheet, at right angles to the imaginary axis and crossing the $p_1 = \pm (\varepsilon_1)^{\frac{1}{2}}$ branch cuts at the zeros of (7C). The constant level paths and decay regions are shown in Figs. (3.3) and (3.4) .

APPENDIX D.

EXTREMUM OF THE LOCUS
OF TURNING POINTS

The purpose of this appendix is to show the relationship between the locus of turning points and the caustic formed in a stratified medium. Let us assume that there exists a stratified medium whose dielectric constant varies continuously in z between free space and $\epsilon_1 < 1$. Rays emitted from a two-dimensional point source located at (o, z') divide into transmitted and returning rays. The ray equation for the returning rays after they have turned is given by

$$ x = - \left[\int_{z'}^{z_t} - \int_{z_t}^{z} \right] \frac{p \, d\tau}{\sqrt{\epsilon(\tau) - p^2}} \quad , \qquad \epsilon(z_t) = p^2 \tag{D-1} $$

where p is the ray parameter, (x_t, z_t) are the coordinates of turning point of the ray and (x, z) are the coordinates of ray. The caustic formed by the rays given in Eq. (D-1) can be obtained by solving the constraint equation,

$$ \frac{d}{dz_t} \left\{ \left[\int_{z'}^{z_t} - \int_{z_t}^{z} \right] \frac{p \, d\tau}{\sqrt{\epsilon(\tau) - p^2}} \right\} = 0 \quad , \tag{D-2} $$

simultaneously with Eq. (D-1). The constraint equation, D-2, was obtained by taking the derivative of Eq. (D-1) with respect to z_t. We see Eq. (D-2) will give p or z_t in terms of z which, in turn, can be used in Eq. (D-1) to obtain the equation for the caustic. For comparison purposes at a later time we will evaluate Eq. (D-2) at $z = z'$. The result is

$$ 2 \frac{d}{dz_t} \left\{ \int_{z'}^{z_t} \frac{p \, d\tau}{\sqrt{\epsilon(\tau) - p^2}} \right\} = 0 \quad . \tag{D-3} $$

The locus of turning points for the turning rays is given by

$$x_t = - \int_{z'}^{z_t} \frac{p \, d\tau}{\sqrt{\epsilon(\tau) - p^2}} \quad .$$

(D-4)

The extremum of this equation is given by $d x_t / d z_t = 0$. By imposing this condition on Eq. (D-4), the resulting equation is Eq. (D-3) . This shows that extremum of the locus of turning points correspond to points on the caustic which coincide with the $z = z'$ line .

APPENDIX E.

UNIFORM ASYMPTOTIC APPROXIMATIONS FOR BESSEL FUNCTIONS

The uniform asymptotic approximations of the Bessel functions and their derivatives are given by Olver[30]. They are :

$$J_\nu(\nu w) \sim \left(\frac{4|\nu|^{2/3}\xi}{1-w^2}\right)^{1/4} \cdot \frac{A_i(|\nu|^{2/3}\xi)}{\nu^{1/2}} \tag{E-1}$$

$$H_\nu^{\binom{1}{2}}(\nu w) \sim 2 e^{\mp i\pi/3} \left(\frac{4|\nu|^{2/3}\xi}{1-w^2}\right)^{1/4} \frac{A_i(|\nu|^{2/3}\xi)}{\nu^{1/2}} \tag{E-2}$$

$$J_\nu'(\nu w) \sim -\frac{2}{w} \left(\frac{1-w^2}{4|\nu|^{2/3}\xi}\right)^{1/4} \frac{A_i'(|\nu|^{2/3}\xi)}{\nu^{1/2}} \tag{E-3}$$

$$H_\nu^{\binom{1}{2}}(\nu w) \sim -\frac{4 e^{\pm 2\pi i/3}}{w} \left(\frac{1-w^2}{4|\nu|^{2/3}\xi}\right)^{1/4} \frac{A_i(|\nu|^{2/3}\xi)}{\nu^{1/2}} \tag{E-4}$$

with

$$\frac{2}{3}\xi^{3/2} = \frac{\nu}{|\nu|} \int_w^1 \frac{\sqrt{1-t^2}}{t} dt \quad . \tag{E-5}$$

The above transformation, E-5 , is a relation between the w-plane and the ξ-plane for a particular value of $\arg\nu$. As can be seen, the transformation is independent of the magnitude of ν . Olver has made a thorough investigation of the relationship between w and ξ . He has shown that by cutting the ξ plane as shown in Fig. E-1 , the asymptotic approximations given in Eqs.(E-1) - (E-4) are valid over the whole w plane, cut as shown in Fig. E-2 with $|\arg\nu| < \pi/2$.
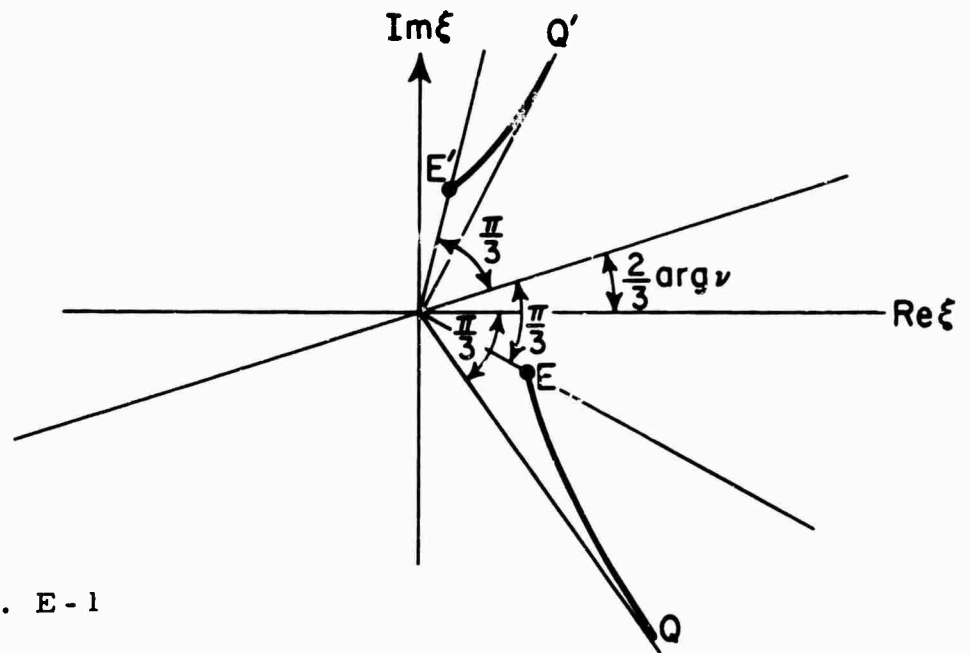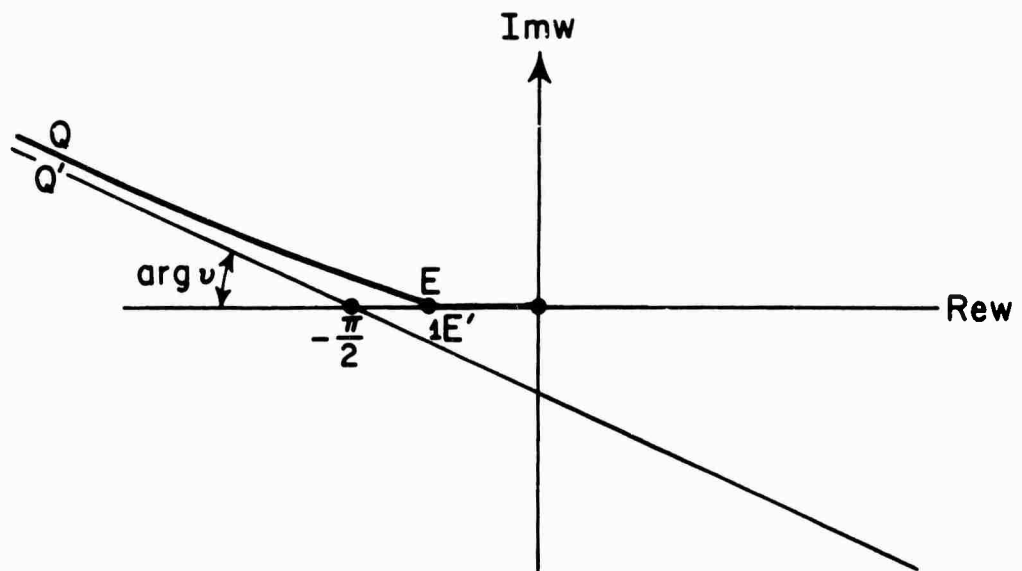
Fig. E - 1

The ξ Plane

Fig. E - 2

The w Plane

The branch cuts in Fig. E-1 are constant level curves of $\exp(-2/3\ \xi^{3/2})$ whose level is $\left(\frac{3}{2}\pi\right)^{2/3}$. When these branch cuts are transformed into the w plane, they fall on top of one another and form a section of the w plane branch cut. The parameter equations of this section of the w plane branch cut are

$$w = \text{sech}\,\sigma \quad , \quad 0 \le t < \infty$$

$$\sigma - \tanh\sigma = -i\pi + t\,e^{i(3/2\,\pi\,-\,\arg\nu)} \quad . \tag{E-6}$$

It is interesting to note that the branch cuts change position as the $\arg\nu$ is varied, however this will not concern us since the branch cuts will always remain out of the region of our interest.

In his paper Olver has obtained the asymptotic approximations to the Bessel functions for $|\arg\nu| < \pi/2$. We will now show that these formulae are valid when $\arg\nu = -\pi/2$ and $0 \le w < \infty$. To show this fact we will find the asymptotic approximations of $J_\nu(\nu w)$ in the region $|\pi - \arg\nu| < \pi/2$. If the asymptotic approximations from the right and left hand sides of the ν plane yield the same results when evaluated at $\arg\nu = -\pi/2$, then Olver's formula is correct at $\arg\nu = -\pi/2$. If the two formulae differ by more than an exponentially small term along some sector of the Re w axis, this will mean that the particular sector is an anti-Stokes line[41] and an oscillating term will be neglected if Olver's original formula is used at $\arg\nu = -\pi/2$. We should not make the faulty conclusion, however that if the two formulae agree, this sector of the Re w axis is not an anti-Stokes line.

First, evaluating Olver's asymptotic formula, E-1, at $\arg\nu = -\pi/2$, w real and $0 \le w \le 1$, we have

$$J_\nu(\nu w) \sim e^{i\pi/2} \left(\frac{4|\nu|^{2/3}|\xi|}{1-w^2} \right)^{1/4} \frac{A_i(|\nu|^{2/3}|\xi|e^{-i\pi/3})}{|\nu|^{1/3}} \quad .$$
(E-7)

Next, we want to find an expression for $J_\nu(\nu w)$ in the region $|\pi - \arg \nu| < \pi/2$. This can be done by making use of the analytic continuation formula given by Watson[42]. The result is

$$J_\nu(\nu w) = J_{-\nu}(\overline{\nu}w e^{i\pi}) = e^{-\overline{\nu}\pi i} J_{-\overline{\nu}}(\overline{\nu}w)$$
(E-8)

where $\nu = \overline{\nu} e^{i\pi}$ and then using the definition of $J_{-\overline{\nu}}(\overline{\nu}w)$, we obtain

$$J_\nu(\nu w) = e^{\overline{\nu}\pi i} \left[\cos \overline{\nu}\pi \, J_{\overline{\nu}}(\overline{\nu}w) - \sin \overline{\nu}\pi \, Y_{\overline{\nu}}(\overline{\nu}w) \right] \quad .$$
(E-9)

This will give us the asymptotic approximation of $J_\nu(\nu w)$ in terms of functions whose asymptotic approximations are valid in the right half of the ν plane. The asymptotic approximation to $Y_{\overline{\nu}}(\overline{\nu}w)$ has not been given as yet but can be obtained from Eq. (E-2) since $Y_\nu(z) = H_\nu^{(1)}(z) - H_\nu^{(2)}(z)$. We now evaluate Eq. (E-9) at $\arg \nu = -\pi/2$, $0 \le w \le 1$ and neglect exponentially small terms. The result is

$$J_\nu(\nu w) = \frac{1}{2} \left[J_{\overline{\nu}}(\overline{\nu}w) - i Y_{\overline{\nu}}(\overline{\nu}w) \right] \quad .$$
(E-10)

Substituting the asymptotic approximations given in Eqs. (E-1) and (E-2), in the right hand side of the above equation, gives us

$$J_\nu(\nu w) \sim \frac{1}{2} \left[\frac{4|\nu|^{2/3}|\xi|}{1-w^2} \right] \frac{e^{-i\pi/4}}{|\nu|^{1/3}} \left[A_i(|\nu|^{2/3}|\xi| e^{+i\pi/3}) \right.$$
(E-11)

$$\left. + i B_i(|\nu|^{2/3}|\xi| e^{i\pi/3}) \right] \quad .$$

Using the connection formula between Airy functions shows us that the asymptotic approximation for $J_\nu(\nu w)$ is the same as Eq. (E-7).

The same procedure can be repeated for $\arg \nu = -\pi/2$, $1 \leq w < \infty$, which shows that Olver's formula can be extended to $\arg \nu = -\pi/2$ for this section of the w plane also. In addition it can be shown that the asymptotic formula for $H_\nu^{(1)}{}^{(\frac{1}{2})}(\nu w)$, $J_\nu'(\nu w)$ and $H_\nu^{(1)}{}^{(\frac{1}{2})'}(\nu w)$ are also valid for $\arg \nu = -\pi/2$, $0 \leq w < \infty$.

REFERENCES

1. Nakamura, Y., J. Geo. Res., Vol. 69, No. 20, 1964, pp. 4349-4354.

2. Brekhovskikh, L. M., "Waves in Layered Media", Academic Press. 1960, pp. 215-225.

3. Hartree, D. R., "The Propagation of Electromagnetic Waves in a Stratified Medium", Proc. Camb. Phil. Soc. Vol. 25, 1929, p. 97.

4. Epstein, P. S., "Reflection of Waves in an Inhomogeneous Absorbing Medium", Proc. Nat. Acad. Sci., Wash., Vol. 16, 1930, pp. 627-637.

5. Heading, J., "Refractive Index Profiles Based on the Hypergeometric Equation and the Confluent Hypergeometric Equation", Proc. Camb. Phil. Soc., Vol. 61, 1965, pp. 897-913.

6. Wait, J. R., "Electromagnetic Waves in Stratified Media", Pergamon Press, 1962, Chapter 3.

7. Jeffreys, H., "Compressional Waves in Two Superposed Layers", Camb. Phil. Trans. Roy Soc., Series A, Vol. 203, 1904, pp. 1-42.

8. Muskat, M., "Theory of Refraction Shooting", Physics (now Journal of App. Phys.), Vol. 4, 1933, pp. 14-28.

9. Ott, H., "Reflection and Refraction of Spherical Waves", Annalen der Physik, Vol. 41, 1942, pp. 443-446.

10. Ref. 2, Chapter 4.

11. Kruger, M., "Die Theorie der in Endlicher Entfernung von der Trennungsebene Zweier Medien Erregten Kugeluelle Fur Endliche Brechungsindezes", Zeitschrift Fur Physik, Vol. 121, 1943, pp. 377-477.

12. Gerjouy, E., "Refraction of Waves From a Point Source Into a Medium of Higher Velocity", Phys. Rev., Vol. 73, No. 12, 1948, pp. 1442-1449.

13. Tamir, T. and L. B. Felsen, "On the Relation Between Pole Waves and Lateral Waves In Slab Configurations", Rpt. R-1245-64, pp. 1-9, Polytechnic Institute of Brooklyn, Microwave Research Institute, 1964.

14. Orlov, Yu. L, "On Some Perculiarities of the Ray Theory of Cylindrical and Spherical Waves Propagating in a Weakly Non-homogeneous Plasma I", Soviet Radiophysics, Vol. 9, No. 3, 1966, p. 491.

15. Felsen, L. B. and N. Marcuvitz, "Modal Analysis and Synthesis", Rpt. 1225-64, Polytechnic Institute of Brooklyn, Microwave Research Institute, 1964.

16. Abramowitz, M. and L Stegun, "Handbook of Mathematical Functions", National Bureau of Standards, U.S. Government Printing Office, 1964, pp. 446-455.

17. Ref. 16, p. 448, No. 10.4.59.

18. Ref. 16, p. 448, No. 10.4.60.

19. Felsen, L. B. and N. Marcuvitz, "Modal Analysis and Synthesis", Rpt. R-776-59, Polytechnic Institute of Brooklyn, Microwave Research Institute, 1959.

20. Orlov, Yu. L., "On the Peculiarities of Refraction and Focusing of Spherical Electromagnetic Wave Incident onto a Weakly Nonuniform Parabolic Plasma Layer", Soviet Radiophysics, Vol. 10, No. 1, 1967, pp. 30-39.

21a. Ref. 16, pp. 692-695.

21b. Olver, F. W. J., "Uniform Asymptotic Expansions for Weber Parabolic Cylinder Functions of Large Order", J. of Res. N.B.S., Vol. 63B, No. 2, 1959, p. 131.

22. Ref. 16, p. 692, No. 19.17.1.

23. Ref. 16, p. 332, No. 8.1.5.

24. Ref. 16, p. 332, Nos. 8.6.1 and 8.6.3.

25. Kelso, J., "Radio Ray Propagation in the Ionosphere", McGraw-Hill, 1964, p. 189.

26. Copson, E. T., "Asymptotic Expansions", Cambridge University Press, 1965, p. 42.

27. Friedman, B., "Principles and Techniques of Applied Mathematics, John Wiley, 1963, Chapter 3.

28. Ref. 16, p. 362, No. 9.1.54.

29. Ref. 16, p. 360, No. 9.1.15.

30. Olver, F.W.J. "The Asymptotic Expansions of Bessel Functions of Large Order", Phil. Trans., Series A, Vol. 247, 1954, pp. 328-368.

31. Watson, G. N., "A Treatise on The Theory of of Bessel Functions", Cambridge University Press, 1962, p. 74.

32. Magus, W., F. Oberhettinger, and R. P. Soni, "Formulas and Theorems for the Special Functions of Mathematical Physics", Springer, Verlag, 1966, pp. 140-141 .

33. Chester, C. and J. B. Keller, "Asymptotic Solution of Systems of Linear Ordinary Differential Equations with Discontinuous Coefficients", Rpt. No. EM-150, New York University, Courant Institute of Mathematical Sciences, Division of Electromagnetic Research, 1959.

34. Ref. 16, p. 360, No. 9.1.10.

35. Schelkunoff, S. A., "The Theory of Electromagnetic Waves", Editor Morris Kline, Dover Publications, (paperback edition) 1965, p. 181.

36. Wait, J. R., "On the Propagation of VLF and ELF Radio Waves When the Ionosphere Is Not Sharply Bounded", J. Res. N. B. S., Vol. 66D, No. 1, 1962, pp. 53-61.

37. Ref. 27. pp. 159-160.

38. Tricomi, F. G., "Integral Equations", Interscience Publishers, 1957, p. 10.

39. Langer, R. E., "The Asymptotic Solutions of Ordinary Linear Differential Equations of The Second Order, With Special Reference to Turning Points", Trans. Am. Math. Soc., Vol. 67, 1949, p. 461.

40. Ref. 27, Chapter 3.

41. Heading, J., "Introduction to Phase-Integral Methods", John Wiley, 1962, p. 69.

42. Ref. 31, p. 75.

DOCUMENT CONTROL DATA - R & D

(Security classification of title, body of abstract and indexing annotation must be entered when the overall report is classified)

1. ORIGINATING ACTIVITY (Corporate author)	2a. REPORT SECURITY CLASSIFICATION
Polytechnic Institute of Brooklyn, Electrophysics Department, Long Island Graduate Center, Route 110, Farmingdale, New York 11735	Unclassified
	2b. GROUP

3. REPORT TITLE

LATERAL WAVES ON DIFFUSE DIELECTRIC INTERFACES

4. DESCRIPTIVE NOTES (Type of report and inclusive dates)

Scientific.   Interim.

5. AUTHOR(S) (First name, middle initial, last name)

Roger Lang
Jerry Shmoys

6. REPORT DATE	7a. TOTAL NO OF PAGES	7b. NO OF REFS
June 1968	194	30

8a. Contract No. F19628-68-C-0072	9a. ORIGINATOR'S REPORT NUMBER(S)
b. Project, Task, Work Unit Nos. 5635-04-01	PIBEP-68-008 Scientific Report No. 4
c. DoD Element 6144501F	9b. OTHER REPORT NO(S) (Any other numbers that may be assigned this report)
d. DoD Subelement 681305	AFCRL-68-0455

10. DISTRIBUTION STATEMENT

1. Distribution of this document is unlimited. It may be released to the Clearinghouse, Department of Commerce, for sale to the general public.

11. SUPPLEMENTARY NOTES	12. SPONSORING MILITARY ACTIVITY
TECH, OTHER	Air Force Cambridge Research Laboratories (CRD) L. G. Hanscom Field Bedford, Massachusetts 01730

13. ABSTRACT In the past the lateral wave has been investigated for the case of a sharply bounded transition layer and a layer with a linear velocity variation. The interpretation of the lateral wave given in these instances cannot be extended to an arbitrary smooth layer, and in many cases, the exact nature of the lateral wave contribution becomes unclear. It is our purpose to clarify these matters and to present the characteristics of lateral wave propagation on a layer of arbitrary variation. The models employed can simulate an inhomogeneous plasma having a number density profile, $n(z)$, which varies continuously between two homogeneous half spaces. An integral representation for the scattered field in the optically denser half space is found and evaluated asymptotically in the high frequency limit. This asymptotic evaluation is carried out in two parameter ranges: first, when the layer is thick compared with wavelength; and second, when the layer thickness is arbitrary but the observation point's distance along the interface is large compared with layer thickness.

When the layer thickness is large compared with wavelength, the asymptotic analysis of the scattered field shows that the interpretation of the lateral wave depends markedly upon the gradient of $n(z)$ at the junction with the optically rarer homogeneous half space. It is found that when a finite gradient of $n(z)$ exists, the conventional interpretation of the lateral wave contribution is correct; however, the lateral wave mechanism is different in the case of a zero gradient. For observation points situated at a large distance along a layer of arbitrary thickness, the asymptotic expression for the lateral wave contribution has an amplitude dependence on distance identical with that for the lateral wave on an abrupt interface. In addition, the lateral wave expression reduces to the thick layer result for large layer thickness and it reduces to the abrupt interface result for thin layer thickness.

DD FORM 1473
1 NOV 65

14 KEY WORDS	LINK A		LINK B		LINK C	
	ROLE	WT	ROLE	WT	ROLE	WT
Lateral Waves						
Geometric optics						
Inhomogeneous medium						